University of South Carolina

Scholar Commons

2017

Synthesis, Characterization and Application of Polymer-Grafted Nanoparticles

Yang Zheng
University of South Carolina

Follow this and additional works at: https://scholarcommons.sc.edu/etd

 Part of the Chemistry Commons

Recommended Citation

SYNTHESIS, CHARACTERIZATION AND APPLICATION OF POLYMER-GRAFTED
NANOPARTICLES

by

Yang Zheng

Bachelor of Science
Nanjing University, 2011

_____

Submitted in Partial Fulfillment of the Requirements

For the Degree of Doctor of Philosophy in

Chemistry

College of Arts and Sciences

University of South Carolina

2017

Accepted by:

Brian Benicewicz, Major Professor

Chuanbing Tang, Committee Member

Thomas Vogt, Committee Member

Harry Ploehn, Committee Member

Cheryl L. Addy, Vice Provost and Dean of the Graduate School

ABSTRACT

This work focused on the synthesis and characterization of polymer-grafted nanoparticles for various applications including drug-delivery, directed self-assembly and mechanical reinforcement applications. The surfaces of inorganic particles were modified with polymers of different composition, chain length, graft density and polymer architecture depending on the specific needs of each project. The surface modifications were mainly achieved by surface-initiated reversible addition fragmentation chain transfer (RAFT) polymerization, which is a very versatile technique to prepare nanocomposites with desired properties.

The first part of this work (Chapters 2 & 3) focused on novel self-assembly techniques. Chapter 2 described the design and characterization of a new self-assembly technique called surface-initiated polymerization-induced self-assembly (SI-PISA). We rationally designed this one-pot synthesis method based on mixed brush grafted silica nanoparticles. Nano-assemblies with different shapes including 1D strings, 2D disks, 3D vesicles and solid spheres were obtained at high solid content in various solvent systems. The scheme is based on sequential SI-RAFT polymerization strategy. A solvent-miscible brush was first grafted onto 15 nm silica NPs, and self-assembly was subsequently induced by the polymerization of a second brush that was solvent-immiscible. Self-assembly occurred in situ with the SI-polymerization of the second brush. The shape of the nano-objects was found to be controlled by the chemical structure of grafted polymers, chain length of grafted polymers, and reaction media.

In Chapter 3, we utilized the low blocking efficiency of reversed monomer addition order in combination with surface initiated RAFT polymerization to establish a facile procedure towards mixed polymer brush grafted nanoparticles SiO_2-g-(PS1, PS1-b-PMAA). The SiO_2-g-(PS, PS-b-PMAA) nanoparticles were analyzed by GPC deconvolution, and the fraction of each polymer component was calculated. Additionally, the SiO_2-g-(PS, PS-b-PMAA) were amphiphilic in nature, and showed unique self-assembly behavior in water.

The second part of this work (Chapter 4) is based on a drug delivery application. A pH and thermal dual-responsive nanocarrier with silica as the core and block copolymer composed of poly(methacrylic acid) (PMAA) and poly(N-isopropylacrylamide) (PNIPAM) as the shell was prepared by surface initiated RAFT polymerization. These dual-responsive nanoparticles were used as carriers to deliver the model drug doxorubicin (DOX) with unusually high entrapment efficiency and loading content. The release rate was controlled by both pH and temperature of the surrounding medium. Moreover, these particles selectively precipitated at acidic conditions with increased temperature, which may enhance their ability to accumulate at tumor sites. Cytotoxicity studies demonstrated that DOX-loaded nanoparticles are highly active against Hela cells, and more effective than free DOX of equivalent dose. A cellular uptake study revealed that SiO_2-PMAA-*b*-PNIPAM nanoparticles could successfully deliver DOX molecules into the nuclei of Hela cells. All these features indicated that SiO_2-PMAA-*b*-PNIPAM nanoparticles are a promising candidate for therapeutic applications.

The third part of this work (Chapter 5 & 6) is surface functionalization of silica nanoparticles with low Tg rubbery polymers, and the use of these polymer-grafted

nanoparticles as mechanical reinforcement fillers. Chapter 5 documented the collaborative work between our research group and Michelin North America Inc. to study the influence of grafting density and molecular weight of grafted polymer on mechanical properties of polyisoprene tire rubber. The grafting of polyisoprene (PIP) to different types of silica has been studied and developed by RAFT polymerization processes. This has been shown to be applicable for preparing grafted nanoparticles that are useful for exploring new surface interactions between silica fillers and rubber materials. Scale up approaches have been successful and detailed mechanical property studies were documented to assess the potential of these new graft architectures on improving rubbery composite properties. Chapter 6 is focused on another rubber material, polychloroprene. Compared with other rubbers, polychloroprene exhibits excellent resistant to oil, grease, wax, ozone and harsh weather conditions. RAFT polymerization and surface-initiated RAFT polymerization (SI-RAFT) of polychloroprene was studied. The SI-RAFT polymerization rate of chloroprene was found to be slower than free solution RAFT polymerization, and further regulated by graft density of the grafted polymers. The resulting polychloroprene-grafted silica nanoparticles were directly crosslinked to get matrix-free polychloroprene nanocomposites that showed good nanoparticle dispersion and superior mechanical properties compared with unfilled polychloroprene rubber

TABLE OF CONTENTS

LIST OF TABLES

LIST OF SCHEMES

CHAPTER 1

INTRODUCTION

1.1 Controlled Radical Polymerization.

Free radical polymerization has been widely used for industrial applications due to its advantages like mild polymerization conditions, wide monomer selections, and high molecular weight of polymers. However, free radical polymerization is often limited by irreversible chain transfer and termination, which results in a large number of branched polymers and polydisperse polymers. Beginning in the 1980's, controlled radical polymerization (CRP) was developed to prepare polymers with controlled molecular weight, narrow polydispersity and complicated architectures. This kind of polymerization is also referred to as living polymerization, in which all chains will be initiated early in the reaction, grow at the same rate, and lack termination reactions.[2] Major CRP techniques include nitroxide mediated polymerization (NMP)[3-4], atom transfer radical polymerization (ATRP)[5-6] and reversible addition-fragmentation (RAFT) polymerization.[7-8]

RAFT polymerization was first discovered and reported by Common-wealth Scientific and Industrial Research Organization (CSIRO) in Australia.[9] As the most recently discovered living radical polymerization, it has a mechanism that is fundamentally different from nitroxide-mediated polymerization (NMP) and atom transfer radical polymerization (ATRP). RAFT polymerization employs a degenerative chain transfer process while the two others rely on a persistent radical effect. The basic mechanism of RAFT can be viewed simply as a free radical polymerization that incorporates a chain transfer agent. Thus, most conventional initiators and monomers can be applied to RAFT polymerization, making it a versatile method for making polymers with narrow molecular weight distribution. A detailed mechanism of RAFT polymerization is shown in Scheme 1.1. Radical-radical termination is minimized through the reversible trapping of active

radicals into dormant species. This process is achieved using dithioester compounds known as RAFT agents. The thiocarbonylthio moiety of the RAFT agent is reactive towards radicals, in particular, they react with propagating radicals to form a carbon centered intermediate. This intermediate will then undergo β-scission, to release a new radical that is capable of reinitiating propagation. The reinitiated chain will then reversible add to another chain transfer agent. Finally, a symmetric equilibrium will be established between propagating radicals and dormant carbon centered radicals. When RAFT agent, monomer, initiator and reaction conditions are well chosen, excellent control can be achieved with PDI as low as 1.1. Another feature for RAFT polymerization is that once polymerization is stopped appropriately, the thiocarbonylthio end group can be preserved, which can serve as a macro-CTA. Upon isolation and addition of another monomer, well controlled block copolymers can be produced.
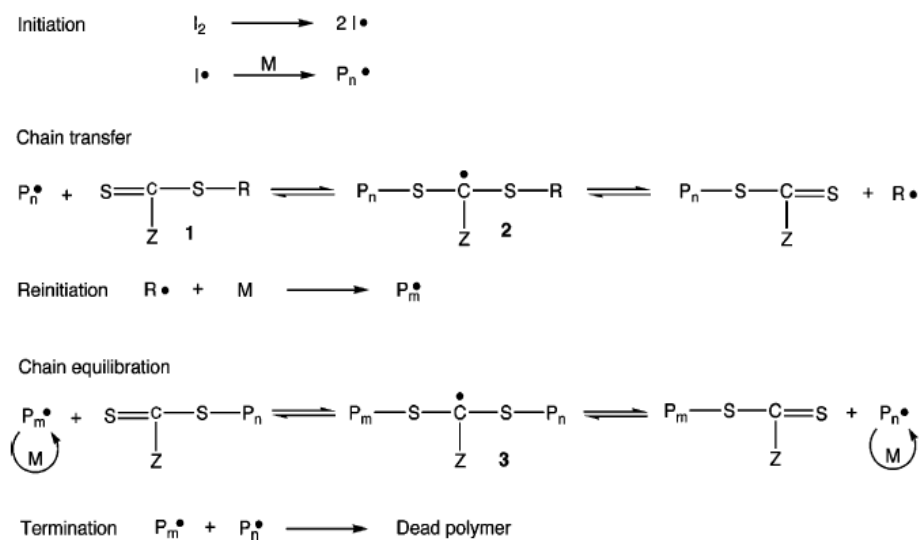
Scheme 1.1. Mechanism of RAFT polymerization[10]

1.2 Nanocomposites.

It is now well accepted that the incorporation of nanoparticles into a polymer matrix can significantly improve the mechanical, optical, and electrical properties of the resulting polymer nanocomposites (PNCs). [11-14] The advantage of nanocomposites comes from the large interfacial area that brings forth the property enhancements not seen with larger scale fillers. However, the large interface increases the unfavorable enthalpic interaction between hydrophobic organic polymer matrix and hydrophilic inorganic filler that often causes the aggregation of nanoparticles. For example, untreated silica nanoparticles easily aggregated into micon-sized clusters in tire rubber matrix, which compromised the mechanical performance of the resulting composites.[15-16] Aggregated nano-fillers will lose the advantage of large exposed surface area and will not be significantly different from micron-sized fillers. To increase nanoparticle dispersion in polymer matrices, it is vital to create a compatible interface by grafting organic molecules, either ligands or polymers, to inorganic particle surfaces.

Grafting polymer brushes to inorganic particle surfaces has shown great success in promoting filler-matrix compatibility.[17-19] Various parameters were found to influence filler dispersion including polymer molecular weight, polymer graft density, polymer architecture and polymer composition. For example, Kumar *et al.* found that dispersion was influenced by the long and short range enthalpic interactions of the nanoparticles and the entropic displacement of polymer chains on the nanoparticle surface. A variety of self-assembled anisotropic structures or well dispersed particles could be realized by manipulating polymer graft density (σ) and chain length (N) in a polystyrene matrix.[20] Figure 1.1 shows the experimentally obtained filler morphologies obtained by Kumar et al.

Evenly dispersed particles were obtained with sufficient polymer coverage. Numerous polymer chemistries have been achieved on filler surfaces though the majority of polymeric species tend to be derived from chain growth monomers.
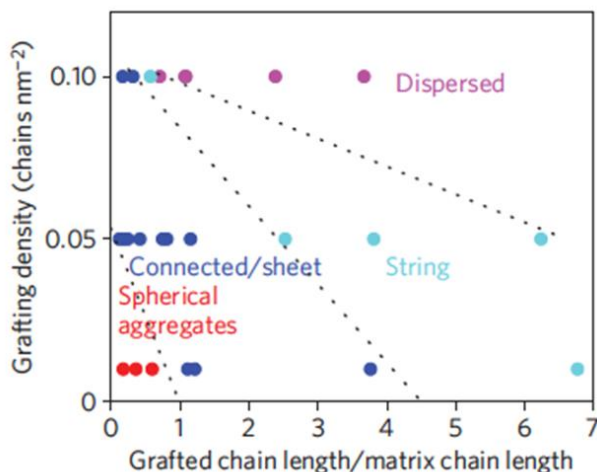
Figure 1.1: Experimentally obtained morphology diagram representing polystyrene grafted silica nanoparticles in polystyrene.[20]

Bimodal brush grafted nanoparticles are nanoparticles with two populations of polymer brushes attached to the surface that usually consists of a long molecular weight, low graft density population and a low molecular weight, high graft density population.[21] Each of these two population of brushes has their own functionality in achieving perfect particle dispersion or particular dispersion states. The long chain population entangles with the matrix and the short chain population screens particle core-core interaction by fully covering the surfaces. The first successful preparation of bimodal polymer grafted nanoparticles was reported by Benicewicz *et al.* using a sequential surface-initiated RAFT polymerization for the synthesis of bimodal styrene brushes on silica nanoparticles.[22] Matyjazewski *at al.* presented a different approach toward bimodal styrene brushes on silica via surface-initiated ATRP.[23] With effective synthetic methodology established

bimodal brush systems have been explored for various thermomechanical, electrical, and optical enhancements.[17, 19, 24]

1.3 Surface grafting strategies.

Generally, surface functionalization of nanoparticles includes two synthetic strategies: grafting-to and grafting-from. In grafting-to method, polymers are pre-made in the first step, which will then react with the nanofiller surface through active chain-end group chemistry. Due to steric hindrance, the graft density depends on the molecular weight and flexibility of the molecules, and is found to be on the lower end compared with grafting-from strategy. Once initial polymers are attached, it becomes increasingly difficult for the following polymer chains to diffuse to the surface and attach.

In the grafting-from method, polymerization is initiated from the particle surface and the polymer grows *in-situ*. This method overcomes the steric hindrance effect and can achieve relatively high graft density. A variety of controlled radical polymerization (CRP) techniques have been employed to graft a wide range of polymers from nanoparticle surfaces such as ATRP[25-26], NMP[27-28] and RAFT[29-30].

1.4 Inorganic substrates.

Many types of NPs have been modified using the above mentioned approaches, including titania,[32] silica,[33] barium titanate,[34] zirconia,[35] iron oxide,[36] CNTs,[37] and others. Each kind of inorganic core has its unique properties and application. For example, silica nanoparticles are widely used for rubber fillers and drug delivery applications due to its biocompatibility.[38-40] Titania nanoparticles are suitable for LED applications because of their high transparency, high refractive index and very low absorption coefficient in the
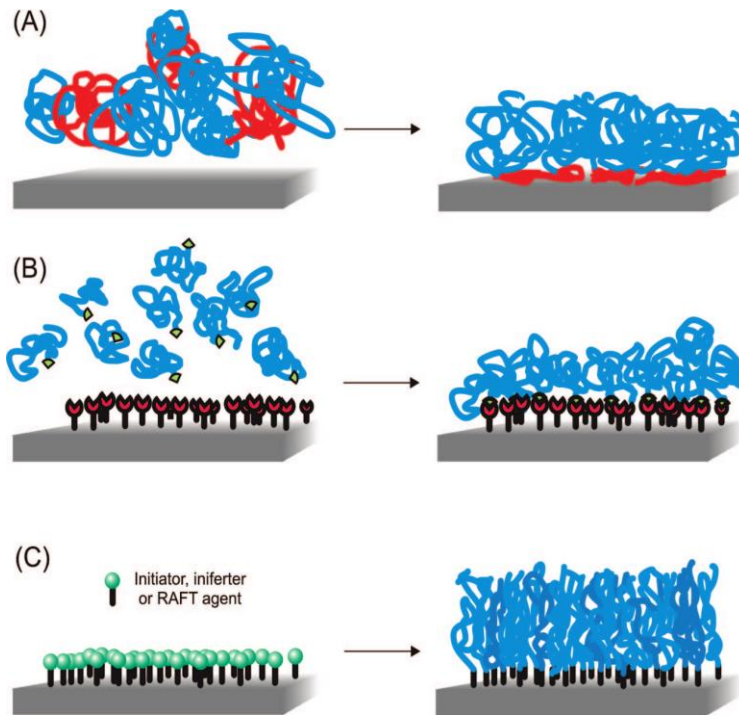
Figure 1.2. Various methods for grafting polymer chains to a substrate surface: A) physisorption, B) grafting-to and C) grafting-from methods. [31]

visible range.[41] Iron oxide nanoparticles are ideal candidates for bioimaging and recyclable delivery system due to their magnetic responsiveness.[42-43] Barium titanate nanoparticles have high dielectric constant and find applications in insulator fillers.[18] In most cases, different nanoparticles possess different surface chemistry and coupling agents need to be chosen carefully that provide sufficient reactivity with the substrate. Silane coupling agents are the most widely used which works well with silica substrates but lacks reactivity with metal oxides. Phosphate/phosphonate and amine based ligands have been used to complement silane coupling agents. Thiol-gold bonding is widely used for functionalization of gold nanoparticles.[44] However it has been reported that the gold-thiol bond with bonding energy 30-50 kcal/mol is not as strong as normal covalent bonds and may result in rearrangement or loss of surface grafted chains.[45]

7
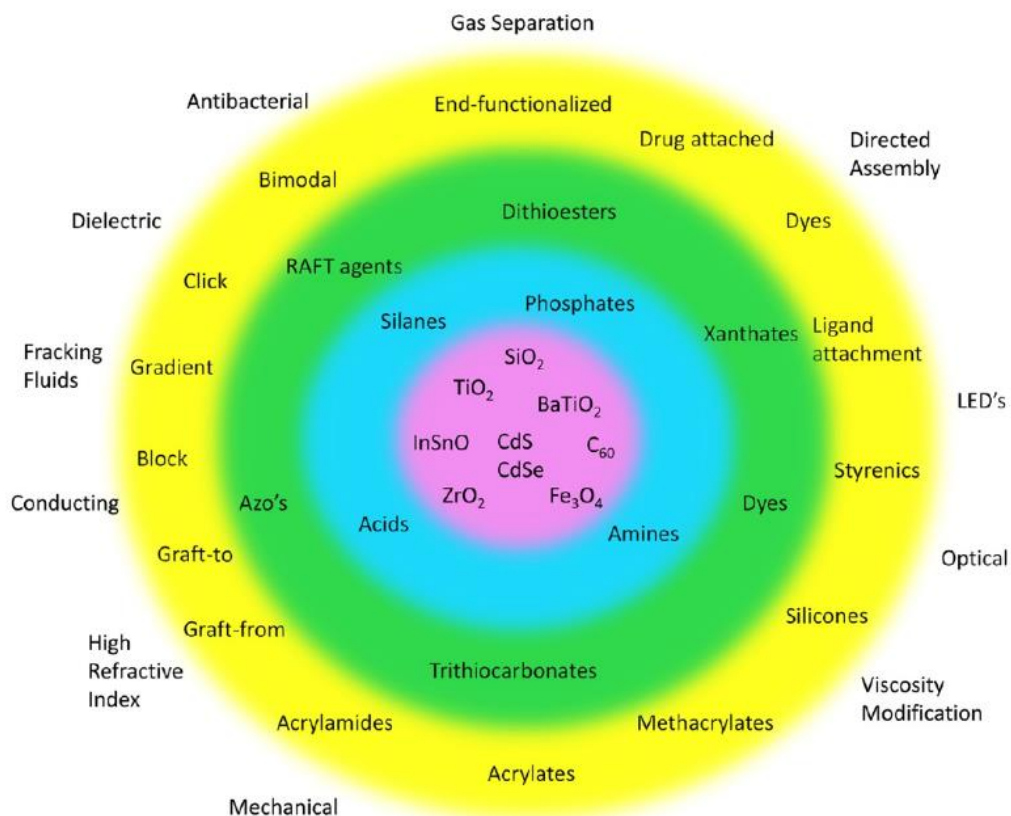
Figure 1.3 Schematic illustration of the various types of NPs available, the forms of surface functionalization, and the applications that these materials can impact.[12]

1.5 Nanocomposites via RAFT polymerization

Nanocomposites via RAFT polymerization is a versatile surface modification method that has been used throughout this dissertation. It could be applied to grafting to, grafting from and physisorption. The polymers prepared by RAFT polymerization will have thiocarbonyl end groups that could be reduced to thiols with $NaBH_4$.[46] Both thiol and thiocarbonyl end groups could easily bind to gold nanoparticle surfaces for the fabrication of gold nanocomposites which are found useful in sensing, nanomedicine and catalytic applications.[47-48] Metal oxide nanoparticles have been modified using RAFT polymers

with organophosphorus moieties. Click chemistry has also been used to functionalize silica nanoparticles where alkyne terminated polymer chains were clicked to azide surface functionalized silica nanoparticles.[49]

The grafting from strategy relies on surface-initiated RAFT polymerization. Compared with grafting to strategy, this method could achieve higher graft density and a better control of obtaining specific graft densities. Benicewicz *et al.* first developed the SI-RAFT procedure by sequentially adding an aminosilane coupling reagent followed by an activated RAFT agent to silica nanoparticle surfaces. Figure 1.8 demonstrates nanoparticle functionalization using an activated RAFT agent.[10] Activated RAFT agents contain a modified carboxylic acid that possess excellent leaving group chemistry by reacting prestine RAFT agents with 2-mecatothiazoline and N-hydroxysuccinimide (NHS) esters. The process proved to be a versatile method for surface modification of silica nanoparticles with effective graft densities of $0.01 - 0.7$ ch/nm^2 being achieved. One advantage of SI-RAFT over SI-ATRP or any other type of surface initiated controlled radical polymerization is that the graft density could be determined prior to polymerization by quantitively measuring the characteristic UV-vis absorption of the RAFT-grafted nanoparticles. The versatility of RAFT has allowed for nanocomposites to be synthesized for many applications including hybrid materials, thermosresponsive, optical, electrical, self-healing, and drug delivery.
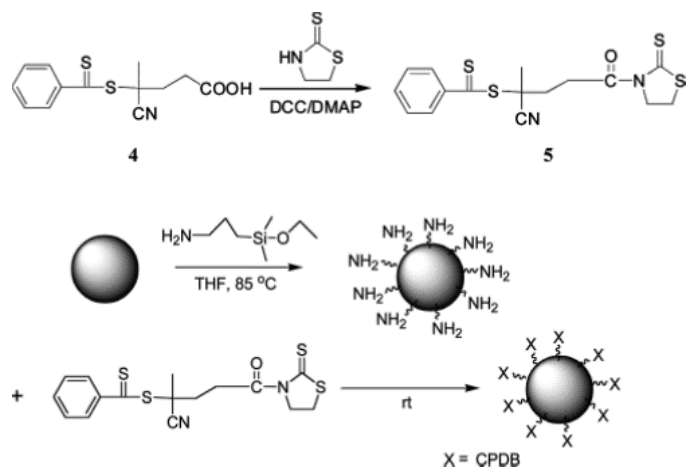
Figure 1.4. Synthesis and attachment of activated RAFT agent to SiO$_2$ nanoparticle.[10]

1.6 Polymerization-induced self-assembly

Self-assembly of amphiphilic block copolymers in selective solvents has been extensively studied in the past twenty years. A broad range of nano-objects have been created including spheres, rods, tubes, and vesicles.[50] These self-assembled nanomaterials have been found useful in biomedical, catalysis, and cosmetic applications. [51] A typical method to induce self-assembly behavior includes several steps. First, block copolymers are prepared in a good solvent for both blocks, followed by purification and redispersion to form a dilute solution. Then, a selective solvent is introduced dropwise to induce the collapse of one of the blocks, generating the desired aggregated structure. These multiple preparation processes are time consuming and more importantly, polymer concentration is limited, which prevents large scale production for commercial applications.[52] In recent years, polymerization-induced self-assembly (PISA) emerged as a more convenient technique to prepare self-assembled nanomaterials in large scale. In PISA, self-assembly

10

occurs in-situ with polymerization, and the solid content of reaction solution could be as high as 30 wt%.

The term "polymerization-induce self-assembly" was first introduced by Pan et al. where they chain extended trithiocarbonate terminated poly(4-vinylpyridine)(P4VP) with styrene in methanol.[1] P4VP was first prepared by reversible addition-fragmentation transfer (RAFT) polymerization with 10kDa molecular weight and narrow PDI. Then, chain extension of styrene was carried out in methanol which is a good solvent for P4VP and styrene monomers, but a none-solvent for polystyrene(PS). As the PS block increases, the polymers get more and more solvophobic, and beyond a certain point, aggregation occurs with PS forming the core and P4VP being the corona. Visually, one could observe the turbidity change of the reaction mixture from a clear, to light blue opalescent, and eventually, a milky-white solution was formed. On the microscopic level revealed by TEM, spherical nanoobjects could be observed after 2 hrs, and then rod-like structures after 24hrs.
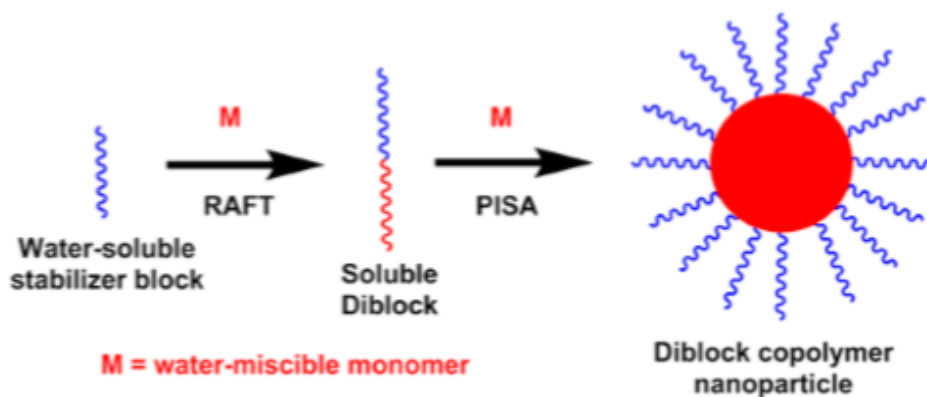
Scheme 1.2. Principle of Polymerization-Induced Self-Assembly Conducted in aqueous media.

By carefully adjusting the ratio between styrene monomer and RAFT agent, vesicle shaped structures could also be created.

Inspired by initial discovery of PISA in methanol and ethanolic solvents, the Armes group conducted a series of PISA experiments in water, a more environmentally friendly and convenient solvent. [53] The succesful PISA in water requires careful selection of a water-miscible monomer, which when polymerized, formed a water-insoluble polymer. Some examples include N-isopropylacrylamide (PNIPAM),[54] N,N-diethylacrylamide (DEAA),[55] 2-methoxyethyl acrylate (MEA),[56] and 2-hydroxypropyl methacrylate (HPMA).[57] However, in most cases, only spherical nanoobjects could be observed. Blanaz et al. performed aqueous dispersion polymerization with HPMA as a core forming
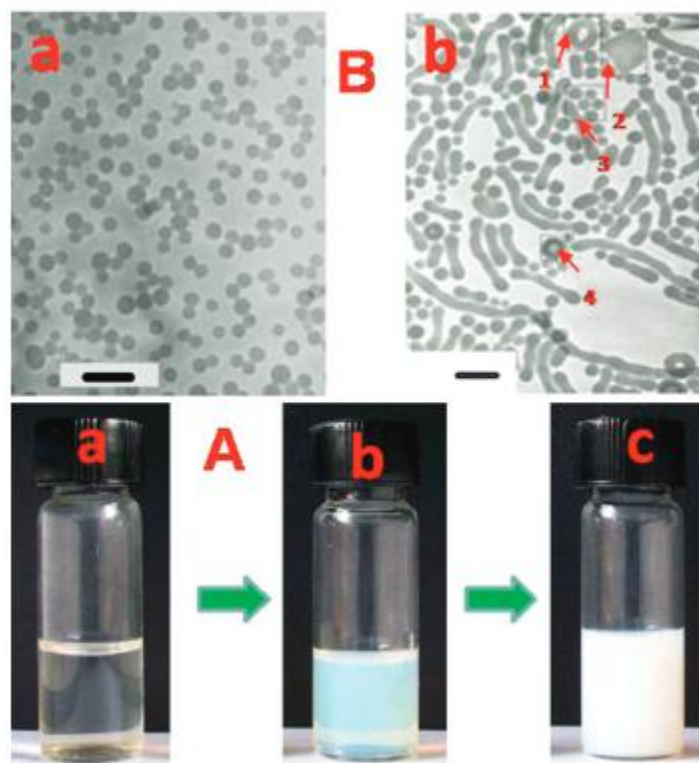
Figure 1.5. Optical photos of the RAFT polymerization and TEM images of the morphologies formed at 2h and 24h.[1]

monomer and poly(ethylene glycol) (PEG) as corona, which provided access to non-spherical morphologies like worms and vesicles.[51] The trend of morphology change (from spheres to worms to vesicles) as the hydrophobic block increaases, is similar to the PISA

cases in organic solutions discussed above. Moreover, the transition from worms to vesicle structures was carefully studied. TEM images clearly provided evidence that highly branched worms swell at junction points, and then wraps around to form jellyfish structures, and finally enclose to form vesicles. [57] All this remarkable evolution in copolymer morphology happened within 2h at 70°C, with high HPMA conversion.

1.7 Research Outline

The goal of this research was to functionalize inorganic nanoparticles with grafted polymers using new surface chemistry and novel polymer architecture and apply these polymer-grafted nanoparticles to various research areas including drug-release, directed self-assembly and mechanical reinforcement. The results are encouraging and proved the versatility of polymer-inorganic composite materials. With the right combination of core material (silica, gold, magnetic, etc.), polymer structure (water soluble polymers, low Tg polymers, stimuli responsive polymers, etc.), and polymer architecture (block copolymer, bimodal polymers, mixed brush polymers, etc.), we were able to fabricate novel materials that meet the specific requirements in a wide range of applications in nanotechnology.

The first part of this work (Chapters 2 & 3) focused on novel self-assembly techniques. Chapter 2 described the design and characterization of a new self-assembly technique called surface-initiated polymerization-induced self-assembly (SI-PISA). We rationally designed this one-pot synthesis method based on mixed brush grafted silica nanoparticles. Nano-assemblies with different shapes including 1D string, 2D disks, 3D vesicles and solid spheres were obtained at high solid content in various solvent systems. The scheme is based on sequential SI-RAFT polymerization strategy. A solvent-miscible

brush was first grafted onto 15 nm silica NPs, and self-assembly was subsequently induced by the polymerization of a second brush that was solvent-immiscible. Self-assembly occurred in situ with the SI-polymerization of the second brush. The shape of the nano-objects was found to be controlled by the chemical structure of grafted polymers, chain length of grafted polymers, and reaction mediums.

In Chapter 3, we utilized the low blocking efficiency of reversed monomer addition order in combination with surface initiated RAFT polymerization to establish a facile procedure towards mixed polymer brush grafted nanoparticles SiO_2-g-(PS_1, PS_1-b-PMAA). The SiO_2-g-(PS, PS-b-PMAA) nanoparticles were analyzed by GPC deconvolution, and the fraction of each polymer component was calculated. Additionally, the SiO_2-g-(PS, PS-b-PMAA) were amphiphilic in nature, and showed unique self-assembly behavior in water.

The second part of this work (Chapter 4) is based on drug delivery application. A pH and thermal dual-responsive nanocarrier with silica as the core and block copolymer composed of poly(methacrylic acid) (PMAA) and poly(N-isopropylacrylamide) (PNIPAM) as the shell was prepared by surface initiated RAFT polymerization. These dual-responsive nanoparticles were used as carriers to deliver the model drug doxorubicin (DOX) with unusually high entrapment efficiency and loading content. The release rate was controlled by both pH and temperature of the surrounding medium. Moreover, these particles selectively precipitated at acidic conditions with increased temperature, which may enhance their ability to accumulate at tumor sites. Cytotoxicity studies demonstrated that DOX-loaded nanoparticles are highly active against Hela cells, and more effective than free DOX of equivalent dose. A cellular uptake study revealed that SiO_2-PMAA-b-PNIPAM nanoparticles could successfully deliver DOX molecules into the nuclei of Hela

cells. All these features indicated that SiO$_2$-PMAA-*b*-PNIPAM nanoparticles are a promising candidate for therapeutic applications.

The third part of this work (Chapter 5 & 6) is surface functionalization of silica nanoparticles with low Tg rubbery polymers, and the use of these polymer-grafted nanoparticles as mechanical reinforcement fillers. Chapter 5 documented the collaborative work between our research group and Michelin North America Inc. to study the influence of grafting density and molecular weight of grafted polymer on mechanical properties of polyisoprene tire rubber. The grafting of polyisoprene (PIP) to different types of silica has been studied and developed by RAFT polymerization processes. This has been shown to be applicable for preparing grafted nanoparticles that are useful for exploring new surface interactions between silica fillers and rubber materials. Scale up approaches have been successful and detailed mechanical property studies were documented to assess the potential of these new graft architectures on improving rubbery composite properties. Chapter 6 is focused on another rubber material, polychloroprene. Compared with other rubbers, polychloroprene exhibits excellent resistant to oil, grease, wax, ozone and harsh weather conditions. RAFT polymerization and surface-initiated RAFT polymerization (SI-RAFT) of polychloroprene was studied. The SI-RAFT polymerization rate of chloroprene was found to be slower than free solution RAFT polymerization, and further regulated by graft density of the grafted polymers. The resulting polychloroprene-grafted silica nanoparticles were directly crosslinked to get matrix-free polychloroprene nanocomposites that showed good nanoparticles dispersion and superior mechanical properties compared with unfilled polychloroprene rubber.

1.8 References

1.   Wan, W.-M.; Hong, C.-Y.; Pan, C.-Y., One-pot synthesis of nanomaterials via RAFT polymerization induced self-assembly and morphology transition. *Chemical Communications* **2009,** (39), 5883-5885.

2.   Braunecker, W. A.; Matyjaszewski, K., Controlled/living radical polymerization: Features, developments, and perspectives. *Progress in Polymer Science* **2007,** *32* (1), 93-146.

3.   Hawker, C. J.; Bosman, A. W.; Harth, E., New Polymer Synthesis by Nitroxide Mediated Living Radical Polymerizations. *Chemical Reviews* **2001,** *101* (12), 3661-3688.

4.   Grubbs, R. B., Nitroxide-Mediated Radical Polymerization: Limitations and Versatility. *Polymer Reviews* **2011,** *51* (2), 104-137.

5.   Matyjaszewski, K., Atom Transfer Radical Polymerization (ATRP): Current Status and Future Perspectives. *Macromolecules* **2012,** *45* (10), 4015-4039.

6.   Matyjaszewski, K.; Xia, J., Atom Transfer Radical Polymerization. *Chemical Reviews* **2001,** *101* (9), 2921-2990.

7.   Perrier, S.; Takolpuckdee, P.; Westwood, J.; Lewis, D. M., Versatile Chain Transfer Agents for Reversible Addition Fragmentation Chain Transfer (RAFT) Polymerization to Synthesize Functional Polymeric Architectures. *Macromolecules* **2004,** *37* (8), 2709-2717.

8.   Moad, G.; Mayadunne, R. T. A.; Rizzardo, E.; Skidmore, M.; Thang, S. H., Synthesis of novel architectures by radical polymerization with reversible addition fragmentation chain transfer (RAFT polymerization). *Macromolecular Symposia* **2003,** *192* (1), 1-12.

9.   Chiefari, J.; Chong, Y. K.; Ercole, F.; Krstina, J.; Jeffery, J.; Le, T. P. T.; Mayadunne, R. T. A.; Meijs, G. F.; Moad, C. L.; Moad, G.; Rizzardo, E.; Thang, S. H., Living Free-Radical Polymerization by Reversible Addition−Fragmentation Chain Transfer: The RAFT Process. *Macromolecules* **1998,** *31* (16), 5559-5562.

10.   Li, C.; Han, J.; Ryu, C. Y.; Benicewicz, B. C., A Versatile Method To Prepare RAFT Agent Anchored Substrates and the Preparation of PMMA Grafted Nanoparticles. *Macromolecules* **2006,** *39* (9), 3175-3183.

11.   Kumar, S. K.; Jouault, N.; Benicewicz, B.; Neely, T., Nanocomposites with Polymer Grafted Nanoparticles. *Macromolecules* **2013,** *46* (9), 3199-3214.

12.   Kumar, S. K.; Benicewicz, B. C.; Vaia, R. A.; Winey, K. I., 50th Anniversary Perspective: Are Polymer Nanocomposites Practical for Applications? *Macromolecules* **2017,** *50* (3), 714-731.

13.   Mittal, G.; Dhand, V.; Rhee, K. Y.; Park, S.-J.; Lee, W. R., A review on carbon nanotubes and graphene as fillers in reinforced polymer nanocomposites. *Journal of Industrial and Engineering Chemistry* **2015,** *21*, 11-25.

14.   Thakur, V. K.; Kessler, M. R., Self-healing polymer nanocomposite materials: A review. *Polymer* **2015,** *69*, 369-383.

15.   Oberdisse, J., Aggregation of colloidal nanoparticles in polymer matrices. *Soft Matter* **2006,** *2* (1), 29-36.

16.   Bagwe, R. P.; Hilliard, L. R.; Tan, W., Surface Modification of Silica Nanoparticles to Reduce Aggregation and Nonspecific Binding. *Langmuir* **2006,** *22* (9), 4357-4362.

17.   Li, Y.; Wang, L.; Natarajan, B.; Tao, P.; Benicewicz, B. C.; Ullal, C.; Schadler, L. S., Bimodal "matrix-free" polymer nanocomposites. *RSC Advances* **2015,** *5* (19), 14788-14795.

18.   Qiao, Y.; Yin, X.; Wang, L.; Islam, M. S.; Benicewicz, B. C.; Ploehn, H. J.; Tang, C., Bimodal Polymer Brush Core–Shell Barium Titanate Nanoparticles: A Strategy for High-Permittivity Polymer Nanocomposites. *Macromolecules* **2015,** *48* (24), 8998-9006.

19.   Zhao, D.; Di Nicola, M.; Khani, M. M.; Jestin, J.; Benicewicz, B. C.; Kumar, S. K., Role of block copolymer adsorption versus bimodal grafting on nanoparticle self-assembly in polymer nanocomposites. *Soft Matter* **2016,** *12* (34), 7241-7247.

20.   Akcora, P.; Liu, H.; Kumar, S. K.; Moll, J.; Li, Y.; Benicewicz, B. C.; Schadler, L. S.; Acehan, D.; Panagiotopoulos, A. Z.; Pryamitsyn, V.; Ganesan, V.; Ilavsky, J.; Thiyagarajan, P.; Colby, R. H.; Douglas, J. F., Anisotropic self-assembly of spherical polymer-grafted nanoparticles. *Nat Mater* **2009,** *8* (4), 354-359.

21.   Li, Y.; Tao, P.; Viswanath, A.; Benicewicz, B. C.; Schadler, L. S., Bimodal Surface Ligand Engineering: The Key to Tunable Nanocomposites. *Langmuir* **2013,** *29* (4), 1211-1220.

22.   Rungta, A.; Natarajan, B.; Neely, T.; Dukes, D.; Schadler, L. S.; Benicewicz, B. C., Grafting Bimodal Polymer Brushes on Nanoparticles Using Controlled Radical Polymerization. *Macromolecules* **2012,** *45* (23), 9303-9311.

23.   Yan, J.; Kristufek, T.; Schmitt, M.; Wang, Z.; Xie, G.; Dang, A.; Hui, C. M.; Pietrasik, J.; Bockstaller, M. R.; Matyjaszewski, K., Matrix-free Particle Brush System with Bimodal Molecular Weight Distribution Prepared by SI-ATRP. *Macromolecules* **2015,** *48* (22), 8208-8218.

24.   Virtanen, S.; Krentz, T. M.; Nelson, J. K.; Schadler, L. S.; Bell, M.; Benicewicz, B.; Hillborg, H.; Zhao, S., Dielectric breakdown strength of epoxy bimodal-polymer-brush-grafted core functionalized silica nanocomposites. *IEEE Transactions on Dielectrics and Electrical Insulation* **2014,** *21* (2), 563-570.

25.   Singh, N.; Wang, J.; Ulbricht, M.; Wickramasinghe, S. R.; Husson, S. M., Surface-initiated atom transfer radical polymerization: A new method for preparation of polymeric membrane adsorbers. *Journal of Membrane Science* **2008,** *309* (1–2), 64-72.

26.   Fristrup, C. J.; Jankova, K.; Hvilsted, S., Surface-initiated atom transfer radical polymerization-a technique to develop biofunctional coatings. *Soft Matter* **2009,** *5* (23), 4623-4634.

27.   Blas, H.; Save, M.; Boissière, C.; Sanchez, C.; Charleux, B., Surface-Initiated Nitroxide-Mediated Polymerization from Ordered Mesoporous Silica. *Macromolecules* **2011,** *44* (8), 2577-2588.

28.   Ghannam, L.; Parvole, J.; Laruelle, G.; Francois, J.; Billon, L., Surface-initiated nitroxide-mediated polymerization: a tool for hybrid inorganic/organic nanocomposites 'in situ' synthesis. *Polymer International* **2006,** *55* (10), 1199-1207.

29.   Li, Y.; Benicewicz, B. C., Functionalization of Silica Nanoparticles via the Combination of Surface-Initiated RAFT Polymerization and Click Reactions. *Macromolecules* **2008,** *41* (21), 7986-7992.

30.   Gonzato, C.; Courty, M.; Pasetto, P.; Haupt, K., Magnetic Molecularly Imprinted Polymer Nanocomposites via Surface-Initiated RAFT Polymerization. *Advanced Functional Materials* **2011,** *21* (20), 3947-3953.

31.   Barbey, R.; Lavanant, L.; Paripovic, D.; Schüwer, N.; Sugnaux, C.; Tugulu, S.; Klok, H.-A., Polymer Brushes via Surface-Initiated Controlled Radical Polymerization: Synthesis, Characterization, Properties, and Applications. *Chemical Reviews* **2009,** *109* (11), 5437-5527.

32.   Fan, X.; Lin, L.; Messersmith, P. B., Surface-initiated polymerization from TiO2 nanoparticle surfaces through a biomimetic initiator: A new route toward polymer–matrix nanocomposites. *Composites Science and Technology* **2006,** *66* (9), 1198-1204.

33.   Perruchot, C.; Khan, M. A.; Kamitsi, A.; Armes, S. P.; von Werne, T.; Patten, T. E., Synthesis of Well-Defined, Polymer-Grafted Silica Particles by Aqueous ATRP. *Langmuir* **2001,** *17* (15), 4479-4481.

34.   Qiao, Y.; Islam, M. S.; Wang, L.; Yan, Y.; Zhang, J.; Benicewicz, B. C.; Ploehn, H. J.; Tang, C., Thiophene Polymer-Grafted Barium Titanate Nanoparticles toward Nanodielectric Composites. *Chemistry of Materials* **2014,** *26* (18), 5319-5326.

35.   Rovira-Bru, M.; Giralt, F.; Cohen, Y., Protein Adsorption onto Zirconia Modified with Terminally Grafted Polyvinylpyrrolidone. *Journal of Colloid and Interface Science* **2001,** *235* (1), 70-79.

36.   Lien, Y.-H.; Wu, T.-M., Preparation and characterization of thermosensitive polymers grafted onto silica-coated iron oxide nanoparticles. *Journal of Colloid and Interface Science* **2008,** *326* (2), 517-521.

37.   Viswanathan, G.; Chakrapani, N.; Yang, H.; Wei, B.; Chung, H.; Cho, K.; Ryu, C. Y.; Ajayan, P. M., Single-Step in Situ Synthesis of Polymer-Grafted Single-Wall Nanotube Composites. *Journal of the American Chemical Society* **2003,** *125* (31), 9258-9259.

38.   Paris, J. L.; Cabañas, M. V.; Manzano, M.; Vallet-Regí, M., Polymer-Grafted Mesoporous Silica Nanoparticles as Ultrasound-Responsive Drug Carriers. *ACS Nano* **2015,** *9* (11), 11023-11033.

39.   Jadhav, S. A.; Brunella, V.; Scalarone, D.; Berlier, G., Poly(NIPAM-co-MPS)-grafted multimodal porous silica nanoparticles as reverse thermoresponsive drug delivery system. *Asian Journal of Pharmaceutical Sciences* **2017,** *12* (3), 279-284.

40.   Kar, M.; Tiwari, N.; Tiwari, M.; Lahiri, M.; Gupta, S. S., Poly-L-Arginine Grafted Silica Mesoporous Nanoparticles for Enhanced Cellular Uptake and their Application in DNA Delivery and Controlled Drug Release. *Particle & Particle Systems Characterization* **2013,** *30* (2), 166-179.

41.   Tao, P.; Li, Y.; Rungta, A.; Viswanath, A.; Gao, J.; Benicewicz, B. C.; Siegel, R. W.; Schadler, L. S., TiO2 nanocomposites with high refractive index and transparency. *Journal of Materials Chemistry* **2011,** *21* (46), 18623-18629.

42.   Lu, A.-H.; Salabas, E. L.; Schüth, F., Magnetic Nanoparticles: Synthesis, Protection, Functionalization, and Application. *Angewandte Chemie International Edition* **2007,** *46* (8), 1222-1244.

43.   Laurent, S.; Forge, D.; Port, M.; Roch, A.; Robic, C.; Vander Elst, L.; Muller, R. N., Magnetic Iron Oxide Nanoparticles: Synthesis, Stabilization, Vectorization, Physicochemical Characterizations, and Biological Applications. *Chemical Reviews* **2008,** *108* (6), 2064-2110.

44.   Corbierre, M. K.; Cameron, N. S.; Lennox, R. B., Polymer-Stabilized Gold Nanoparticles with High Grafting Densities. *Langmuir* **2004,** *20* (7), 2867-2873.

45.   Love, J. C.; Estroff, L. A.; Kriebel, J. K.; Nuzzo, R. G.; Whitesides, G. M., Self-Assembled Monolayers of Thiolates on Metals as a Form of Nanotechnology. *Chemical Reviews* **2005,** *105* (4), 1103-1170.

46.   Willcock, H.; O'Reilly, R. K., End group removal and modification of RAFT polymers. *Polymer Chemistry* **2010,** *1* (2), 149-157.

47.	Saha, K.; Agasti, S. S.; Kim, C.; Li, X.; Rotello, V. M., Gold Nanoparticles in Chemical and Biological Sensing. *Chemical Reviews* **2012,** *112* (5), 2739-2779.
48.	Alexandridis, P., Gold Nanoparticle Synthesis, Morphology Control, and Stabilization Facilitated by Functional Polymers. *Chemical Engineering & Technology* **2011,** *34* (1), 15-28.
49.	Li, J.; Wang, L.; Benicewicz, B. C., Synthesis of Janus Nanoparticles via a Combination of the Reversible Click Reaction and "Grafting to" Strategies. *Langmuir* **2013,** *29* (37), 11547-11553.
50.	Mai, Y.; Eisenberg, A., Self-assembly of block copolymers. *Chemical Society Reviews* **2012,** *41* (18), 5969-5985.
51.	Blanazs, A.; Armes, S. P.; Ryan, A. J., Self-Assembled Block Copolymer Aggregates: From Micelles to Vesicles and their Biological Applications. *Macromolecular Rapid Communications* **2009,** *30* (4-5), 267-277.
52.	Ji, W.; Yan, J.; Chen, E.; Li, Z.; Liang, D., In Situ and Online Monitoring Polymerization-Induced Micellization. *Macromolecules* **2008,** *41* (13), 4914-4919.
53.	Warren, N. J.; Armes, S. P., Polymerization-Induced Self-Assembly of Block Copolymer Nano-objects via RAFT Aqueous Dispersion Polymerization. *Journal of the American Chemical Society* **2014,** *136* (29), 10174-10185.
54.	An, Z.; Shi, Q.; Tang, W.; Tsung, C.-K.; Hawker, C. J.; Stucky, G. D., Facile RAFT Precipitation Polymerization for the Microwave-Assisted Synthesis of Well-Defined, Double Hydrophilic Block Copolymers and Nanostructured Hydrogels. *Journal of the American Chemical Society* **2007,** *129* (46), 14493-14499.
55.	Grazon, C.; Rieger, J.; Sanson, N.; Charleux, B., Study of poly(N,N-diethylacrylamide) nanogel formation by aqueous dispersion polymerization of N,N-diethylacrylamide in the presence of poly(ethylene oxide)-b-poly(N,N-dimethylacrylamide) amphiphilic macromolecular RAFT agents. *Soft Matter* **2011,** *7* (7), 3482-3490.
56.	Liu, G.; Qiu, Q.; An, Z., Development of thermosensitive copolymers of poly(2-methoxyethyl acrylate-co-poly(ethylene glycol) methyl ether acrylate) and their nanogels synthesized by RAFT dispersion polymerization in water. *Polymer Chemistry* **2012,** *3* (2), 504-513.
57.	Blanazs, A.; Madsen, J.; Battaglia, G.; Ryan, A. J.; Armes, S. P., Mechanistic Insights for Block Copolymer Morphologies: How Do Worms Form Vesicles? *Journal of the American Chemical Society* **2011,** *133* (41), 16581-16587.

CHAPTER 2

SURFACE-INITIATED POLYMERIZATION-INDUCED SELF-ASSEMBLY

2.1 Abstract

The self-assembly behavior of amphiphilic polymer grafted nanoparticles are systematically studied in this chapter. A new self-assembly technique, namely surface-initiated polymerization-induced self-assembly (SI-PISA) was developed that enabled the one-pot synthesis of hybrid nano-objects with different shapes including 1D strings, 2D disks, 3D vesicles and solid spheres. This SI-PISA was established based on a bimodal polymer-grafted NPs structure. A solvent-miscible brush was first grafted onto 15 nm silica NPs, and self-assembly was subsequently induced by the polymerization of a second brush that was solvent-immiscible. Self-assembly occurred *in situ* with the SI-polymerization of the second brush. The shape of the nano-objects was found to be controlled by the chemical structure of grafted polymers, chain length of grafted polymers, and reaction media.

2.2 Introduction

Polymerization-induced self-assembly of block copolymers (PISA) has drawn considerable attention over the past ten years since the seminal reports by Pan *et al*. [1-2] Compared with the traditional method of preparing block copolymer assemblies, PISA has the advantages of a one-step reaction and relatively high solids content (20-50% w/w).[3-4] Typically, a soluble homopolymer is synthesized and chain-extended with a second monomer that when polymerized, becomes insoluble and drives *in situ* self-assembly to form stable nano-objects. A wide range of nanostructures have been observed, including spherical micelles, worms, octopi structures, jellyfish structures and vesicles.[5] A variety of controlled radical polymerization methods (NMP[6], ATRP[7], RAFT[8-10]) have been used for PISA with RAFT being the most widely studied. Despite great versatility of PISA in terms of polymerization techniques, reaction solvent and monomer selection, as far as we know,

very few attempts have been made to prepare hybrid assemblies that are composed of polymers and inorganic nanoparticles.[11] Recently, Tan *et al*. and Armes *et al*. successfully encapsulated silica nanoparticles within vesicles during PISA synthesis.[12-13] However, there was no control over the assembly of the encapsulated nanoparticles. Currently, polymer-directed self-assembly of inorganic nanoparticles remains a challenging task. Typically, it has been achieved via a solvent switching method that is relatively tedious and limited by low nanoparticle concentration.[14-16] These observations suggest an intriguing question: can we utilize PISA to direct the self-assembly of inorganic nanoparticles *in situ* during the polymerization process and form well-defined nano-objects? To address this question, we designed a system based on bimodal polymer grafted nanoparticles. The procedure to synthesize such mixed brushes has been established using a sequential surface-initiated RAFT (SI-RAFT) polymerization strategy.[17] After the first SI-RAFT polymerization, active chain-end groups were removed by reacting with an excess of AIBN. Then, a second population of RAFT agent was grafted onto the particles surface and a second monomer was polymerized. The polymerizations were well-controlled, showing the common characteristics of living polymerization.

In this work, the first case of surface-initiated polymerization-induced self-assembly by polymerizing benzyl methacrylate(BzMA) from SiO_2-g-(PHEMA, CPDB) nanoparticles which served as both chain transfer agent and stabilizer is demonstrated. Hybrid nano-objects with string-shaped morphologies were obtained in one step. [18] However, we did not observe higher ordered assemblies before macroscopic phase separation occurred, probably due to the poor stabilizing effect of PHEMA in methanol. [19]

An improved(SI-PISA) was designed then employed that leads to stable 3D assemblies at high NP concentration (~10mg/ml). Self-assembly occurred spontaneously during polymerization, which is analogous to PISA of block copolymers. 3D nanovesicles were obtained in one pot. Nanovesicles are of particular interest because of their hollow structures that enable applications in drug delivery,[20] catalysis,[21] bioimaging,[22] and cancer therapy.[23-24] In recent literature, such vesicles were prepared by coating inorganic NPs with amphiphilic ligands[25] or polymers.[14-15] As for polymer-directed self-assembly, both mixed brush grafted NPs[15, 20] and block copolymer tethered NPs[14, 21, 23] have been prepared that successfully assembled into thin-layer vesicles. Typically, the polymer-grafted NPs were first prepared in a good solvent for each component followed by purification steps to remove free polymers. Then, self-assembly was triggered by addition of a selective solvent[23, 25] or film rehydration[14-15], which required multiple steps of sample preparation and was limited by low NP concentration. For example, NP concentration was kept below 260 µg/ml for the film rehydration method[3, 8]; Nie *et al*. studied the concentration effect on self-assembly of PEG-b-PCL tethered gold NPs by solvent switching and found that nanoscale vesicle formation was limited to particle concentrations less than 250 µg/ml, otherwise huge submicron-sized assemblies were formed.[26] Thus, gram-scale production of such hybrid vesicular assemblies still remains a challenging task.

This approach establishes a method to prepare nanovesicles at relatively high NP concentration, and does not require any post-polymerization processing. Moreover, this strategy provided an opportunity to observe the evolution of nanovesicle formation from well-dispersed NPs, that aided our understanding of how surface-grafted polymers direct the vesicular assembly of NPs.

2.3 Experimental Section

Materials: 2-Hydroxyethyl methacrylate (Acros, 99%) and benzyl methacrylate (Acros, 96%) were passed through basic aluminum column to remove inhibitors before use. 2.2'-Azobisisobutyronitrile (AIBN) was purified by recrystallization from methanol and dissolved in methanol to make a 10mM solution. All other reagents were used as received.

Synthesis of PHEMA grafted silica nanoparticles. 4-Cyanopentanoic acid dithiobenzoate (CPDB) anchored 15nm silica nanoparticles were prepared according to the literature. Graft density was determined by measuring the UV-vis peak at 304 nm, and calculated from CPDB calibration curve. A solution of 2-hydroxyethyl methacrylate (2.27 g), AIBN (263µl of 10mM solution in methanol), CPDB-anchored silica nanoparticles (0.76g, 23µmol/g) and DMF (5ml) was prepared in a Schlenk tube. The mixture was degassed by three freeze-pump-thaw cycles, backfilled with nitrogen, and then placed in an oil bath at 65°C for 5 hours. The polymerization solution was quenched in an ice bath and poured into diethyl ether to precipitate the SiO_2-g-PHEMA nanoparticles. The SiO_2-g-PHEMA nanoparticles were redispersed in DMF and precipitated in diethyl ether two more times to remove excess monomers and initiators.

Chain End Deactivation of SiO_2-g-PHEMA. Solid AIBN [58mg (20 eq)] was added to a solution of SiO_2-g-PHEMA in DMF and heated at 65°C for 1 hour. The resulting solution was poured into a large amount of diethyl ether and centrifuged at 5000rpm for 5

min. The recovered SiO$_2$-g-PHEMA completely lost its original pink color and appeared to be white in color.

Second RAFT Agent attachment to SiO$_2$-g-PHEMA. SiO$_2$-g-PHEMA nanoparticles from the previous step were dispersed in ~15ml DMF, to which 17μl of 3-aminopropyl(dimethyl)ethoxysilane (APTES) was added to react with the remaining surface hydroxyl groups under N$_2$ for 1.5 hours. Excess AIBN was washed out by ether precipitation and activated CPDB (50 mg) was added to anchor a second population of RAFT agent to give SiO$_2$-g-(PHEMA, CPDB) nanoparticles. Graft density was determined by measuring the UV-vis peak at 304 nm, and calculated from the CPDB calibration curve. TGA results were used to adjust the calculation (55% weight percent silica in PHEMA grafted NPs)[17]. (It is worth noting that the added APTES will not react with hydroxyl groups on the PHEMA chains. In a control experiment, free PHEMA was synthesized, followed by RAFT agent cleavage, reaction with APTES and then activated CPDB using the same procedure. As a result, no RAFT agent was attached as detected by UV-vis absorption.)

Surface-initiated RAFT polymerization of BzMA using SiO$_2$-g-(PHEMA, CPDB) as a macro chain transfer agent and stabilizer. SiO$_2$-g-(PHEMA, CPDB) nanoparticles (0.22g, 45wt% silica), BzMA (0.76 g), AIBN (56μl of 10mM solution in methanol) and methanol (8ml) were mixed together and added to a Schlenk flask with rubber stopper. The mixture was degassed by three freeze-pump-thaw cycles, backfilled with nitrogen and then placed in an oil bath of 80°C. In a sealed tube environment, the tube

is under slight pressure and the internal measured temperature was consistent with the bath temperature. Aliquots of the reaction solution were withdrawn from the flask at 1h, 1.5h, 2h, 2.5h, 3.5h, 4.5h respectively.

Synthesis of PHPMA grafted silica nanoparticles. 4-Cyanopentanoic acid dithiobenzoate (CPDB) anchored 15nm silica nanoparticles were prepared according to literature. A solution of 2-hydroxypropyl methacrylate (3.8 g), AIBN (266µl of 10mM solution in methanol), CPDB-anchored silica nanoparticles (1g, 23µmol/g) and DMF (8ml) was prepared in a Schlenk tube. The mixture was degassed by three freeze-pump-thaw cycles, backfilled with nitrogen, and then placed in an oil bath at 65°C for 3 hours. The polymerization solution was quenched in an ice bath and poured into 1:1 mixture of diethyl ether and petroleum ether to precipitate the SiO_2-g-PHPMA nanoparticles. The SiO_2-g-PHPMA nanoparticles were redispersed in DMF and precipitated two more times to remove excess monomers and initiators.

Chain End Deactivation of SiO_2-g-PHPMA. 80mg (20 eq) solid AIBN was added to a solution of SiO_2-g-PHPMA in DMF and heated at 65°C for 1 hour. The resulting solution was poured into large amount of 1:1 mixture of diethyl ether and petroleum ether and centrifuged at 5000rpm for 5 min. The recovered SiO_2-g-PHPMA completely lost its original pink color and appeared to be white in color.

Second RAFT Agent attachment to SiO_2-g-PHPMA. SiO_2-g-PHPMA nanoparticles from the previous step were dispersed in ~15ml DMF, to which 20 µl of 3-

aminopropyl(dimethyl)ethoxysilane was added to react with the remaining surface hydroxyl groups under N_2 for 1.5 hours. Excess AIBN was washed out by ether precipitation and activated CPDB (50 mg) was added to anchor a second population of RAFT agent to give SiO$_2$-g-(PHPMA, CPDB) nanoparticles, which regained the characteristic pink color of the RAFT agent. Graft density was determined by measuring the UV-vis peak at 304 nm, and calculated from CPDB calibration curve. The TGA result was used to adjust calculation (60% weight percent silica in PHPMA grafted NPs). (It is worth noting that the added APTES will not react with hydroxyl groups on PHPMA chains. In a control experiment, free PHPMA was synthesized, followed by RAFT agent cleavage, reaction with APTES and then activated CPDB using the same procedure. As a result, no RAFT agent was attached as detected by UV-vis absorption.)

Surface-initiated RAFT polymerization of BzMA using SiO$_2$-g-(PHPMA, CPDB) as macro chain transfer agent and stabilizer. SiO$_2$-g-(PHPMA, CPDB) nanoparticles (0.143g, 70wt% silica), BzMA (0.42 g), ACVA (36μl of 10mM solution in ethanol) and ethanol (8ml) were mixed together and added to a Schlenk flask with rubber stopper. The mixture was degassed by three freeze-pump-thaw cycles, backfilled with nitrogen and then placed in an oil bath of 70°C. Aliquots of the reaction solution were withdrawn from the flask periodically since the beginning of polymerization. Grafted polymer chains were cleaved from silica nanoparticles by reacting with an excess amount of HF. Toluene was then used to selectively dissolve PBzMA for GPC analysis.

Synthesis of PHPMA grafted silica nanoparticles. A solution of methacrylic acid (2.6 g), AIBN (300µl of 10mM solution in methanol), CPDB-anchored silica nanoparticles (1g, 23µmol/g) and DMF (6ml) was prepared in a Schlenk tube. The mixture was degassed by three freeze-pump-thaw cycles, backfilled with nitrogen, and then placed in an oil bath at 65°C for 2.5 hours. The polymerization solution was quenched in an ice bath and poured into diethyl ether to precipitate the SiO_2-g-PMAA nanoparticles. The SiO_2-g-PHPMA nanoparticles were redispersed in DMF and precipitated two more times to remove excess monomers and initiators.

Surface-initiated RAFT polymerization of BzMA using SiO_2-g-(PMAA, CPDB) as macro chain transfer agent and stabilizer. SiO_2-g-(PMAA, CPDB) nanoparticles (0.16g), BzMA (1.5 g), ACVA (86µl of 10mM solution in ethanol) and ethanol (20ml) were mixed together and added to a Schlenk flask equipped with a rubber stopper. The mixture was degassed by three freeze-pump-thaw cycles, backfilled with nitrogen and then placed in an oil bath of 70°C. Aliquots of the reaction solution were withdrawn from the flask periodically since the beginning of polymerization. Grafted polymer chains were cleaved from the silica nanoparticles by reacting with an excess amount of HF. Toluene was then used to selectively dissolve PBzMA for GPC analysis.

Characterization.

^{1}H NMR (Bruker ARX 300/ARX 400) was conducted using CD_3OD as the solvent. Molecular weights and dispersity were determined using a gel permeation chromatography (GPC) equipped with a 515 HPLC pump, a 2410 refractive index detector, and three

Styragel columns. The columns consisted of HR1, HR3 and HR4 in the effective molecular weight ranges of 100-5000, 500-30000, and 5000-500000, respectively. THF was used as eluent at 30°C and flow rate was adjusted to 1.0mL/min. Molecular weights were calibrated with poly(methyl methacrylate) standards obtained from Polymer Laboratories. Dynamic Light Scattering characterizations were conducted using Zetasizer Nano ZS90 from Malvern. Each sample was diluted with methanol to ~1mg/ml prior to DLS analysis. The transmission electron microscopy (TEM) was performed on a Hitachi H8000 TEM at an accelerating voltage of 200 KV. The samples were prepared by depositing a drop of the diluted nanoparticle solution in methanol on copper grids.

2.4 Results and Discussion

2.4.1 Self-assembly of SiO$_2$-g-(PHEMA, CPDB) nanoparticles into 1D strings.

Scheme 2.1 shows the synthetic route toward SiO$_2$-g-(PHEMA, CPDB) from bare 15nm silica nanoparticles. Poly(2-hydroxyethyl methacrylate) (PHEMA) was selected as the first polymer brush since it is miscible with methanol, and has been previously reported as a stabilizing block for PISA.[19] The graft density of PHEMA was 0.1 ch/nm^2, as calculated from the characteristic RAFT UV-vis peak at 304nm. The medium graft density secured enough polymer content to solubilize the silica nanoparticles, and yet left enough surface space for the growth of the second polymer population. Surface-initiated polymerization of HEMA was carried out in DMF at 65 °C, with molar ratio between species [RAFT]:[HEMA]:[AIBN]= 1:1000:0.15. After 5 hours, 19% conversion was achieved, corresponding to 190 repeat units and 24.7 KDa molecular weight (assuming 100% CTA efficiency). RAFT end groups were subsequently removed by reacting with 20eq AIBN.[17, 27] The resulting PHEMA grafted nanoparticles were then treated with

aminopropyldimethylethoxysilane and activated CPDB to immobilize a second RAFT agent. The second graft density was determined to be 0.15 ch/nm^2 based on UV analysis and TGA result (Figure 2.1).
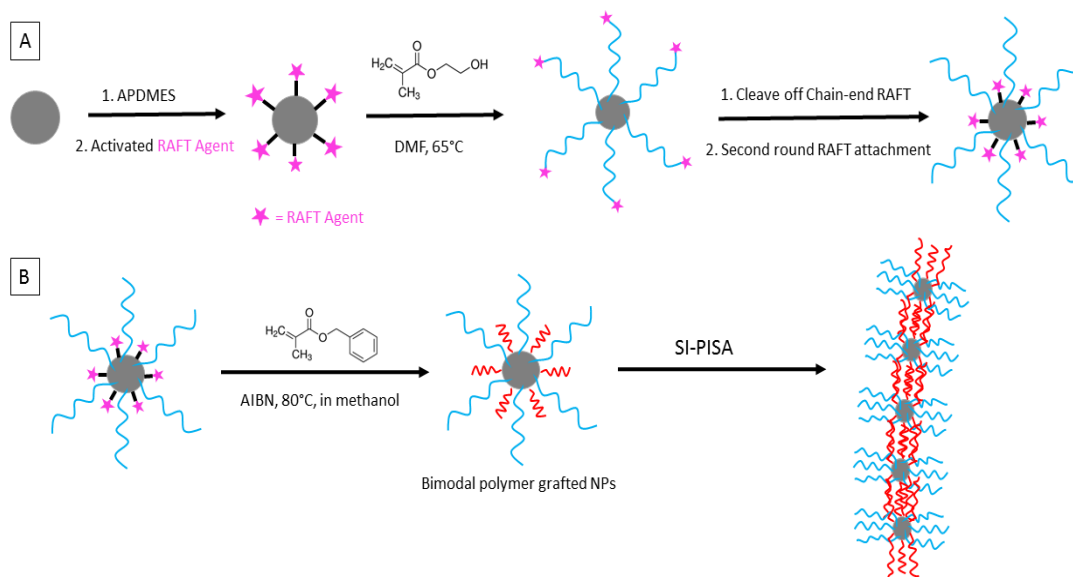
Scheme 2.1. (A) Synthesis of SiO$_2$-g-(PHEMA, CPDB) nanoparticles. (B) Surface-initiated RAFT dispersion polymerization of BzMA from SiO$_2$-g-(PHEMA, CPDB) nanoparticles in methanol.
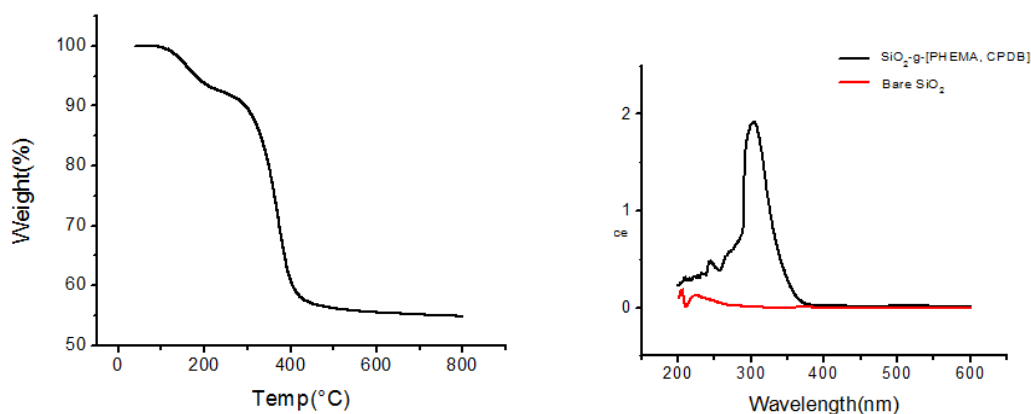
Figure 2.1. TGA and UV-vis analysis of SiO$_2$-g-[PHEMA, CPDB].

The SiO$_2$-g-(PHEMA, CPDB) nanoparticles prepared in the previous steps were used to perform surface-initiated dispersion RAFT polymerization of BzMA in methanol (Scheme 2.1B). The SiO$_2$-g-(PHEMA, CPDB) nanoparticles were well-dispersed in methanol to form a homogenous solution, to which BzMA, AIBN, and trioxane were added. The molar ratio between RAFT: BzMA: AIBN was set at 1:1200:0.15, with solid content 12% (w/w%). BzMA was selected since it has been widely used as core forming material in alcoholic PISA systems and showed fast polymerization rate and high conversion.[28-29] The experimental design allows the surface PHEMA chains to solubilize each individual silica nanoparticle in methanol at the beginning of the polymerization. As the polymerization was initiated, PBzMA chains grew from the silica surface, forming (PHEMA, PBzMA) bimodal polymer-grafted nanoparticles. These bimodal nanoparticles were individually stable at the early stages when PBzMA chains were relatively short. However, with the continuous increase of insoluble PBzMA chain lengths, each particle became more and more solvophobic and beyond a certain point, self-assembly occurred to minimize the contact between PBzMA chains and the solvent.

Visual observation during polymerization indicated formation of assemblies (Figure 2.2A). The polymerization solution was pink and transparent at 0h, and gradually faded in color to become almost colorless, but still transparent at 1h. Significant visual turbidity change began at 1.5 h, when a slightly turbid solution was formed. The turbidity increased with time and eventually formed a milky-white solution at 4.5h. All the turbid solutions formed in the first 4.5 hours were homogenous and stable, with no macroscopic precipitation. However, samples after 5 hours were less stable with white precipitates forming on the walls of the reaction flask.

31
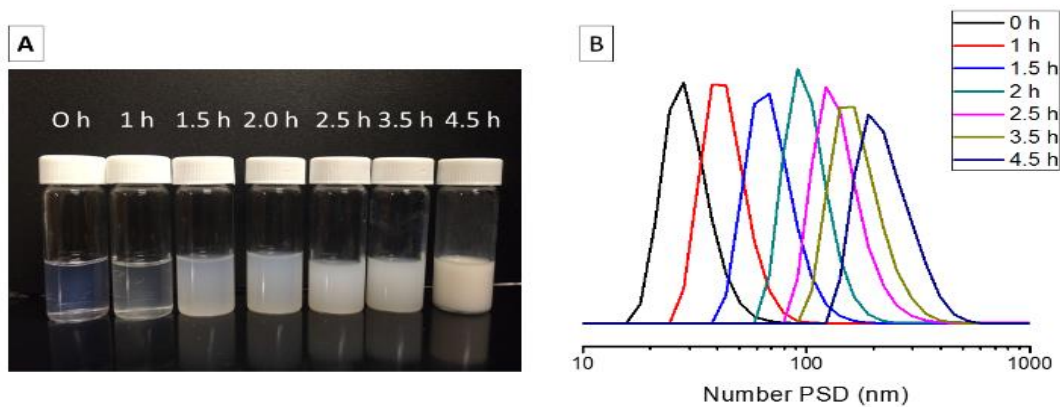
Figure 2.2. (A) Optical digital photo of the surface-initiated RAFT polymerization at different times (B) DLS of polymerization solution at different times.
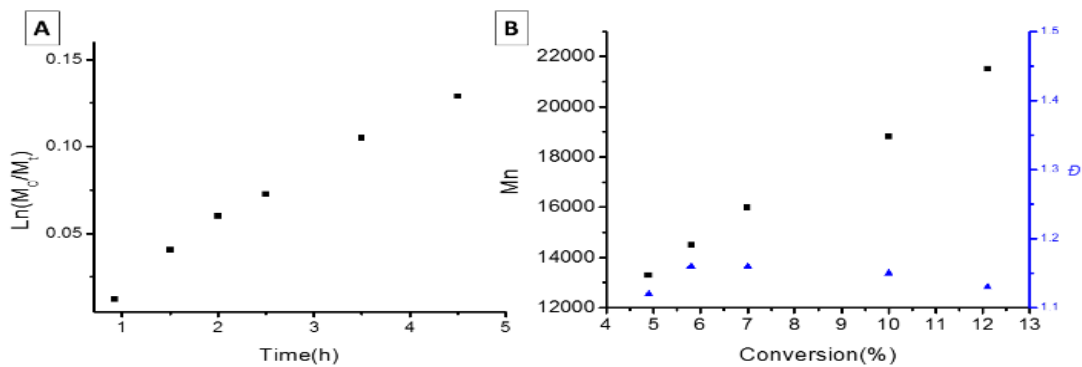
Figure 2.3. (A) Ln(M_0/M_t) vs time plot for surface-initiated BzMA polymerization in methanol. (B) Mn and Đ vs monomer conversion plots for surface-initiated BzMA polymerization in methanol.

Table 2.1. Summary of reaction time, monomer conversions, GPC data, DLS data, and visual appearance obtained for a series of SiO$_2$-g-(PHEMA, PBzMA) nanoparticles.

Entry No.	Reaction Time (h)	Conversion (%)[a]	Bimodal polymer composition[b]	Mn of PBzMA (g/mol)[c]	Mw/Mn[d]	Number Average Size (nm)[e]	Visual appearance
153-0	0	-	PHEMA$_{190}$			28	Pink transparent solution
153-1	1	1.2	PHEMA$_{190}$ PBzMA$_{12}$	N/A	N/A	55	Very light pink transparent solution
153-2	1.5	4.9	PHEMA$_{190}$ PBzMA$_{49}$	13000	1.12	71	Slightly turbid solution
153-3	2	5.8	PHEMA$_{190}$ PBzMA$_{58}$	14500	1.16	100	Slightly turbid solution
153-4	2.5	7.0	PHEMA$_{190}$ PBzMA$_{70}$	16000	1.16	142	Turbid solution
153-5	3.5	10.0	PHEMA$_{190}$ PBzMA$_{100}$	18800	1.15	169	Turbid solution
153-6	4.5	12.1	PHEMA$_{190}$ PBzMA$_{121}$	21500	1.13	225	Milky-white solution

[a] Determined by ^{1}H NMR spectroscopy. [b] Determined by ^{1}H NMR spectroscopy, assuming 100% RAFT agent efficiency. [c] Determined by size exclusion chromatography using PMMA as standard. [d] Determined by size exclusion chromatography. [e] Determined by dynamic light scattering. Number average size reported for all samples.

The initial pink color loss was quite interesting and worth noting, as it has not been observed in normal surface-initiated polymerization of methacrylates. We reason that the disappearance of pink color occurred at the onset of self-assembly, when the insoluble PBzMA chains collapsed and became wrapped into the core part of the assemblies. The surface-initiated RAFT polymerization was followed by ^{1}H NMR and gel permeation

chromatography (GPC). Monomer conversion was calculated based on the ratio between the monomer vinyl peak at 5.6 ppm and the internal standard peak at 5.1 ppm (trioxane). GPC analysis was conducted by reacting polymer grafted nanoparticles with HF to cleave the chains from the silica surfaces, and then THF was used to selectively dissolve PBzMA. Details of reaction time, monomer conversions, GPC data, DLS data, and visual appearance are summarized in Table 2.1. Polymerization kinetics showed a linear relationship between $\ln([M]_0/[M]_t)$ and time (Figure 2.3A). The onset of turbidity at *ca.* 1.5h corresponded to 49 repeat units of PBzMA, which is the critical degree of polymerization for phase separation in this case. The molecular weight of PBzMA increased linearly with conversion, with dispersity remaining below 1.2 (Figure 2.3B). GPC traces showed a gradual shift toward higher molecular weights as the polymerization proceeded (Figure 2.4). All the results suggested that the surface-initiated RAFT dispersion polymerization of PBzMA was well controlled with PHEMA grafted nanoparticles as stabilizer.

DLS studies indicated an increase in the hydrodynamic size of nanoparticles with reaction time, which is consistent with the turbidity change observed during polymerization. Number average sizes were reported to offer comparison with the size of aggregates observed with TEM.[11] The solution before reaction (0 h) had a number-average diameter of 28 nm, which corresponds to individually dispersed PHEMA grafted nanoparticles. At 1.5h, when the initial turbidity change could be visually observed, the average particle size increased to 71 nm, indicating a slight degree of agglomeration between nanoparticles. The mean particle diameter grew progressively with
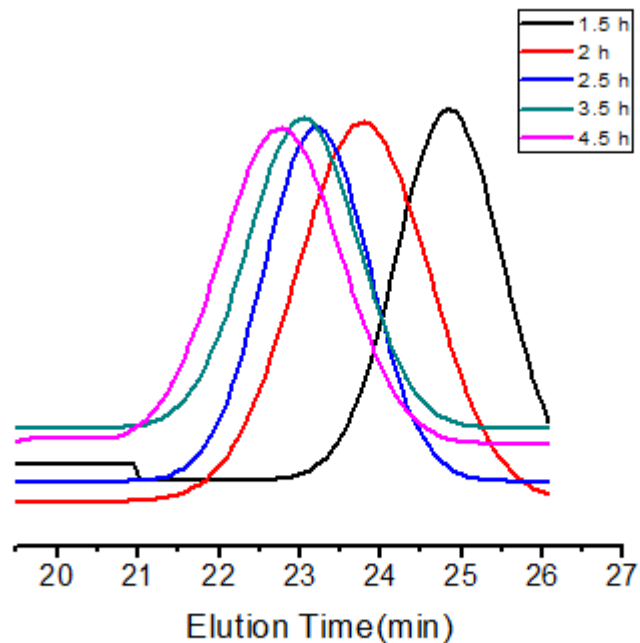
Figure 2.4. GPC traces of BzMA chains cleaved from silica nanoparticle surfaces.

polymerization time, and reached 225nm at 4.5hour, when a milky-white solution was formed.

In order to investigate the morphology of nanoparticle assemblies, TEM was used to follow the polymerization and representative images are shown in Figure 2.5. Figure 2.5A showed that particles were individually dispersed in methanol before reaction. At 1.5h, particles began to connect with each other and formed mostly one-dimensional short strings composed of several nanoparticles (Figure 2.5B). As the polymerization continued, the strings became longer and formed branched structures (Figure 2.5C). At 4.5h, highly branched string structures were formed, accompanied with higher degree of aggregation at
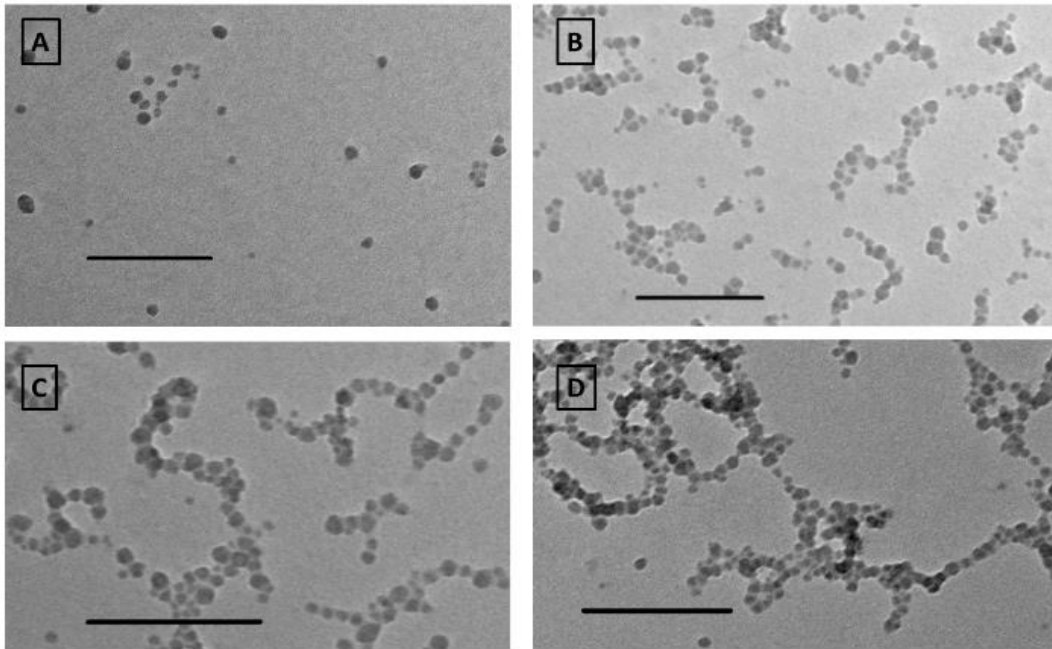
Figure 2.5. TEM images of the morphologies formed at 0 h (A), 1.5 h (B), 2 h(C), and 4.5 h (D). All scale bars: 200nm.
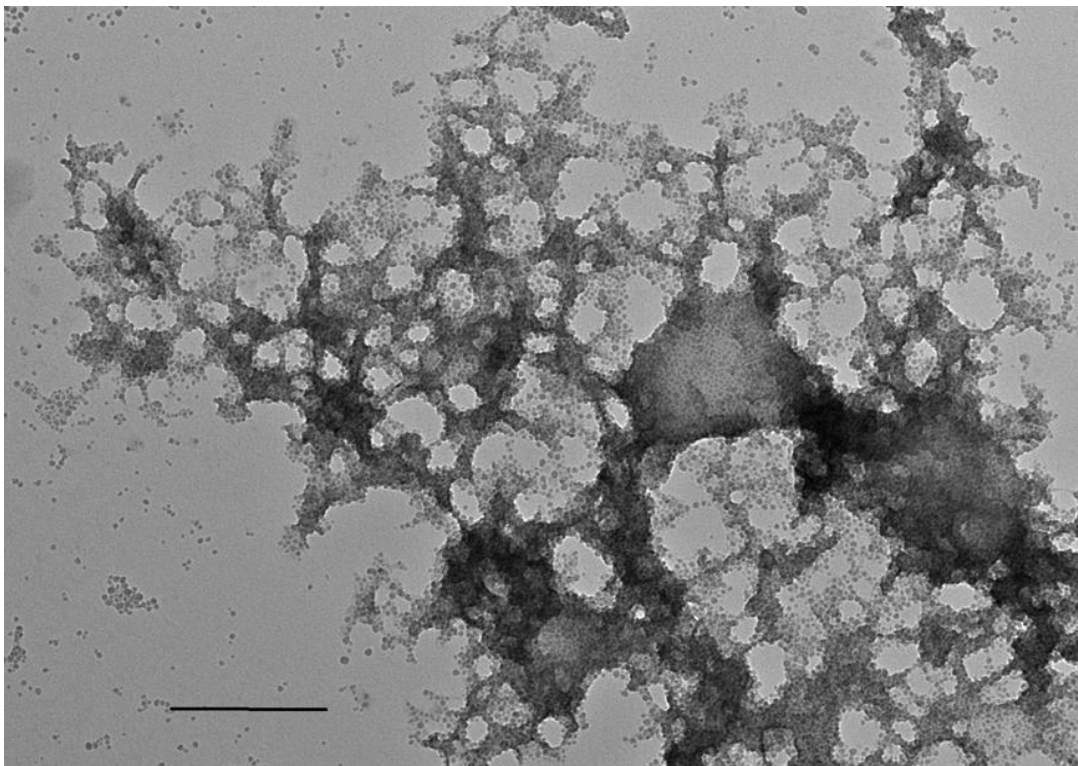
Figure 2.6. TEM of polymerization sample after 5h. Scale bar 500nm.

junction points. Samples after 5h formed cross-linked nanoparticle networks (Figure 2.6) that eventually precipitated from solution.

The basis for the self-assembly process is explained in Scheme 2.2. When the PBzMA chains became sufficiently long, the mixed polymer brushes will first phase separate (due to polymer-

polymer immiscibility) by chain-stretching and rearranging to form surface PHEMA domains and surface PBzMA domains. Then, the PBzMA domains between nanoparticles will aggregate (due to polymer-solvent immiscibility) with each other to form nanoparticle pairs. The closely associated nanoparticle pairs lead to a higher PHEMA polymer density around the centre than the poles of nanoparticle pairs. As a result, the following nanoparticles could only approach from the ends, forming nanoparticle strings. This self-assembly mechanism is supported by TEM images at high magnification (Figure 2.7). It is clear that the nanoparticles were not in direct contact with each other. Instead,
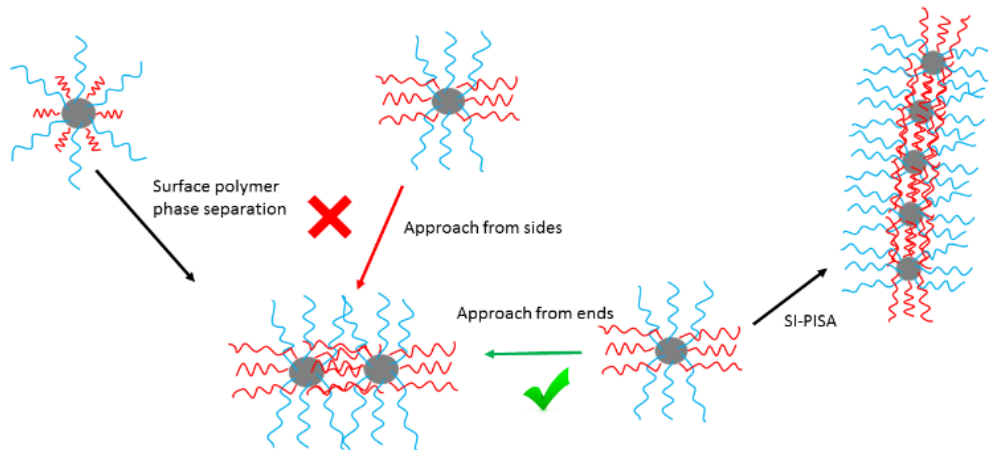
Scheme 2.2. Proposed mechanism of SI-PISA of silica nanoparticles into strings.

37
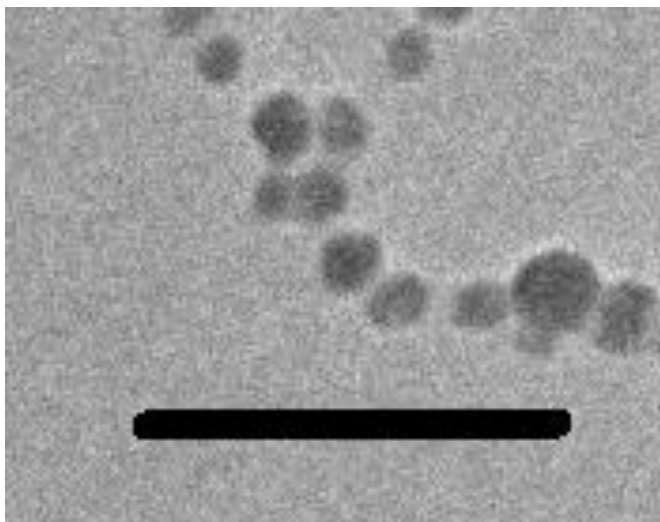
Figure 2.7. High magnificatio TEM nanoparticle strings. Scale bar 100nm.

there was a 5-8 nm gap between each nanoparticle pair, which represents the collapsed PBzMA domain.

It is worth noting that the self-assembly mechanism of these bimodal polymer grafted nanoparticles is different from most of the polymer-directed 1D colloidal assemblies reported previously, where sparsely grafted homopolymers[30] or block copolymers[31-32] were used to direct the anisotropic assembly. The anisotropy, in this case, originated from the phase separation of immiscible polymer brushes and guided the in situ formation of 1D assemblies without the need of any post-polymerization process.

2.4.2 Self-assembly of SiO_2-g-(PHPMA, CPDB) nanoparticles into 3D vesicles.

To further explore SI-PISA for higher-order self-assemblies, an improved design of surface-initiated polymerization-induced self-assembly (SI-PISA) that leads to stable 3D assemblies at high NP concentration (~10mg/ml) was designed by replacing PHEMA brushes with PHPMA brushes and using ethanol as solvent instead of methanol. Self-

assembly occurred spontaneously during polymerization, which is analogous to PISA of block copolymers. However, in contrast to block copolymer PISA, the polymer chains were anchored onto inorganic NP surfaces, forming mixed brush grafted NPs which directed the self-assembly of NPs into hybrid assemblies. In the current approach homopolymer brushes were first grafted onto inorganic NPs that were compatible with the target solvent (ethanol) to disperse NPs, and then a second population of brushes was polymerized that were immiscible in the solvent. As the growth of the second brush population proceeded, the increased "solvophobicity" of the immiscible chains induced interparticle collapse, and directed the self-assembly of inorganic cores. Hybrid vesicles with sizes on the nanometer scale were produced *in situ* with polymerization, without the need for any post-polymerization steps. Moreover, by taking samples periodically after the polymerization started, we observed the entire evolution process from well-dispersed NPs to short nanostrings, to nanorings, to nanovesicles and eventually, micron-sized aggregates, that provided interesting mechanistic insights about the birth and death of NP vesicles.

The mixed brush grafted NPs were synthesized using a sequential surface-initiated RAFT polymerization strategy that provided precise control over the composition of both brushes. In the first step, SiO_2-g-(PHPMA, CPDB) NPs were prepared as shown in Scheme 2.3A. Poly(hydroxypropyl methacrylate) (PHPMA), which has been used to successfully stabilize 3D assemblies of block copolymer PISA was grafted onto 15 nm silica NPs using surface-initiated RAFT polymerization in DMF at 65 °C. PHPMA with a molecular weight of 16 kDa and 0.1 ch/nm^2 graft density was achieved, which was confirmed by NMR and TGA characterization. Chain-end RAFT groups were removed by reacting with excess AIBN, to deactivate the first polymer brush.[17, 33]

Then, a second RAFT agent was attached onto the unreacted surface with 0.1 ch/nm^2 graft density, which was calculated from the characteristic UV absorption at 304 nm and TGA data. The resulting NPs, SiO$_2$-g-(PHPMA, CPDB) appeared as viscous pink solids after solvent removal, and could be easily re-dispersed in ethanol and used as precursors to vesicular assemblies.
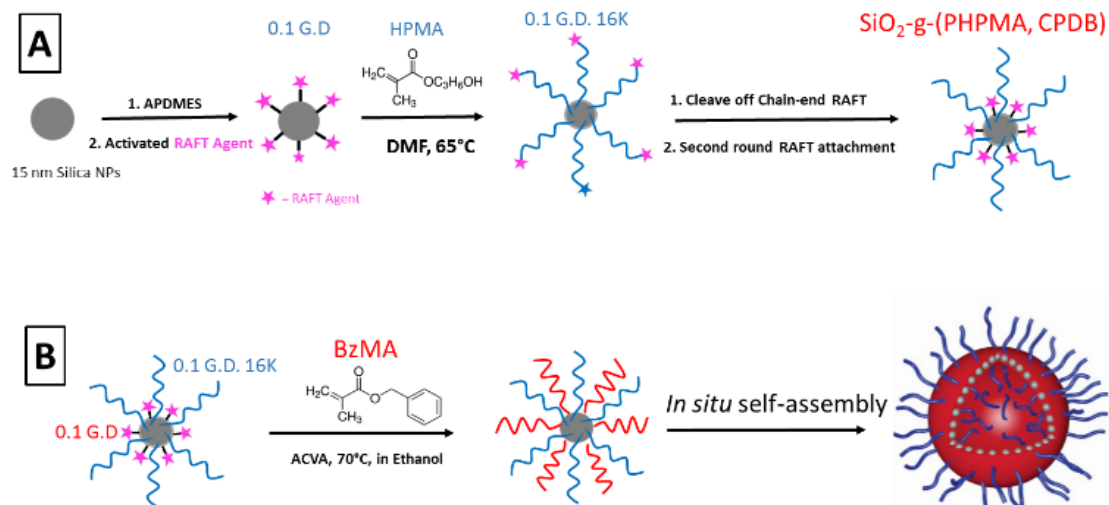
Scheme 2.3. (A) Synthesis of SiO$_2$-g-(PHPMA, CPDB). (B) One-pot surface-initiated RAFT polymerization-induced self-assembly of grafted NPs into vesicles.

Surface-initiated polymerization of a second monomer benzyl methacrylate (BzMA) from SiO$_2$-g-(PHPMA, CPDB) was conducted at 70 °C with the molar ratio of RAFT: BzMA: ACVA: = 1:1000:0.15. Ethanol was added as solvent to achieve ~10mg/ml
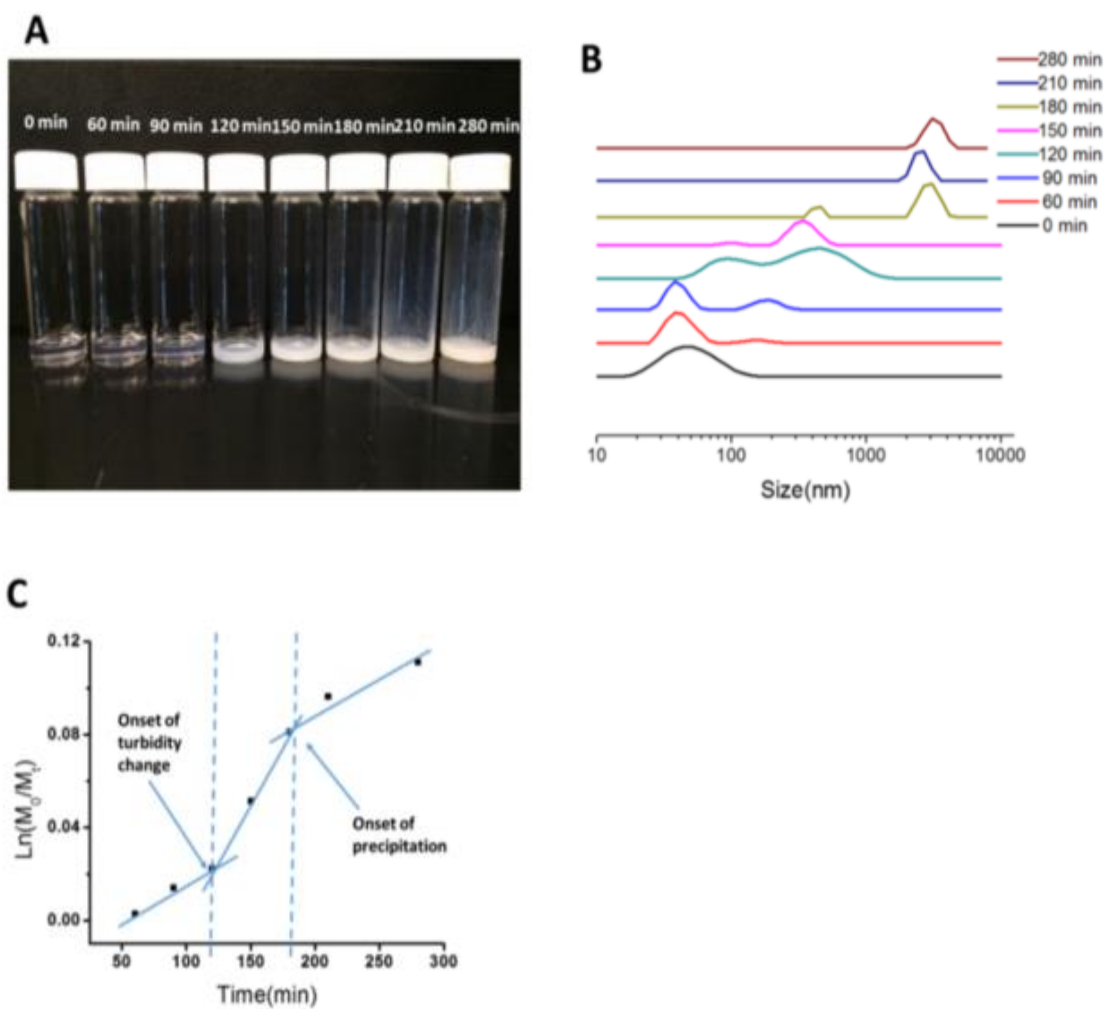
Figure 2.8. (A) Visual appearance of each sample withdrawn during polymerization. (B) DLS of each sample withdrawn during polymerization. (C) Polymerization kinetics of surface-initiated RAFT polymerization of BzMA from SiO$_2$-g-(PHPMA, CPDB) in ethanol at 70°C.

NP concentration. Both reaction solvent and monomer were carefully selected as ethanol is a good solvent for PHPMA grafted NPs and BzMA monomer, but a poor solvent for PBzMA. As the polymerization proceeded, the growing PBzMA chains promoted self-assembly by interparticle collapse, while PHPMA chains served as stabilizers to prevent uncontrolled agglomeration. (Scheme 2.3B)

The formation of assemblies during polymerization could be observed from the turbidity changes of the reaction solution. A small sample was withdrawn from the reaction flask periodically throughout polymerization and the visual appearance of each sample is shown in Figure 2.8A. The polymerization system started as a clear, light-pink, homogenous solution, which remained unchanged during the first 1.5 hours. The onset of turbidity changes occurred at 120min, when a slightly turbid solution was observed. At this time, the solution was still homogenous with no macroscopic precipitate. The turbidity increased with time and macroscopic precipitates were observed after 180 min. White precipitates formed and adhered onto the wall of glass vials (Figure 2.8, right 3 vials in C), indicating formation of unstable assemblies.

To better understand the self-assembly mechanism, each sample displayed in Figure 2.8A was analysed by dynamic light scattering (DLS) to obtain NP size distributions (Figure 2.8B). The trend in nanoparticle diameter measured by DLS agreed with visual observations, and clearly indicated the formation of assemblies. At 0 min, only one peak at 45 nm was observed, which corresponded to individually dispersed SiO_2-g-(PHPMA, CPDB) NPs. A second peak centred at *ca.* 200nm appeared soon after the reaction started, indicating initial formation of aggregates. As the polymerization proceeded, the individual NP peak gradually disappeared, while the aggregates peak increased as well as shifted towards larger size. As the polymerization proceeded even further, a new peak at micron-scale size appeared, and quickly became the dominant size in the distribution. These data indicated that there were two stages of self-assembly where well-dispersed nanoparticles first self-assembled into nanoscale assemblies, which then further evolved into microscale assemblies.
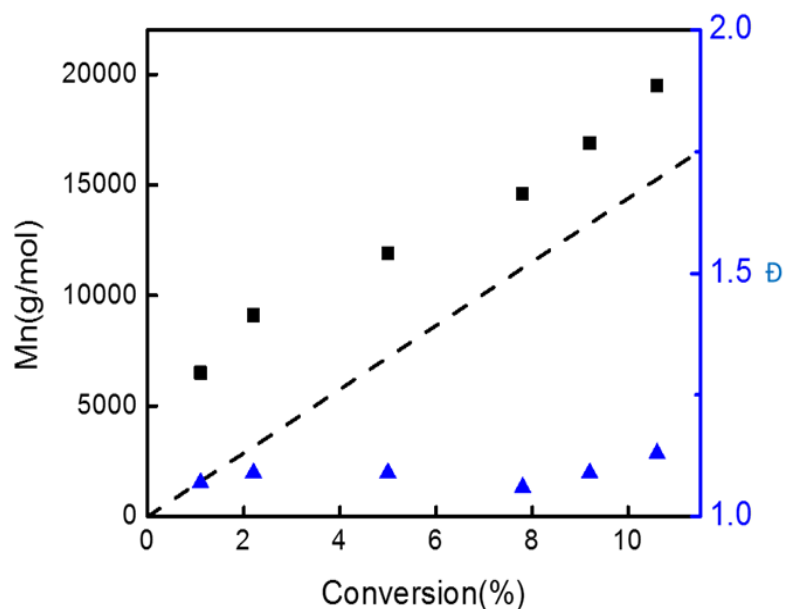
Figure 2.9. Molecular weight versus conversion and polydispersity for surface-initiated polymerization of BzMA from SiO_2-g-(PHPMA, CPDB) NPs at 70°C in ethanol
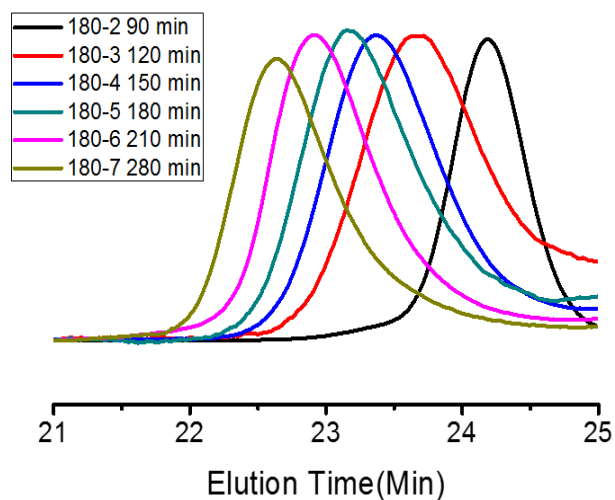
Figure 2.10. THF gel permeation chromatograms (vs poly (methyl methacrylate) standards) obtained from PBzMA chains cleaved-off from SiO_2-g-(PHPMA, PBzMA) NPs.

The polymerization of BzMA was also monitored by ^{1}H NMR to obtain monomer conversion. Interestingly, the polymerization kinetics curve, $Ln(M_0/M_t)$ vs time, displayed three different stages (Figure 2.8C), even though the reaction temperature remained constant at 70°C. Additionally, the three stages were separated by specific points correlated with the onset of initial cloudiness and the onset precipitate formation, which provides some interesting mechanistic insights. The kinetics of the first stage at 0 to 120 min corresponded to normal solution based surface-initiated controlled radical polymerization, when short PBzMA chains grew from well-dispersed NPs. The rate of polymerization increased in the second stage from 120 to 180 min, which corresponded to the onset of aggregation as observed both visually and by DLS. At this stage, PBzMA chains reached a critical length and nascent assemblies formed with insoluble PBzMA chains collapsing with each other, and the unreacted BzMA monomers preferentially remaining within the PBzMA regime, thus increasing the local monomer concentration. Similar behaviour has been reported in block copolymer PISA in both alcoholic medium and aqueous solution. [5] The third stage, from 180 to 280 min, was marked by the onset of precipitation. At this stage, micron-sized assemblies. were formed that tended to precipitate from the reaction medium. As a result, chain-transfer agents and monomers were no longer in the same phase, chain end mobility was restricted, and the reaction kinetics decreased. Overall the Mn of the BzMA chains showed a linear increase with conversion during the entire polymerization period and polydispersity of PBzMA remained below 1.1 (Figure 2.9). The corresponding GPC traces of PBzMA chains shifted to higher molecular weights during the polymerization, with unimodal distributions, (Figure 2.10) indicating that the polymerization of BzMA proceeded with good control, and resulted in a well-defined

mixed brush polymer structure. The details of the reaction time, monomer conversions, GPC data, DLS data, and visual appearance obtained for a series of SiO2-g-(PHPMA, PBzMA) NPs are summarized in Table 2.2.

Table 2.2 Summary of reaction time, monomer conversions, GPC data, DLS data, and visual appearance obtained for a series of SiO$_2$-g-(PHPMA, PBzMA) nanoparticles.

Entry No.	Reaction Time (min)	BzMA Conversion (%)[a]	Bimodal polymer composition[b]	Mn of PBzMA (g/mol)[c]	Mw/Mn [d]	Hydrodynamic radius (nm)[e]	Visual appearance
180-0	0	0	PHPMA$_{111}$	N/A	N/A	45.12	Clear
180-1	60	0.3	PHPMA$_{111}$ PBzMA$_3$	N/A	N/A	51.46	Clear
180-2	90	1.1	PHPMA$_{111}$ PBzMA$_{11}$	6500	1.07	54.15	Clear
180-3	120	2.2	PHPMA$_{111}$ PBzMA$_{22}$	9100	1.09	171.3	Slight Cloudy
180-4	150	5.0	PHPMA$_{111}$ PBzMA$_{50}$	11900	1.09	343.6	Cloudy
180-5	180	7.8	PHPMA$_{111}$ PBzMA$_{78}$	14600	1.06	1740	Cloudy
180-6	210	9.2	PHPMA$_{111}$ PBzMA$_{92}$	16900	1.09	2952	Milky/Phase Separate
180-7	280	10.6	PHPMA$_{111}$ PBzMA$_{106}$	19500	1.13	2960	Milky/Phase separate

[a] Determined by ^{1}H NMR spectroscopy. [b] Determined by ^{1}H NMR spectroscopy. Assuming 100% RAFT agent efficiency. [c] Determined by size exclusion chromatography using PMMA as standard. [d] Determined by size exclusion chromatography. [e] Determined by dynamic light scattering. Z-average size reported for all samples.

The morphologies of the self-assembled structures during polymerization were investigated by transmission electron microscopy (TEM) and revealed the early formation and growth of nano-sized assemblies into thin-layer vesicles. Initially, PHPMA grafted NPs were well-dispersed in ethanol (0 min, Figure 2.11A). When the polymerization was initiated, NPs first organized into short strings of a small number of NPs (60 min Figure 2.11B). With continued growth of the PBzMA, the connectivity of the short strings increased and formed ring-like structures which then served as templates for fully enclosed vesicles. (Figure 2.11C, D, 90 min). Samples at 120 min contained highly mixed morphologies of nascent vesicles, half-vesicles, disks and dispersed NPs (Figure 2.11E, F), which was consistent with DLS data that showed a fairly large polydispersity of sizes. The filling and wrapping of the nanorings into vesicles progressed with time and was mostly complete at 150 min (Figure 2.11G), when most of the observed structures were complete vesicles. DLS data also showed that most components in solution at this time were self-assembled structures with ~340nm diameter. The duration of the pure vesicle phase was fairly short, probably due to the increased polymerization rate at this stage. By 180 min, most of the vesicle structures had disappeared and were replaced by collapsed structures. Figure 2.11H shows the progression involving wall thickening, followed by intervesicle collapse. Eventually (280 min Figure 2.11I), all the vesicles had evolved into micron-sized clusters with irregular shapes.
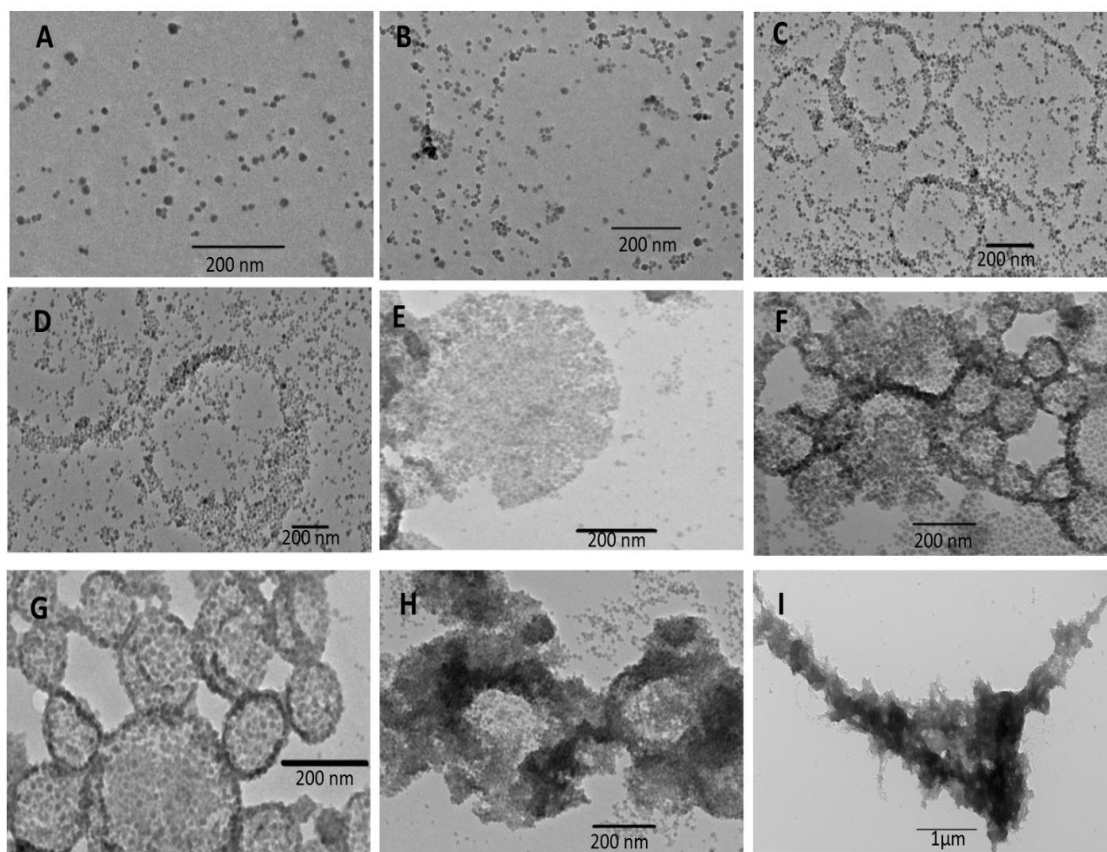
Figure 2.11. Representative TEM images of the assemblies at different polymerization times: 0 min (A), 60 min (B), 90 min (C, D), 120 min (E,F), 150 min (G), 180 min (H), 280 min (I).
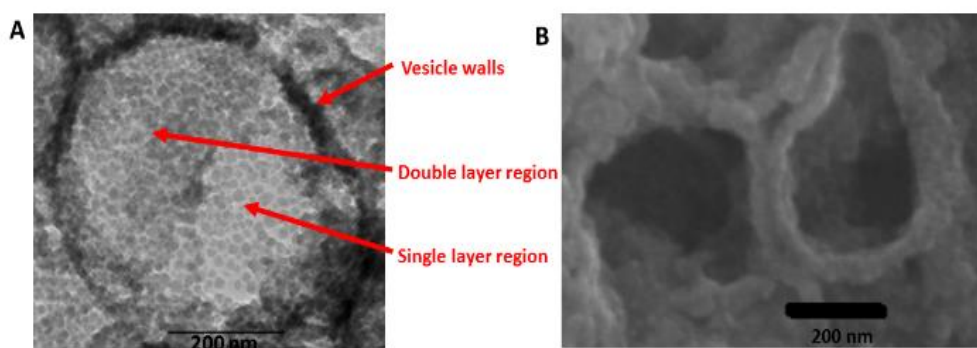
Figure 2.12. (A) Close-up TEM view of an individual self-assembled vesicle with broken shell (left image). (B) SEM image of self-assembled vesicles showing inner cavities and single-layer walls (right image).
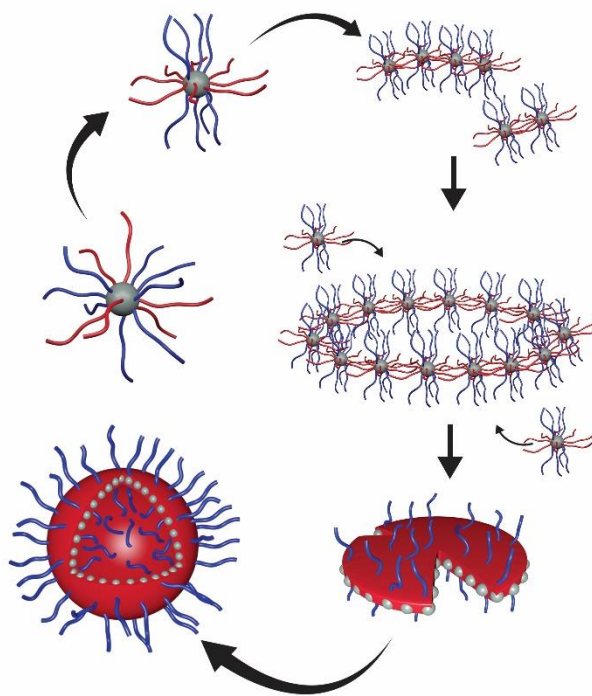
Scheme 2.4. Proposed mechanism of surface-initiated polymerization-induced self-assembly of NPs into nanovesicles.

The hollow nature of self-assembled structures at 150min after reaction started was further revealed by both TEM and scanning electron microscopy (SEM) studies. Figure 2.12A shows a close-up view of one vesicle structure with a broken fraction of its shell. The peripheral region has the darkest contrast, representing a thin layer of vesicle walls collapsed on a flat TEM grid. The left part of inner region represents the double layer of NPs which is a typical projection of a 3D thin-layer hollow sphere onto a 2D image. The right-hand section of the inner space showed the lightest contrast and was apparently composed of a single-layer of 15 nm NPs, which is the result of a partially enclosed shell. SEM images (Figure 2.12B) further confirmed that the vesicles have hollow cavities enclosed by walls made from the grafted nanoparticles.

Based on the step-by-step assembly process from dispersed NPs to nanovesicles presented in Figure 2.12, we propose a detailed mechanism for the formation of vesicles from the SI-PISA of NPs (Scheme 2.4). When the insoluble PBzMA chains reached a critical length, the mixed brush grafted NPs underwent a localized phase separation of the soluble PHPMA chains from the insoluble PBzMA chains. Initial self-assembly occurred by interparticle collapse between PBzMA domains, forming short strings and nanorings. The nanorings directed the orientation and addition of further NPs to grow inward, forming nanodisks composed of NPs embedded in the collapsed PBzMA domain that were stabilized by PHPMA chains extending into the solvent. The round-shaped disks then formed wedge shaped defects around their perimeter, which facilitated folding of the nanoparticle disks into single-walled vesicles.
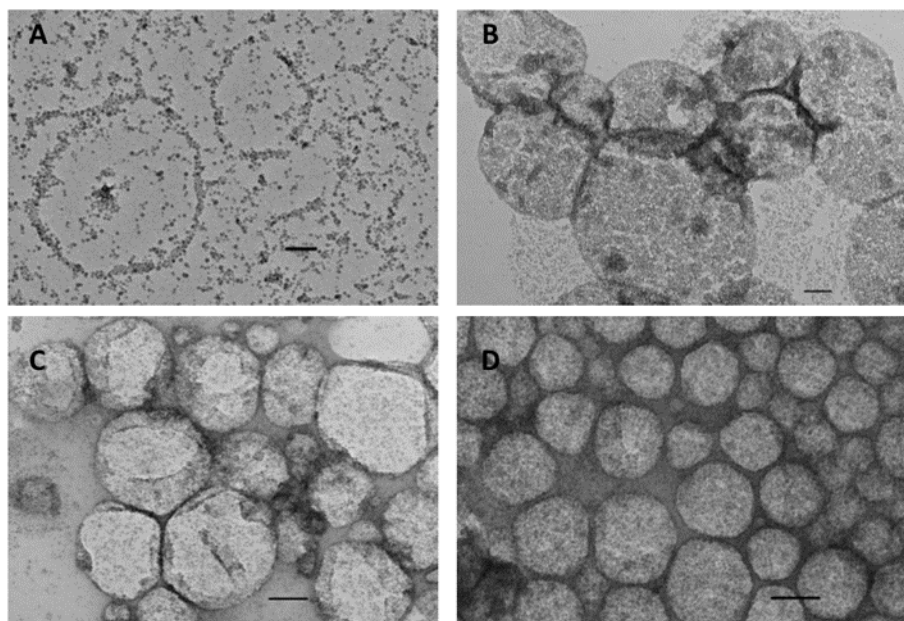
Figure 2.13. Representative TEM images of assembled structures from SiO_2-g-(PMAA, PBzMA) NPs with 23 kDa PMAA. All scale bars: 200nm.

In order to demonstrate SI-PISA as a general one-step strategy towards well-defined nanovesicles, we further explored another system using SiO_2-g-(PMAA, PBzMA) NPs as building blocks. The synthetic route is the same as the SiO_2-g-(PHPMA, PBzMA) case described above, but poly(methacrylic acid) (PMAA) (23kDa) was used as stabilizing brush instead of PHPMA (Scheme 2.5). As a result, similar self-assembly behaviour was observed from surface-initiated polymerization of BzMA using SiO_2-g-(PMAA, CPDB) as stabilizer. Vesicles were formed during polymerization at 10mg/ml. Additionally, we also observed the intermediate stages as rings, disks, half enclosed vesicles, and fully enclosed vesicles (Figure 2.13). It is also worth mentioning that an early attempt to perform SI-PISA using shorter PMAA (5.8K) as stabilizing brushes failed to result in any well-organized
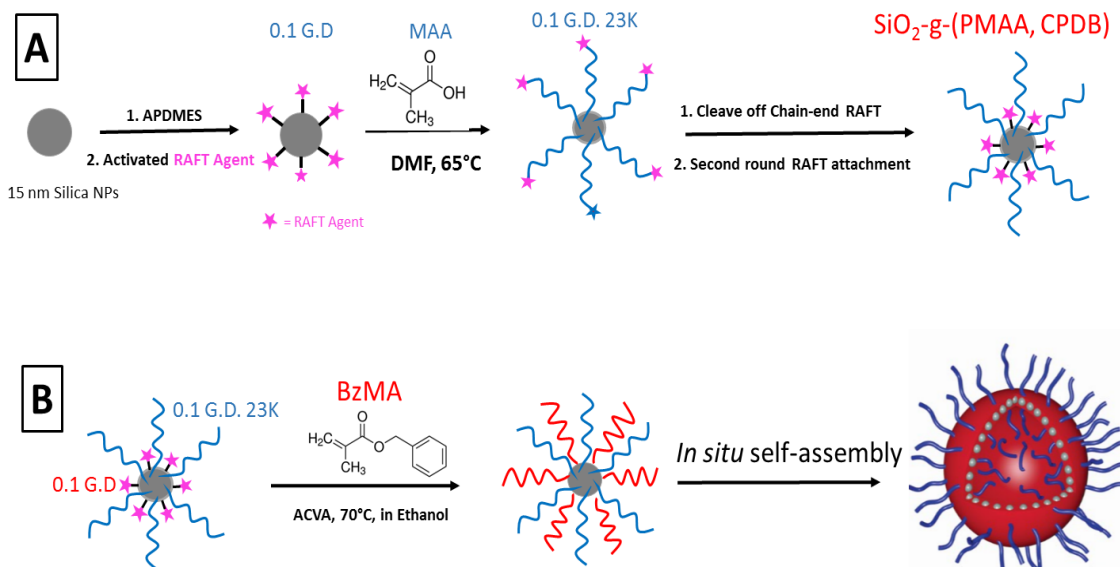
Scheme 2.5. (A) Synthesis of SiO_2-g-(PMAA, CPDB). (B) One-pot surface-initiated RAFT polymerization-induced self-assembly of grafted NPs into vesicles

structures. Instead, NP clusters in random shapes were observed. These observations indicated that the length of the stabilizing brushes plays an important role in the self-assembly process. Understanding the critical molecular length of the stabilizing block would be an interesting topic to further define this SI-PISA strategy.

2.5 Conclusions

In conclusion, we demonstrated a facile and efficient way using surface-initiated polymerization to induce self-assembly of inorganic NPs into strings, disks and single-layer nanovesicles. This SI-PISA strategy represents a new aspect of PISA, that utilizes the growth of polymer chains from NP surfaces to direct the self-assembly of inorganic nanoparticles. Compared with the traditional way of preparing hybrid nanovesicles by solvent switching and film rehydration, this newly developed self-assembly method requires no post-polymerization process and can be operated at high NP concentration(~10mg/ml), which is important for large production of such hybrid assemblies. This approach also offered insights into the evolution of nanovesicles, including their birth from well-dispersed NPs and nanorings, and their death into micron-sized aggregates. We believe that this strategy could be further extended to prepare nanovesicles in other media (i.e. non-polar solvents and water) with different polymer brush selection. Moreover, we could expect the self-assembly of NPs with various shapes like nanotubes and solid spheres, by fine-tuning the chain length and graft density of the first brush and the graft density of the second brush. We believe that the SI-PISA strategy described in this work could open up many possibilities of preparing functional hybrid materials from polymer-grafted NPs.

2.6 References

1.   Zheng, G.; Pan, C., Reversible Addition−Fragmentation Transfer Polymerization in Nanosized Micelles Formed in Situ. *Macromolecules* **2006,** *39* (1), 95-102.

2.   Wan, W.-M.; Pan, C.-Y., One-pot synthesis of polymeric nanomaterials via RAFT dispersion polymerization induced self-assembly and re-organization. *Polymer Chemistry* **2010,** *1* (9), 1475-1484.

3.   Charleux, B.; Delaittre, G.; Rieger, J.; D'Agosto, F., Polymerization-Induced Self-Assembly: From Soluble Macromolecules to Block Copolymer Nano-Objects in One Step. *Macromolecules* **2012,** *45* (17), 6753-6765.

4.   Warren, N. J.; Armes, S. P., Polymerization-Induced Self-Assembly of Block Copolymer Nano-objects via RAFT Aqueous Dispersion Polymerization. *Journal of the American Chemical Society* **2014,** *136* (29), 10174-10185.

5.   Blanazs, A.; Madsen, J.; Battaglia, G.; Ryan, A. J.; Armes, S. P., Mechanistic Insights for Block Copolymer Morphologies: How Do Worms Form Vesicles? *Journal of the American Chemical Society* **2011,** *133* (41), 16581-16587.

6.   Delaittre, G.; Charleux, B., Kinetics of in-Situ Formation of Poly(acrylic acid)-b-polystyrene Amphiphilic Block Copolymers via Nitroxide-Mediated Controlled Free-Radical Emulsion Polymerization. Discussion on the Effect of Compartmentalization on the Polymerization Rate. *Macromolecules* **2008,** *41* (7), 2361-2367.

7.   Wan, W.-M.; Pan, C.-Y., Atom Transfer Radical Dispersion Polymerization in an Ethanol/Water Mixture. *Macromolecules* **2007,** *40* (25), 8897-8905.

8.   Canning, S. L.; Smith, G. N.; Armes, S. P., A Critical Appraisal of RAFT-Mediated Polymerization-Induced Self-Assembly. *Macromolecules* **2016,** *49* (6), 1985-2001.

9.   Zhou, H.; Liu, C.; Gao, C.; Qu, Y.; Shi, K.; Zhang, W., Polymerization-induced self-assembly of block copolymer through dispersion RAFT polymerization in ionic liquid. *Journal of Polymer Science Part A: Polymer Chemistry* **2016,** *54* (11), 1517-1525.

10.   Derry, M. J.; Fielding, L. A.; Armes, S. P., Polymerization-induced self-assembly of block copolymer nanoparticles via RAFT non-aqueous dispersion polymerization. *Progress in Polymer Science* **2016,** *52*, 1-18.

11.   Bleach, R.; Karagoz, B.; Prakash, S. M.; Davis, T. P.; Boyer, C., In Situ Formation of Polymer–Gold Composite Nanoparticles with Tunable Morphologies. *ACS Macro Letters* **2014,** *3* (7), 591-596.

12.   Tan, J.; Sun, H.; Yu, M.; Sumerlin, B. S.; Zhang, L., Photo-PISA: Shedding Light on Polymerization-Induced Self-Assembly. *ACS Macro Letters* **2015,** *4* (11), 1249-1253.

13.   Mable, C. J.; Gibson, R. R.; Prevost, S.; McKenzie, B. E.; Mykhaylyk, O. O.; Armes, S. P., Loading of Silica Nanoparticles in Block Copolymer Vesicles during Polymerization-Induced Self-Assembly: Encapsulation Efficiency and Thermally Triggered Release. *Journal of the American Chemical Society* **2015,** *137* (51), 16098-16108.

14.   He, J.; Liu, Y.; Babu, T.; Wei, Z.; Nie, Z., Self-Assembly of Inorganic Nanoparticle Vesicles and Tubules Driven by Tethered Linear Block Copolymers. *Journal of the American Chemical Society* **2012,** *134* (28), 11342-11345.

15.   Song, J.; Cheng, L.; Liu, A.; Yin, J.; Kuang, M.; Duan, H., Plasmonic Vesicles of Amphiphilic Gold Nanocrystals: Self-Assembly and External-Stimuli-Triggered Destruction. *Journal of the American Chemical Society* **2011,** *133* (28), 10760-10763.

16. Wang, J.; Li, W.; Zhu, J., Encapsulation of inorganic nanoparticles into block copolymer micellar aggregates: Strategies and precise localization of nanoparticles. *Polymer* **2014,** *55* (5), 1079-1096.

17. Rungta, A.; Natarajan, B.; Neely, T.; Dukes, D.; Schadler, L. S.; Benicewicz, B. C., Grafting Bimodal Polymer Brushes on Nanoparticles Using Controlled Radical Polymerization. *Macromolecules* **2012,** *45* (23), 9303-9311.

18. Zheng, Y.; Huang, Y.; Abbas, Z. M.; Benicewicz, B. C., Surface-initiated polymerization-induced self-assembly of bimodal polymer-grafted silica nanoparticles towards hybrid assemblies in one step. *Polymer Chemistry* **2016,** *7* (34), 5347-5350.

19. Zehm, D.; Ratcliffe, L. P. D.; Armes, S. P., Synthesis of Diblock Copolymer Nanoparticles via RAFT Alcoholic Dispersion Polymerization: Effect of Block Copolymer Composition, Molecular Weight, Copolymer Concentration, and Solvent Type on the Final Particle Morphology. *Macromolecules* **2013,** *46* (1), 128-139.

20. Song, J.; Fang, Z.; Wang, C.; Zhou, J.; Duan, B.; Pu, L.; Duan, H., Photolabile plasmonic vesicles assembled from amphiphilic gold nanoparticles for remote-controlled traceable drug delivery. *Nanoscale* **2013,** *5* (13), 5816-5824.

21. Bian, T.; Shang, L.; Yu, H.; Perez, M. T.; Wu, L.-Z.; Tung, C.-H.; Nie, Z.; Tang, Z.; Zhang, T., Spontaneous Organization of Inorganic Nanoparticles into Nanovesicles Triggered by UV Light. *Advanced Materials* **2014,** *26* (32), 5613-5618.

22. Lin, J.; Wang, S.; Huang, P.; Wang, Z.; Chen, S.; Niu, G.; Li, W.; He, J.; Cui, D.; Lu, G.; Chen, X.; Nie, Z., Photosensitizer-Loaded Gold Vesicles with Strong Plasmonic Coupling Effect for Imaging-Guided Photothermal/Photodynamic Therapy. *ACS Nano* **2013,** *7* (6), 5320-5329.

23. He, J.; Huang, X.; Li, Y.-C.; Liu, Y.; Babu, T.; Aronova, M. A.; Wang, S.; Lu, Z.; Chen, X.; Nie, Z., Self-Assembly of Amphiphilic Plasmonic Micelle-Like Nanoparticles in Selective Solvents. *Journal of the American Chemical Society* **2013,** *135* (21), 7974-7984.

24. Niikura, K.; Iyo, N.; Matsuo, Y.; Mitomo, H.; Ijiro, K., Sub-100 nm Gold Nanoparticle Vesicles as a Drug Delivery Carrier enabling Rapid Drug Release upon Light Irradiation. *ACS Applied Materials & Interfaces* **2013,** *5* (9), 3900-3907.

25. Niikura, K.; Iyo, N.; Higuchi, T.; Nishio, T.; Jinnai, H.; Fujitani, N.; Ijiro, K., Gold Nanoparticles Coated with Semi-Fluorinated Oligo(ethylene glycol) Produce Sub-100 nm Nanoparticle Vesicles without Templates. *Journal of the American Chemical Society* **2012,** *134* (18), 7632-7635.

26. Huang, P.; Lin, J.; Li, W.; Rong, P.; Wang, Z.; Wang, S.; Wang, X.; Sun, X.; Aronova, M.; Niu, G.; Leapman, R. D.; Nie, Z.; Chen, X., Biodegradable Gold Nanovesicles with an Ultrastrong Plasmonic Coupling Effect for Photoacoustic Imaging and Photothermal Therapy. *Angewandte Chemie International Edition* **2013,** *52* (52), 13958-13964.

27. Perrier, S.; Takolpuckdee, P.; Mars, C. A., Reversible Addition−Fragmentation Chain Transfer Polymerization: End Group Modification for Functionalized Polymers and Chain Transfer Agent Recovery. *Macromolecules* **2005,** *38* (6), 2033-2036.

28. Derry, M. J.; Fielding, L. A.; Armes, S. P., Industrially-relevant polymerization-induced self-assembly formulations in non-polar solvents: RAFT dispersion polymerization of benzyl methacrylate. *Polymer Chemistry* **2015,** *6* (16), 3054-3062.

29. Yeow, J.; Xu, J.; Boyer, C., Polymerization-Induced Self-Assembly Using Visible Light Mediated Photoinduced Electron Transfer–Reversible Addition–Fragmentation Chain Transfer Polymerization. *ACS Macro Letters* **2015,** *4* (9), 984-990.

30. Nikolic, M. S.; Olsson, C.; Salcher, A.; Kornowski, A.; Rank, A.; Schubert, R.; Frömsdorf, A.; Weller, H.; Förster, S., Micelle and Vesicle Formation of Amphiphilic Nanoparticles. *Angewandte Chemie International Edition* **2009,** *48* (15), 2752-2754.

31. Liu, Y.; He, J.; Yang, K.; Yi, C.; Liu, Y.; Nie, L.; Khashab, N. M.; Chen, X.; Nie, Z., Back Cover: Folding Up of Gold Nanoparticle Strings into Plasmonic Vesicles for Enhanced Photoacoustic Imaging (Angew. Chem. Int. Ed. 52/2015). *Angewandte Chemie International Edition* **2015,** *54* (52), 15916-15916.

32. Kang, Y.; Erickson, K. J.; Taton, T. A., Plasmonic Nanoparticle Chains via a Morphological, Sphere-to-String Transition. *Journal of the American Chemical Society* **2005,** *127* (40), 13800-13801.

33. Wang, L.; Cole, M.; Li, J.; Zheng, Y.; Chen, Y. P.; Miller, K. P.; Decho, A. W.; Benicewicz, B. C., Polymer grafted recyclable magnetic nanoparticles. *Polymer Chemistry* **2015,** *6* (2), 248-255.

CHAPTER 3

A Useful Method for Preparing Mixed Brush Polymer Grafted

Nanoparticles by Polymerizing Block Copolymers from Surfaces

with Reversed Monomer Addition Sequence

3.1 Abstract

The preparation of well-defined block copolymers using controlled radical polymerization depends on the proper order of monomer addition. The reversed order of monomer addition results in a mixture of block copolymer and homopolymer and thus has typically been avoided. In this chapter, we utilized the low blocking efficiency of reversed monomer addition order in combination with surface initiated RAFT polymerization to establish a facile procedure towards mixed polymer brush grafted nanoparticles SiO_2-g-(PS_1, PS_1-*b*-PMAA). The SiO_2-g-(PS, PS-*b*-PMAA) nanoparticles were analyzed by GPC deconvolution, and the fraction of each polymer component was calculated. Additionally, the SiO_2-g-(PS, PS-*b*-PMAA) were amphiphilic in nature, and showed unique self-assembly behavior in water.

3.2 Introduction

It is now well accepted that the order of monomer addition is pivotal in the preparation of well-cdefined block copolymers using controlled radical polymerization.[1-2] Because of the better leaving group ability, monomers that produce tertiary propagating radicals (e.g., methacrylates) should be polymerized prior to those that produce secondary propagating radicals (e.g., acrylates and styrene). For example, the chain extension of styrene from PMMA macroinitiator is considered the "right sequence" towards well-defined PMMA-b-PS. In contrast, the reversed monomer addition sequence leads to mixed products of homopolymer and block copolymer because of the slow initiation of the macro-initiators. Thus, only some of the macro-initiators can be successfully chain extended which leads to the mixture of homopolymers and block copolymers.[3] This reversed

monomer addition order, sometimes called the "wrong sequence" has always been avoided when making block copolymers using controlled radical polymerization methods. Indeed, the product as a copolymer/homopolymer mixture is not of interest for most research and applications. However, we envision that this scenario could be synthetically and practically attractive when the macro-initiators are anchored onto the surface of a substrate or nanoparticles. When the polymer chains are grafted on a substrate or particle surfaces and surface-initiated polymerizations are performed, it is possible that we could advantageously utilize the outcome of this "wrong sequence" to prepare mixed brush polymer grafted nanoparticles in a simplified process.

Nanoparticles with two different populations of polymer brushes have been a topic of increasing importance in ligand engineering of polymer nanocomposites.[4-8] Recent advances in SI-polymerization creates the possibility to fabricate such composite materials with good interfacial properties via control of the graft density, molecular weight, and chemistry of the grafted polymers. However, the preparation procedures are typically time consuming and involve multiple steps. For example, the preparation of bimodal polymer grafted nanoparticles using SI-RAFT polymerization include at least five steps: 1) polymerization of first brush, 2) chain end RAFT agent cleavage 3) aminosilane attachment, 4) second RAFT attachment, and 5) polymerization of second brush. Each step is accompanied by at least two washings and precipitations, making the whole process relatively time-consuming.[6, 9-10] Similarly, the preparation of such materials using SI-ATRP includes multiple steps to partially deactivate the chain end of the first population of polymer brushes.[8]

In this work, we explored surface initiated RAFT polymerization using reversed monomer addition sequence as a simple two step method of preparing mixed brush grafted nanoparticles consisting of a shorter polystyrene homopolymer brush and a longer polystyrene-b-polymetharcylic acid brush. Moreover, these amphiphilic nanoparticles showed unique self-assembly behavior in water, forming nanoparticle clusters with controlled aggregation number.

3.3 Experimental Section

Materials: Styrene (TCI, 97%) and methacrylic acid (Acros, 96%) were passed through a basic aluminum column to remove inhibitors before use. 2.2'-Azobisisobutyronitrile (AIBN) was purified by recrystallization from methanol and dissolved in ethanol to make 10mM solution. All other reagents were used as received.

Synthesis of PS grafted silica nanoparticles. 4-Cyanopentanoic acid dithiobenzoate (CPDB) anchored 15nm silica nanoparticles were prepared according to the literature.[1] A solution of styrene (7.96g), AIBN (255µl of 10mM solution in methanol), CPDB-anchored silica nanoparticles (0.4, 63.8µmol/g) and THF (8ml) was prepared in a Schlenk tube. The mixture was degassed by three freeze-pump-thaw cycles, backfilled with nitrogen, and then placed in an oil bath at 65°C for 11 hours. The polymerization solution was quenched in an ice bath and poured into 1:1 mixture of hexane to precipitate the SiO_2-g-PS nanoparticles. The SiO_2-g-PS nanoparticles were redispersed in THF and precipitated two more times to remove excess monomers and initiators. The purified SiO_2-g-PS nanoparticles were dispersed in DMF for the next reaction step.

Synthesis of SiO₂-g-(PS₁, PS₁-*b*-PMAA) nanoparticles. SiO₂-g-PS nanoparticles (0.2 g), methacrylic acid (0.975 g), AIBN (134 µl of 10 mM solution in ethanol) and DMF (10ml) were mixed together and added to a Schlenk flask equipped with a rubber stopper. The mixture was degassed by three freeze-pump-thaw cycles, backfilled with nitrogen and then placed in an oil bath of 80 °C. Aliquots of the reaction solution were withdrawn from the flask periodically after the start of the polymerization. Grafted polymer chains were cleaved from silica nanoparticles by reacting with excess amount of HF.

Methylation of SiO₂-g-(PS₁, PS₁-*b*-PMAA) nanoparticles

SiO₂-g-PS-b-PMAA nanoparticles (~ 20 mg) were dissolved in 10 mL DMF. An excess of the yellow solution of trimethylsilyldiazomethane was added dropwise into the nanoparticle solution at room temperature (rt). After complete addition, the solution was stirred for 3h at rt. Approximately 10% by volume of methanol was added to enhance the conversion of the methylation. The excess trimethylsilyldiazomethane was quenched by acetic acid. This process was used to improve the compatibility between polymer and THF phase GPC. The PS-b-PMAA block copolymers were converted to PS-b-PMMA to prevent self-assembly of PS-b-PMAA in THF due to the incompatibly between PMAA and THF solvent.

Characterization.

^{1}H NMR (Bruker ARX 300/ARX 400) was conducted using CD₃OD as the solvent. Molecular weights and dispersity were determined using a gel permeation chromatography (GPC) with a 515 HPLC pump, a 2410 refractive index detector, and three Styragel columns. The columns consist of HR1, HR3 and HR4 in the effective molecular weight

ranges of 100-5000, 500-30000, and 5000-500000, respectively. THF was used as eluent at 30°C and flow rate was adjusted to 1.0mL/min. Molecular weights were calibrated with poly(methyl methacrylate) standards obtained from Polymer Laboratories. Dynamic Light Scattering characterizations were conducted using Zetasizer Nano ZS90 from Malvern. Infrared spectra were obtained using a BioRad Excalibur FTS3000 spectrometer. The transmission electron microscopy (TEM) was performed on a Hitachi H8000 TEM at an accelerating voltage of 200 KV. The samples were prepared by depositing a drop of the diluted nanoparticle solution in methanol on copper grids. Scanning electron microscopy (SEM) was performed by drop-casting 10 µl of diluted nanoparticle solution on copper grids with carbon film.

GPC Deconvolution Analysis.

The GPC deconvolution analysis was used to quantify blocking efficiency. GPC traces were split into three peaks: the block copolymer, the "unreacted" homopolymer PS and PS homopolyer by coupling. The different dn/dc values for each component were taken into account when integrating the area of each peak. Since the PMAA block was converted to PMMA prior to GPC analysis, the dn/dc value of 0.086 for PMMA and 0.186 for PSt in THF was used for calculation of the dn/dc values of the block copolymer together with weight fraction of the two blocks (w_{p1}, w_{p2}) calculated from ^{1}HNMR.

$$\left(dn/dc \right)_{BCP} = w_{p1} \left(dn/dc \right)_{p1} + wp_2 \left(dn/dc \right)_{p2}$$

To estimate the mole fraction of each peak, the areas of the peaks were obtained via Origin Peak Analyzer and normalized with respect to molecular weight and dn/nc.

$$x_1 = \frac{\dfrac{A_1}{\left(\frac{dn}{dc}\right)_1 * M_1}}{\dfrac{A1}{\left(\frac{dn}{dc}\right)_1 * M_1} + \dfrac{A2}{\left(\frac{dn}{dc}\right)_2 * M_2} + \dfrac{A3}{\left(\frac{dn}{dc}\right)_3 * M_3}}$$

$$x_2 = \frac{\dfrac{A_2}{\left(\frac{dn}{dc}\right)_2 * M_2}}{\dfrac{A1}{\left(\frac{dn}{dc}\right)_1 * M_1} + \dfrac{A2}{\left(\frac{dn}{dc}\right)_2 * M_2} + \dfrac{A3}{\left(\frac{dn}{dc}\right)_3 * M_3}}$$

$$x_3 = \frac{\dfrac{A_3}{\left(\frac{dn}{dc}\right)_3 * M_3}}{\dfrac{A1}{\left(\frac{dn}{dc}\right)_1 * M_1} + \dfrac{A2}{\left(\frac{dn}{dc}\right)_2 * M_2} + \dfrac{A3}{\left(\frac{dn}{dc}\right)_3 * M_3}}$$

Reproducibility was ensured with five deconvolutions to obtain an average and standard deviation within 2%. This method follows the procedure established by Bartels et al. and Jennings et al.[11-12]

3.4 Results and Discussion

3.4.1. Synthesis of SiO₂-g-(PS, PS-*b*-PMAA) using reversed monomer addition sequence.
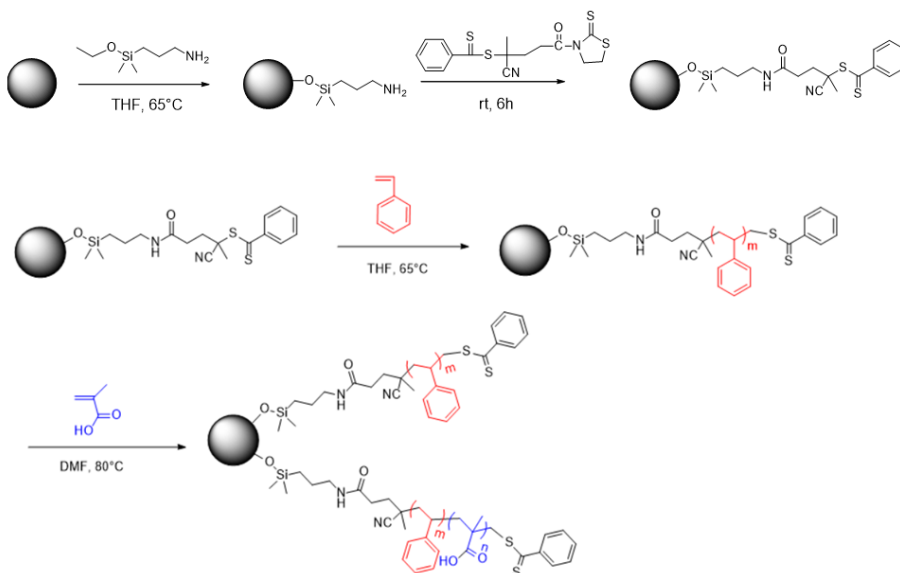
Figure 3.1. Synthetic scheme of SiO₂-g-(PS, PS-*b*-PMAA) using reversed monomer addition sequence.

A 4-cyanopentanoic acid dithiobenzoate (CPDB) RAFT agent was initially attached to 15 nm silica nanoparticles, as reported previously.[6] The graft density was determined by UV-vis analysis to be 0.27 ch/nm². To perform the polymerization in reversed sequence, we graft polymerized styrene first, followed by the chain extension of the macroinitiator with methacrylic acid (Figure 3.1). The initial SI-RAFT of PS was performed in THF for 11 hours at 65 °C. From a small sample, the grafted polymers were cleaved from the silica particle surface and characterized using GPC (21 kDa, Đ = 1.1). The PS grafted nanoparticles were purified, redispersed in DMF, and chain extended with methacrylic acid. The polymerization of MAA was conducted at 80°C at various times.

The resulting polymer grafted particles were treated with HF to etch the silica, and the polymers were subjected to GPC analysis.
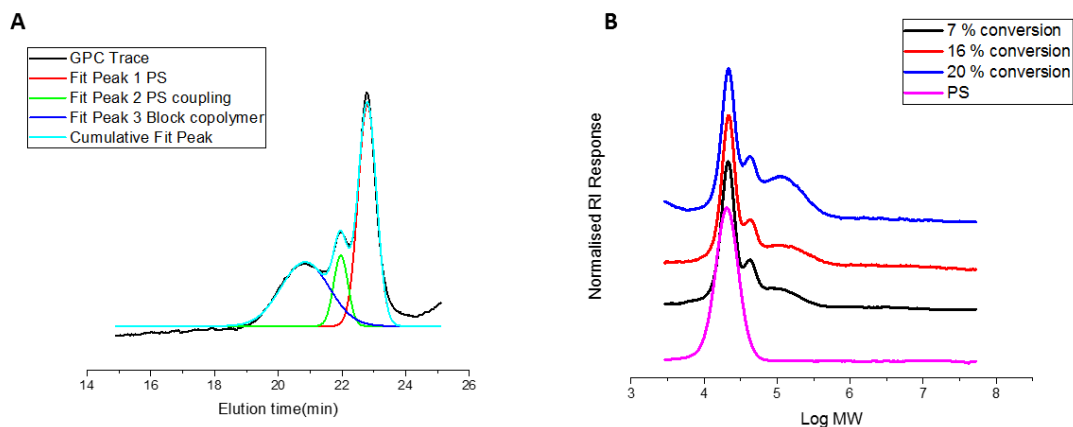
Figure 3.2. (A) An example of a typical GPC curve and fitted peaks for cleaved PS-b-PMAA copolymer. (B) Stacked GPC traces of PS-b-PMAA copolymers synthesized by polymerization of MAA from surface anchored PS macro-initiator.

Figure 3.2 shows a typical GPC curve of PS-b-PMAA copolymer cleaved from the nanoparticle surfaces. It should be noted that the PS-b-PMAA was treated with trimethylsilyldiazomethane to convert the carboxylic groups of the PS-b-PMMA to methyl esters before GPC injection to improve the compatibility between the polymer and the THF phase GPC (experimental section). The curves were analyzed using a deconvolution method with an Origin peak analyzer. Further calculations based on mathematical deconvolution of the GPC peaks provided a multipeak fitting for all polymer peaks. The weight fraction and mole fraction of each component was then calculated based on Mn values from GPC and adjusted by the dn/dc values of each component (see experimental

section for details). This GPC deconvolution method has been used by Wooley et al. and Howdle et al. as a reliable method for calculating block efficiency.[11-12]

Table 3.1. Characteristics of PS-b-PMAA synthesized at different conversions.

	Time [h]	Conversion [%]	Peak 1 Mn [kDa]	Peak 1 percent [%]	Peak 2 Mn [kDa]	Peak 2 percent [%]	Peak 3 Mn [kDa]	Peak 3 percent [%]
0	0	0	20	100				
1	2	7	21	84.8	43	8.4	104	6.7
2	4	16	20	82.9	43	8.0	126	9.1
3	7	20	21	80.6	43	8.5	132	10.9

The results show that the block copolymer GPC curves could be separated into three peaks. The first peak (~21 kDa) appeared at the exact position as the PS macroinitiator, and thus was ascribed to the PS homopolymer which did not participate in the chain extension reaction. This inactive polymer was the major component of the grafted polymers. The second peak (~43 kDa) had twice the molecular weight of the PS homopolymer and its position did not change during the subsequent polymerizations. This indicated the presence of dead PS chains likely formed by radical recombination during the addition of AIBN at the start of the chain extension or second polymerization step. The third peak had the largest molecular weight. Furthermore, the molecular weight as well as its mole fraction increased during polymerization, indicating the formation of block copolymer. At 20% monomer conversion, ~80% of the PS macro-initiators remained

"unreacted" and 8.5% of the PS chains underwent coupling thus forming PS homopolymer with double the molecular weight as the unreacted chains. Finally, 10.9% of the PS chains successfully chain extended with MAA forming block copolymers. Compared with literature data of block copolymerizations crossing from secondary radicals to tertiary radicals, [3] the block efficiency was relatively low. However, the peak ascribed to homopolymer coupling was not observed in the free solution polymerization. Here, we consider the differences between grafting-from polymerization and free solution polymerization. In the case of grafting-from polymerization, the PS macro-initiators were in close proximity as their motion was restricted by tethering onto the nanoparticle surface. Therefore, due to the slow initiation process and inefficient chain extension, the radicals on the particle surface had greater possibility to undergo termination by combination prior to polymerization. In order to demonstrate that this radical coupling occurred within each nanoparticle instead of inter-particle crosslinking, another polymerization was conducted under diluted conditions. The radical coupling peak was observed without a change in mole fraction.

3.4.2. Self-assembly behavior of SiO$_2$-g-(PS, PS-*b*-PMAA).

The self-assembly of grafted nanoparticles has been a topic of recent interest to us, thus we studied the self-assembly behavior of these (PS, PS-*b*-PMAA) grafted nanoparticles in aqueous solution.

Self-assembly was induced by the solvent switching method. Typically, PS-b-PMAA grafted nanoparticles were purified and dispersed in DMF, a good solvent for all components, and then water was introduced dropwise to induce the self-assembly. The

solution changed from transparent to translucent, indicating the formation of nano-assemblies. The morphology of the assemblies was characterized with TEM to be solid sphere aggregates. As discussed earlier, the SiO_2-g-(PS, PS-b-PMAA) nanoparticles have bimodal structures that not only change in chain length of PMAA during the polymerization but also change slightly in the portion of block copolymer. To facilitate comparisons between samples, in this section, we prepared a series of SiO_2-g-(PS_{396}, PS_{396}-b-$PMAA_x$) nanoparticles with the same PS homo-brush chain length but different PS_{396}-b-$PMAA_x$ lengths. The subscripts denote the number of repeating units calculated from [1] HNMR and assumes 10% block copolymer fraction in all cases.
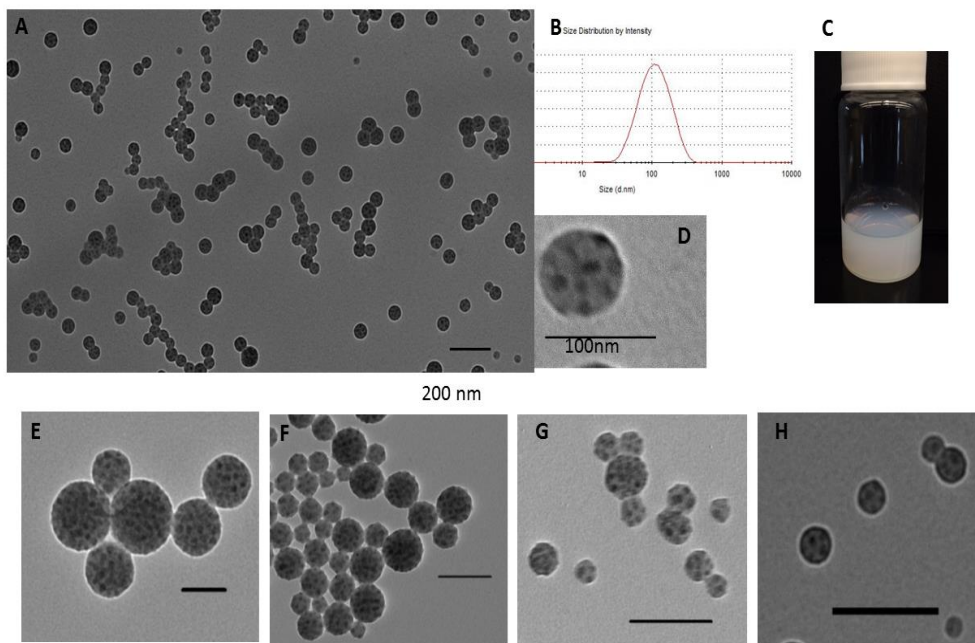
Figure 3.3. A-D. TEM, DLS and visual appearance of assemblies prepared from SiO_2-g-(PS_{396}, PS_{396}-b-$PMAA_{1660}$) nanoparticles. E-H. Comparison of assembled nanospheres with different PS/PMAA ratios. Scale bars :200nm. E. SiO_2-g-(PS_{396}, PS_{396}-b-$PMAA_{350}$), F. SiO_2-g-(PS_{396}, PS_{396}-b-$PMAA_{500}$), G. SiO_2-g-(PS_{396}, PS_{396}-b-$PMAA_{1000}$), H, SiO_2-g-(PS_{396}, PS_{396}-b-$PMAA_{1660}$)

For the experiment using SiO_2-g-(PS_{396}, PS_{396}-b-$PMAA_{1660}$) the average size of the spheres was ~100 nm, which agreed with the value measured by DLS (Figure 3.3A-D).

Each sphere aggregate was composed of tens of smaller spherical silica nanoparticles that showed as darker contrast under TEM. We use the number ratio between PS and PMAA calculated form NMR to represent the difference of hydrophobic/hydrophilic ratio between each sample.

The size of aggregates as well as the aggregation number could be controlled by manipulating the hydrophilic/hydrophobic ratio of the nanoparticles. We studied the assembled structures of a series of samples with the same chain length of the PS block but different lengths of the PMAA block. It was clear that decreasing of size of the PMAA block produced an increase of the aggregation number. The spherical aggregates from SiO_2-g-(PS_{396}, PS_{396}-b-$PMAA_{350}$) nanoparticles consisted of tens-to-hundreds of primary silica nanoparticles, while the aggregates from SiO_2-g-(PS_{396}, PS_{396}-b-$PMAA_{1660}$) consisted of only a few (<10) primary silica nanoparticles.

The size of the aggregates as well as the aggregation number could also be controlled by adjusting the initial concentration of the solution using the identical sample. We prepared a series of solutions with different initial concentrations using the same SiO_2-g-(PS_{396}, PS_{396}-b-$PMAA_{1660}$) nanoparticle sample. As shown in Figure 3.4, the size of the aggregates increased with increasing concentration of the initial solution. At higher concentration (50mg/ml), the aggregate size increased to ~150nm while at low concentration (1mg/ml), the degree of aggregation was very low, and the particles were mostly singly dispersed.
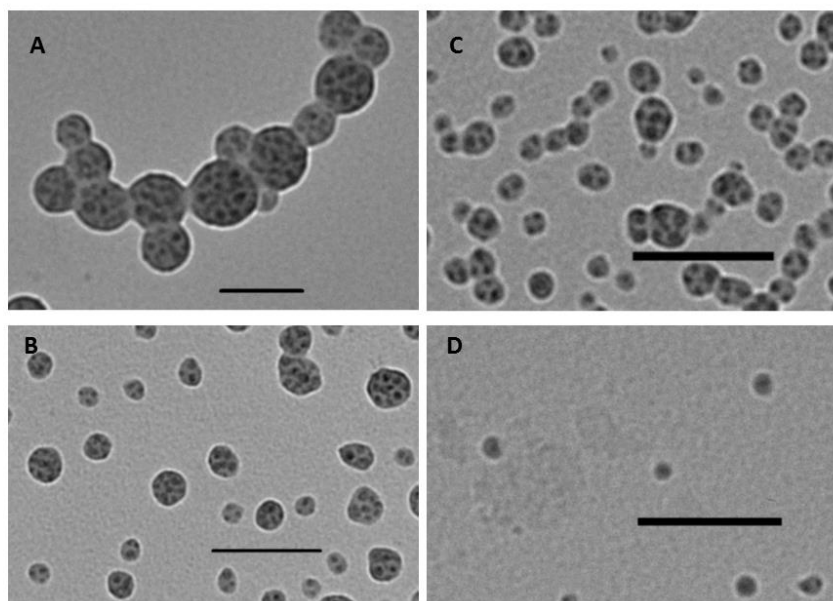
Figure 3.4. Change in aggregate size with decreasing particle solution concentration for SiO$_2$-g-(PS$_{396}$, PS$_{396}$-*b*-PMAA$_{1660}$) sample: A. 50mg/mL, B. 25 mg/mL, C. 10 mg/mL, D. 1mg/mL.

3.5 Conclusions

A reversed monomer addition sequence was successfully utilized to prepare bimodal polymer grafted nanoparticles and resulted in a significantly condensed synthetic procedure. The composition of the grafted polymers was analyzed by GPC deconvolution. Approximately 10% of the grafted PS macro-initiators were chain extended while the majority remained "unreacted" or were terminated by radical coupling. It was shown that this procedure of grafting block polymers with reversed monomer addition sequence could be employed as a "quick and dirty" method of preparing mixed brush polymer grafted nanoparticles. The SiO$_2$-g-(PS$_{396}$, PS$_{396}$-*b*-PMAA$_x$) nanoparticles showed unique self-assembly behavior and formed solid spherical aggregates. The degree of aggregation could be controlled in the range between 1 to several hundred by adjusting the PS/PMAA ratio

and initial nanoparticle concentration. It is expected that these assemblies will find wide

application in the nanotechnology field.

3.6 References

1.   Keddie, D. J., A guide to the synthesis of block copolymers using reversible-addition fragmentation chain transfer (RAFT) polymerization. *Chemical Society Reviews* **2014,** *43* (2), 496-505.
2.   Matyjaszewski, K., Atom Transfer Radical Polymerization (ATRP): Current Status and Future Perspectives. *Macromolecules* **2012,** *45* (10), 4015-4039.
3.   Tang, C.; Kowalewski, T.; Matyjaszewski, K., Preparation of Polyacrylonitrile-block-poly(n-butyl acrylate) Copolymers Using Atom Transfer Radical Polymerization and Nitroxide Mediated Polymerization Processes. *Macromolecules* **2003,** *36* (5), 1465-1473.
4.   Qiao, Y.; Yin, X.; Wang, L.; Islam, M. S.; Benicewicz, B. C.; Ploehn, H. J.; Tang, C., Bimodal Polymer Brush Core–Shell Barium Titanate Nanoparticles: A Strategy for High-Permittivity Polymer Nanocomposites. *Macromolecules* **2015,** *48* (24), 8998-9006.
5.   Li, Y.; Tao, P.; Viswanath, A.; Benicewicz, B. C.; Schadler, L. S., Bimodal Surface Ligand Engineering: The Key to Tunable Nanocomposites. *Langmuir* **2013,** *29* (4), 1211-1220.
6.   Rungta, A.; Natarajan, B.; Neely, T.; Dukes, D.; Schadler, L. S.; Benicewicz, B. C., Grafting Bimodal Polymer Brushes on Nanoparticles Using Controlled Radical Polymerization. *Macromolecules* **2012,** *45* (23), 9303-9311.
7.   Zhao, B.; Zhu, L., Mixed Polymer Brush-Grafted Particles: A New Class of Environmentally Responsive Nanostructured Materials. *Macromolecules* **2009,** *42* (24), 9369-9383.
8.   Yan, J.; Kristufek, T.; Schmitt, M.; Wang, Z.; Xie, G.; Dang, A.; Hui, C. M.; Pietrasik, J.; Bockstaller, M. R.; Matyjaszewski, K., Matrix-free Particle Brush System with Bimodal Molecular Weight Distribution Prepared by SI-ATRP. *Macromolecules* **2015,** *48* (22), 8208-8218.
9.   Zheng, Y.; Huang, Y.; Abbas, Z. M.; Benicewicz, B. C., Surface-initiated polymerization-induced self-assembly of bimodal polymer-grafted silica nanoparticles towards hybrid assemblies in one step. *Polymer Chemistry* **2016,** *7* (34), 5347-5350.
10.   Zheng, Y.; Huang, Y.; Abbas, Z. M.; Benicewicz, B. C., One-pot synthesis of inorganic nanoparticle vesicles via surface-initiated polymerization-induced self-assembly. *Polymer Chemistry* **2017,** *8* (2), 370-374.
11.   Jennings, J.; Beija, M.; Kennon, J. T.; Willcock, H.; O'Reilly, R. K.; Rimmer, S.; Howdle, S. M., Advantages of Block Copolymer Synthesis by RAFT-Controlled Dispersion Polymerization in Supercritical Carbon Dioxide. *Macromolecules* **2013,** *46* (17), 6843-6851.
12.   Bartels, J. W.; Cauët, S. I.; Billings, P. L.; Lin, L. Y.; Zhu, J.; Fidge, C.; Pochan, D. J.; Wooley, K. L., Evaluation of Isoprene Chain Extension from PEO Macromolecular

Chain Transfer Agents for the Preparation of Dual, Invertible Block Copolymer Nanoassemblies. *Macromolecules* **2010,** *43* (17), 7128-7138.

CHAPTER 4

PH AND THERMAL DUAL-RESPONSIVE NANOPARTICLES FOR CONTROLLED DRUG DELIVERY WITH HIGH LOADING CONTENT

4.1 Abstract

A pH and thermal dual-responsive nanocarrier with silica as the core and block copolymer composed of poly(methacrylic acid) (PMAA) and poly(N-isopropylacrylamide) (PNIPAM) as the shell was prepared by surface initiated RAFT polymerization. The resulting SiO_2-PMAA-b-PNIPAM particles dispersed individually in aqueous solution at high pH and low temperature but reversibly agglomerated at acidic conditions or at elevated temperature. These dual-responsive nanoparticles were used as carriers to deliver the model drug doxorubicin (DOX) with unusually high entrapment efficiency and loading content which is due to the small size (15 nm), light weight of the cores and high graft density (0.619 chains/nm^2) achieved by surface initiated RAFT polymerization. The release rate was controlled by both pH and temperature of the surrounding medium. Moreover, these particles selectively precipitated at acidic conditions with increased temperature, which may enhance their ability to accumulate at tumor sites. Cytotoxicity studies demonstrated that DOX-loaded nanoparticles are highly active against Hela cells, and more effective than free DOX of equivalent dose. A cellular uptake study revealed that SiO_2-PMAA-b-PNIPAM nanoparticles could successfully deliver DOX molecules into the nuclei of Hela cells. All these features indicated that SiO_2-PMAA-b-PNIPAM nanoparticles are a promising candidate for therapeutic applications.

4.2 Introduction

Polymer-grafted nanoparticles have gained significant attention because of their wide application in materials science, bioimaging and drug delivery.[1-5] The surface initiated reversible addition-fragmentation chain-transfer polymerization (SI-RAFT)

technique has been developed as a robust method to graft polymers from silica surfaces with predetermined density and controlled molecular weights.[6-8] A variety of polymers with well-defined architectures (homopolymer, block copolymer, bimodal brushes) have been successfully grafted to demonstrate the effectiveness of this method.[9-12] Stimuli-responsive polymers are materials that can adapt to environmental changes like pH, temperature, ionic strength and light.[13-17] Poly(methacrylic acid) (PMAA) and poly(N-isopropylacrylamide) (PNIPAM) are typical stimuli-responsive polymers that have been widely studied. PMAA chains change conformation in water in response to pH changes. In basic conditions, the carboxylic groups along the polymer chains are deprotonated, creating charges that make the polymer swell in water. At low pH (<5), carboxylic groups are protonated, making the chains hydrophobic and adapt a collapsed conformation.[18-19] Comparatively, PNIPAM chains can perform similar conformational transformations in response to temperature. Below the Lower Critical Solution Temperature (LCST), PNIPAM chains stretch out and swell in aqueous solution. A phase transition occurs with temperature above LCST, when the chains become hydrophobic and collapse into a condensed conformation.[20]

Grafting stimuli-responsive polymers onto inorganic nanoparticles is an interesting topic since the combined assembly could exhibit properties inherent from both the inorganic cores and grafted polymers. A common application of these core-shell structures is the controlled delivery of active species into biological targets. For example, Ma *et al.* prepared magnetic colloid nanocrystal clusters covered with cross-linked poly(acrylic acid) that conjugated Doxorubicin (DOX) and released them upon reduction in pH,[21] Xu *et al.* synthesized multifunctional carriers with silicon as the core and a

biocompatible block copolymer as the shell. The release rate was found to be regulated by both pH and chain length of the outer block.[22] However, drug loading contents and entrapment efficiency were relatively low compared with pure polymer systems presumably because of the high weight content of the cores and low graft density of polymers achieved by the "grafting to" process.

Our group has reported surface-initiated RAFT polymerization of methacrylic acid from 15nm silica nanoparticles.[18, 23] This direct "grafting from" strategy offers a convenient way to achieve high graft densities and subsequently, high polymer content. Based on this work, a rationally designed core-shell drug delivery system is described using 15nm silica nanoparticles as cores and poly(methacrylic acid)-b-poly(PNIPAM) block copolymer as shells. Poly(methacylic acid), as the inner block, was used to conjugate with drug molecules through electrostatic attraction forces. The PNIPAM outer block not only introduced temperature responsiveness, but also helped to prevent premature drug leaking. These nano-carriers exhibited unusually high entrapment efficiency and loading content when using doxorubicin as a model drug. The drug release rate was found to be affected by both pH and temperature. Specifically, the release rate was enhanced at acidic pH and high temperature, which is the typical environment of tumor cells.[20] It is also worth noting that these nanoparticles are well dispersed at low temperature, but self-assembled into clusters and eventually precipitated at elevated temperature which may enhance their ability to accumulate around tumor cells.

4.3 Experimental Section

Materials： All chemicals were obtained from Acros or Fisher and used as received unless otherwise specified. N-isopropylacrylamide (PNIPAM) was obtained from TCI, and recrystallized twice from hexane to remove inhibitor. Methacrylic acid (MAA) was purified by passing through an activated neutral alumina column. AIBN was recrystallized from methanol and dissolved in DMF solution at a concentration of 10mmol/L.

Instrumentation.

^{1}H NMR (Bruker ARX 300/ARX 400) was conducted using CD_3OD as the solvent. Molecular weights and PDI were determined using a gel permeation chromatography (GPC) with a 515 HPLC pump, a 2410 refractive index detector, and three Styragel columns. The columns consists of HR1, HR3 and HR4 in the effective molecular weight ranges of 100-5000, 500-30000, and 5000-500000, respectively. THF was used as eluent at 30°C and flow rate was adjusted to 1.0mL/min. Molecular weights were calibrated with poly (methyl methacrylate) standards obtained from Polymer Laboratories. Dynamic Light Scattering characterizations were conducted using Zetasizer Nano ZS90 from Malvern. Infrared spectra were obtained using a BioRad Excalibur FTS3000 spectrometer. Optical spectroscopy was conducted by measuring the transmittance at 300nm using a Perkin-Elmer Lambda 4C UV-Vis spectrometer.

Surface-Initiated RAFT Polymerization of Methacrylic acid from CPDB Anchored Silica Nanoparticles.

4-Cyanopentanoic acid dithiobenzoate (CPDB) anchored 15nm silica nanoparticles were prepared according to the literature.[6] For a typical reaction, 400mg CPDB anchored silica nanoparticles ($0.619chs/nm^2$, 146.7 µmol/g), 5.05g methacrylic acid (58.7mmol), 400mg trioxane were mixed in 12ml DMF and subject to sonication for 2 minutes. AIBN solution in DMF (1.17ml 10mmol/L) was then added. The above mixture was transferred to a Schlenk Tube and degassed by three freeze-pump-thaw cycles, backfilled with nitrogen, and placed in an oil bath of 65 °C for 2.5 hours. The polymerization was stopped by quenching in an ice bath. The resulting solution was washed twice with diethyl ether to remove monomers and initiator and the PMAA grafted particles were redispersed in 20ml DMF for subsequent reaction.

Surface-Initiated RAFT Polymerization of poly(N-isopropylacrylamide)-b-poly(methacrylic acid) from surface anchored Macro-Initiator.

A 10mL solution of PMAA grafted silica nanoparticles with active RAFT agent chain end was mixed with 3.22g N-isopropylacrylamide monomer, 0.58ml of a 1mmol/L AIBN solution, and 500mg trioxane. The above mixture was degassed by three freeze-pump-thaw cycles and placed in an oil bath of 80°C for 12 hours. The polymerization was stopped by quenching in an ice bath.

Preparation of Doxorubicin (DOX) Loaded SiO$_2$-PMAA-b-PNIPAM particles.

A typical process to load DOX onto SiO$_2$-PMAA-b-PNIPAM particles is described as follows: 12ml of a 1mg/mL DOX solution was added into a solution of 40 mg particles and the mixture was stirred overnight in dark conditions. The DOX loaded particles were recovered by ultracentrifugation at 20,000 rpm, 40°C, for 1h and washed twice by DI water to remove free DOX. All supernatant was collected and subject to UV-vis analysis to determine drug encapsulation efficiency (EE) and drug loading contents (DL). A calibration curve of DOX in water was made as reference. EE and DL were determined using the equations:

$$Drug\ loading\ contents(\%) = \frac{weight\ of\ drug\ loaded}{weight\ of\ nanoparticles} * 100$$

$$Drug\ entrapment\ efficiency(\%) = \frac{weight\ of\ drug\ loaded}{weight\ of\ drug\ injected} * 100$$

In vitro drug release from DOX @ SiO$_2$-PMAA-b-PNIPAM

Nanoparticles loaded with doxorubicin were redispersed in 16ml of DI water. The dispersion was then transferred into dialysis bags. The bags were subsequently placed in beakers of different solutions (pH5.0 sodium acetic acid buffer or pH7.0 PBS buffer) at different temperatures (25 °C or 40 °C). 2ml of each solution was sampled with a certain

period of time and analysis using UV-vis spectrometer to determine the amount of released DOX. All drug release data were averaged with three measurements.

Cell culture

Hela cells were obtained from ATCC. They were grown on standard tissue culture plastic in a 5% CO_2 humidified incubator at 37 °C. The cell culture medium was DMEM with 10% fetal bovine serum (FBS) and 1% penicillin/streptomycin antibiotics.

Cell viability assay

Biocompatibility of SiO_2-PMAA-b-PNIPAM nanoparticles, free DOX and DOX loaded nanoparticles were tested on Hela cells, and cell viability was determined by CellTiter-Blue assay. Briefly, cells were seeded on 96-well plate at a density of 1.0×10^4 cell/well and incubated at 37 °C with 5% CO_2 for 24 hr. Then, cell culture medium was replaced with 100 µL of fresh medium containing various concentrations of testing samples. After 24 hr of incubation, testing samples were removed and 10% CellTiter-Blue Reagent was added to each well and incubated for 4 hr. The fluorescence was recorded on a Spectramax Gemini EM spectrophotometer with excitation wavelength of 560 nm and emission wavelength of 590 nm.

Cellular uptake study

Cells were seeded on 12-well plate with a glass cover slip at the bottom of each well (5×10^4 cells/well) and incubated at 37 °C with 5% CO_2 for 24 hr. The medium was replaced respectively with free DOX and DOX loaded nanoparticles (2 µg/mL of DOX) for another 4 hr incubation. Cells were washed 3 times with PBS and fixed by 4%

78

paraformaldehyde (PFA) for 20 min at room temperature. After washing 3 times with PBS, cells were stained by 4', 6-Diamidino-2-Phenylindole (DAPI) for 10 min and kept in PBS. Confocal microscope was used to visualize and take images.

4.4 Results and Discussion
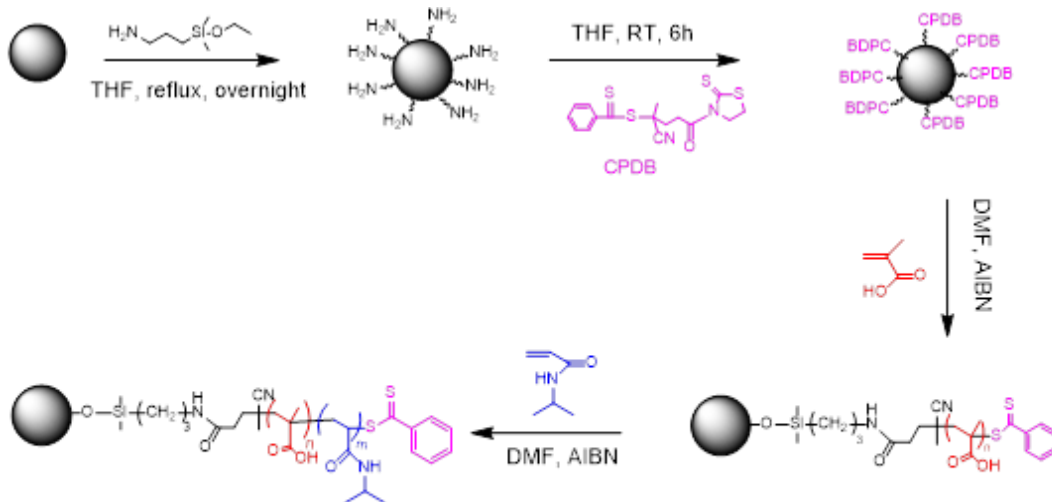
Scheme 4.1. Synthetic scheme for the preparation of PNIPAM-b-PMAA grafted silica nanoparticles.

The strategy for the preparation of PNIPAM-b-PMAA grafted silica nanoparticles is shown in Scheme 4.1. Two separate surface-initiated RAFT polymerizations were conducted sequentially to build well-defined diblock copolymers onto 15 nm silica nanoparticle surfaces. The polymerization of the first block was conducted employing a ratio among species of [MAA]/[RAFT]/[AIBN] = 1000:1:0.1 at 65°C. The monomer conversion, followed by ^{1}H NMR, was found to be 18.5% after 2.5 hours, indicating 185 repeat units of each PMAA chain on average. Thermogravimetric analysis (TGA) showed that the grafted polymer accounted for about 70wt% of the nanoparticles. The PMAA grafted nanoparticles were washed several times by diethyl ether to remove excess

monomer and initiator. The polymerization of the second block was conducted using N-isopropylacrylamide (NIPAM) as monomer with a ratio among species [NIPAM]/[RAFT]/[AIBN] = 1000:1:0.1 in DMF at 65˚C. The reaction was followed by ^{1}H NMR to calculate conversion. The final product was characterized to be SiO_2-$PMAA_{185}$-b-$PNIPAM_{573}$, where subscripts represent the number of repeat units. TGA showed that the total polymer content was ~ 90% (Figure 4.3A). Fourier transform infrared spectroscopy (FTIR) (Figure 4.3B) of the nanoparticles confirmed the existence of block copolymer. The presence of a broad peak at ~3400 cm^{-1} ascribed to hydroxyl groups and the strong absorption at ~1700 cm^{-1} corresponding to C=O double bonds confirmed the successful attachment of PMAA chains. An additional peak at ~1546 cm^{-1} appeared after the second polymerization which is reported to be characteristic of N-H stretching,[24] confirmed the attachment of the PNIPAM block.

Figure 4.1. ^{1}H NMR characterization of surface-initiated polymerization of methacrylic acid.

Figure 4.2. ^{1}H NMR characterization of surface initiated polymerization of n-isopropylacyamide

400nm.
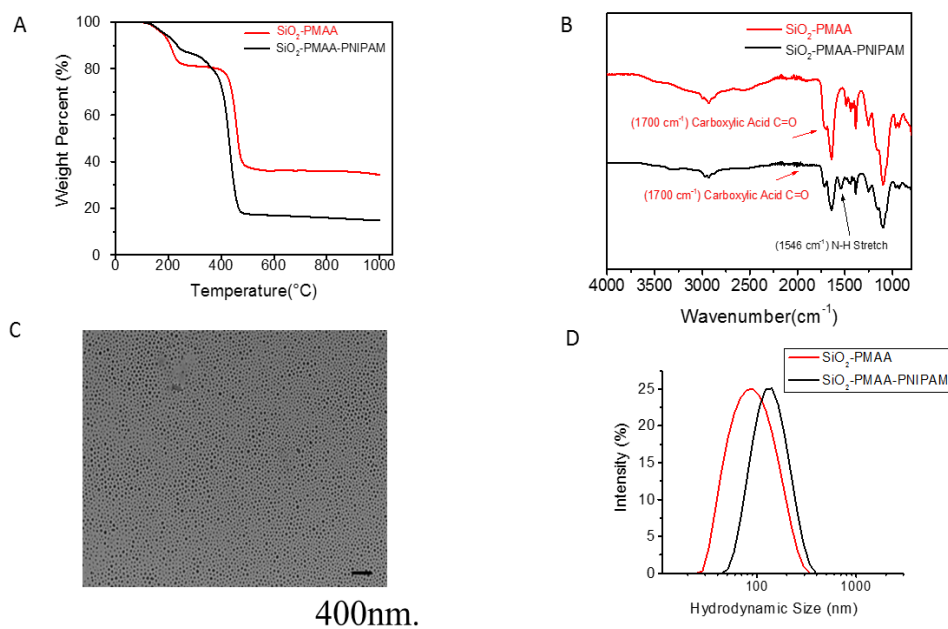
Figure 4.3. Characterization of SiO$_2$-PMAA and SiO$_2$-PMAA-b-PNIPAM nanoparticles. (A) Thermogravimetric analysis. (B) Infrared spectra. (C) TEM of aqueous solution of SiO$_2$-PMAA-b-PNIPAM particles. (D) Hydrodynamic size determined by DLS.

TEM and DLS studies. Both of the PMAA grafted and PMAA-b-PNIAPM grafted silica nanoparticles could be readily dispersed in water at neutral pH and room temperature. The individual nature of the nanoparticles was confirmed using transmission electron microscopy (TEM) as shown in Figure 4.3C. The hydrodynamic diameter of the particles was measured by dynamic light scattering (DLS) (Figure 4.3D). PMAA-SiO$_2$ particles had a Z-average diameter of 79.99nm with a narrow PDI of 0.168 indicating that particles were uniform in size. The SiO$_2$-PMAA-b-PNIPAM particles were found to have a Z-average diameter of 122.9nm, ~43nm larger than SiO$_2$-PMAA particles, which further confirmed the successful attachment of the second block.
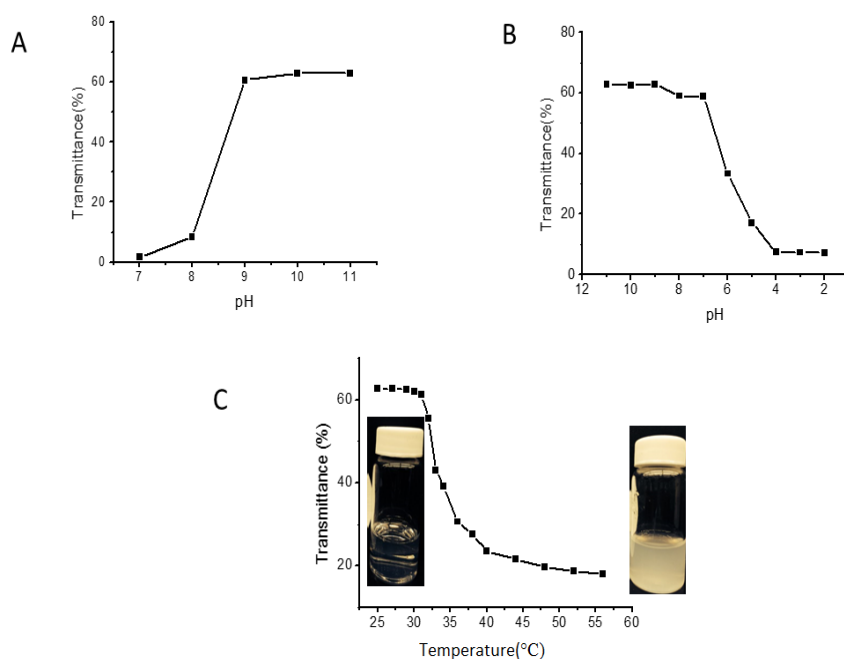
Figure 4.4. Transmittance curves with base (A) and acid (B) additions to aqueous SiO$_2$-PMAA-b-PNIPAM solution. (C) Transmittance change @300nm with increasing temperature of a SiO$_2$-PMAA-b-PNIPAM solution at pH 7.

Double Stimuli-Responsive Properties of SiO₂-PMAA-b-PNIPAM. The as-prepared SiO$_2$-PMAA-b-PNIPAM nanoparticles in aqueous solution responded to both pH and temperature as expected. Initial mixing between dried nanoparticles and DI water resulted in a slightly turbid solution, which cleared up immediately after addition of a small amount of base to break interpolymer hydrogen bonding.[25-26] Acid (1 equivalent) was then

Table 4.1. Loading content and entrapment efficiency with different feed ratios

DOX/particles weight ratio	Loading Content (%)	Entrapment Efficiency (%)
3:10	21.2 ± 0.2	89.8 ± 2.6
5:10	31.4 ± 0.4	91.6 ± 2.4
7.5:10	40.3 ± 0.2	90.2 ± 0.8
10:10	49.4 ± 0.3	97.5 ± 1.2

added to adjust the pH back to neutral and no aggregation occurred during the process. The turbidity change during the process was measured by UV-vis at 300 nm as shown in Figure 4.4.

The thermal responsive behavior of SiO$_2$-PMAA-b-PNIPAM particles was investigated using both optical spectroscopy and DLS. A transparent solution of particles dispersed in water at pH 7 was heated from room temperature to 57°C. As shown in Figure 4.4C, the transmittance decreased dramatically at 32°C, corresponding to the LCST of PNIPAM, indicating formation of aggregates due to decreased solubility of the PNIPAM corona. The aggregation of particles with increasing temperature was also monitored using

DLS. At room temperature, only one sharp peak was found corresponding to monodispersed particles. When temperature was raised above 32°C, a second peak centered at approximately 600nm appeared which represented the formation of aggregates.

In Vitro Drug Release of Doxorubicin. Doxorubicin (DOX) is a widely studied model drug that conjugates well with negatively charged polymers via electrostatic interactions.[21] At neutral pH, DOX molecules, with pKa 8.6, are positively charged, which leads to a strong interaction with negatively charged PMAA polymer chains. The loading content (LC) and entrapment efficiency (EE) of DOX in SiO_2-PMAA-b-PNIPAM were calculated to be 21.2% and 89.8% respectively when the weight percent of initial DOX feeding was 30%.[27] Compared with other core-shell type drug carriers[28-31], the ones prepared in this work showed significantly higher EE and LC. At least two factors contributed to this unusually high amount of DOX loading. First, high polymer content was achieved because of the small size of the cores and high graft density. TGA results showed that 90 wt% of the nanoparticles were polymer while the silica cores accounted for only 10 wt%. Second, once DOX was loaded onto PMAA chains, the outer PNIPAM layer will act as a shield to prevent loaded drug from escaping. Even higher loading content could be achieved with 50%, 75% and 100% feed ratio (Table 1). The *in vitro* DOX release profile from SiO_2-PMAA-b-PNIPAM particles (3:10 feed ratio) under different conditions is shown in Figure 4.5. The release performance was studied at both physiological pH (7.4) and lysosomal pH (5.0) conditions at temperatures of 25°C and 40 °C. The release profiles revealed that release rates depended on both pH and temperature. Only limited amounts of loaded DOX were released at pH 7, regardless of temperature; while under acidic condition, significant amounts of DOX could be released during the same period of time.

Approximately 50% of the loaded drugs were released at pH 5, 25°C, while more than 80% were released at pH 5, 40°C. The best release result was obtained at conditions of acidic pH and elevated temperature, which is the typical environment for cancer cells. The mechanism behind differences in release rates is depicted in Scheme 4.2. Electrostatic attraction between negatively charged polymer and positively charge DOX prevented significant release at neutral pH. However, at acidic conditions, protonation of the carboxylic acid groups of PMAA weakened the electrostatic interaction, enhanced DOX release. The release rate was further boosted by increasing temperature above LCST which collapsed the PNIPAM chains and caused the nanoparticles to agglomerate. The agglomeration process greatly reduced inter-particle spacing and squeezed out DOX at a higher rate. This temperature-controlled agglomeration behavior also allowed particles to

Equation	y = a + b*x		
Weight	No Weighting		
Residual Sum of Squares	0.00142		
Pearson's r	0.99759		
Adj. R-Square	0.99359		
		Value	Standard Error
	Intercept	-0.0515	0.02297
B	Slope	18.0229	0.72343
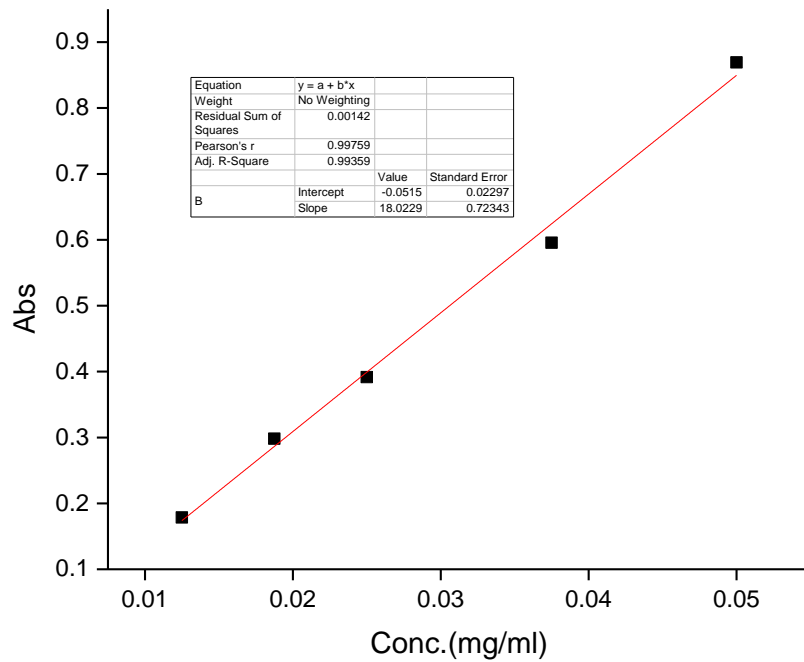
Figure 4.5. Calibration curve of Doxorubicin in water.
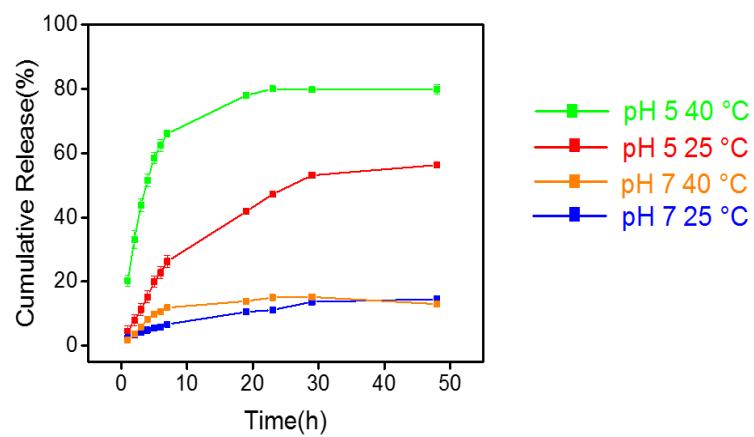
Figure 4.6. In vitro DOX release profile at different pH's and
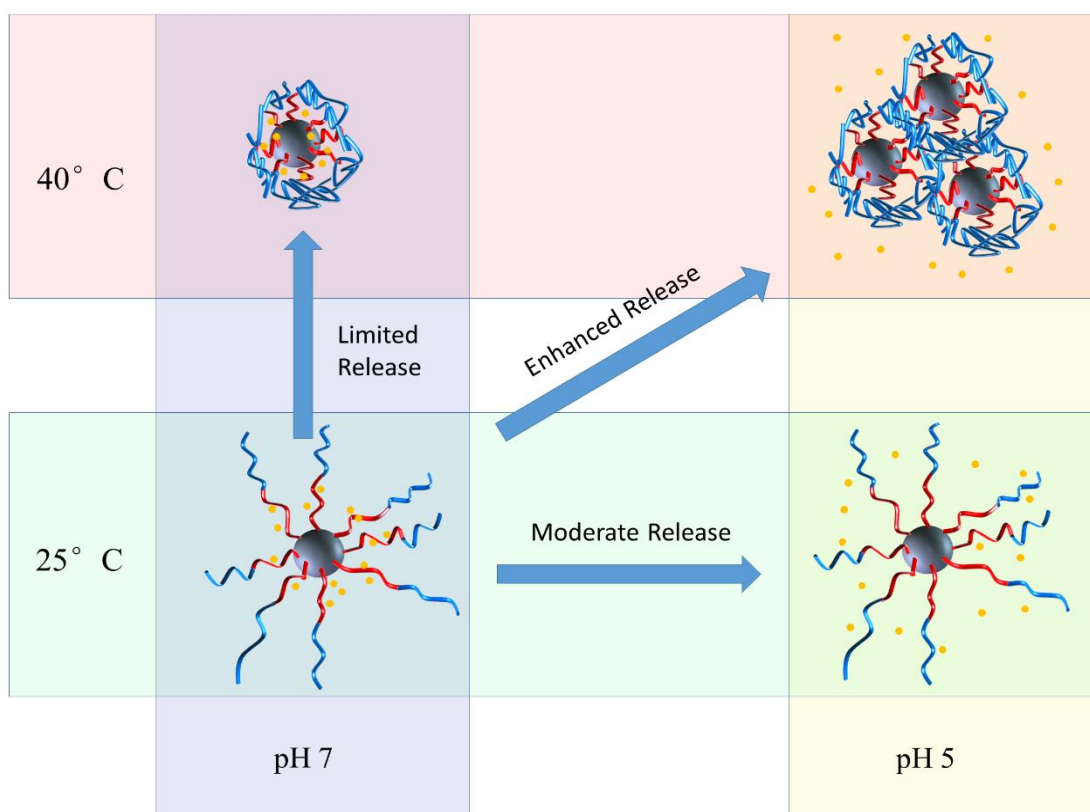
Scheme 4.2. Mechanism of stimuli-responsive drug release.
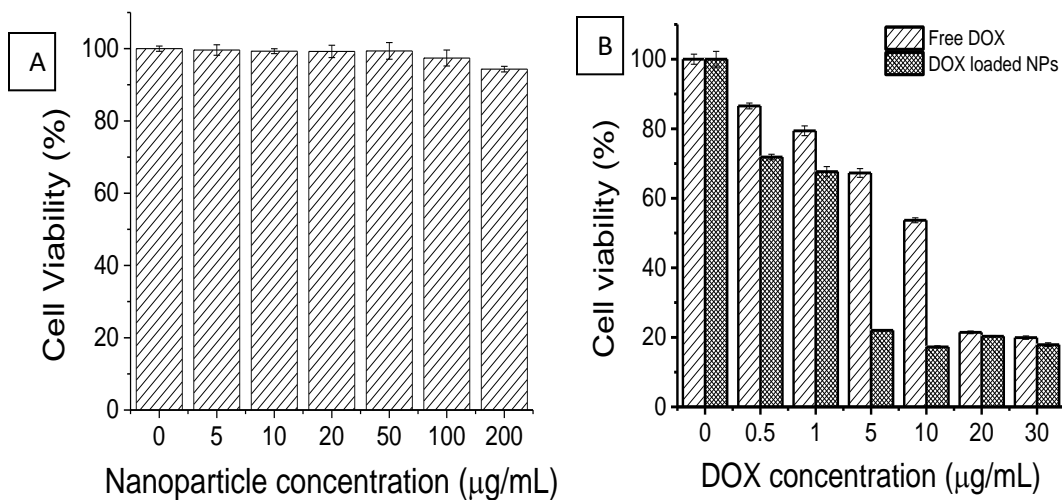
Figure 4.7 Relative cell viabilities of HeLa cells incubated with difference concentrations of (A) SiO_2-PMAA-b-PNIPAM nanoparticles and (B) DOX and DOX loaded SiO_2-PMAA-b-PNIPAM nanoparticles
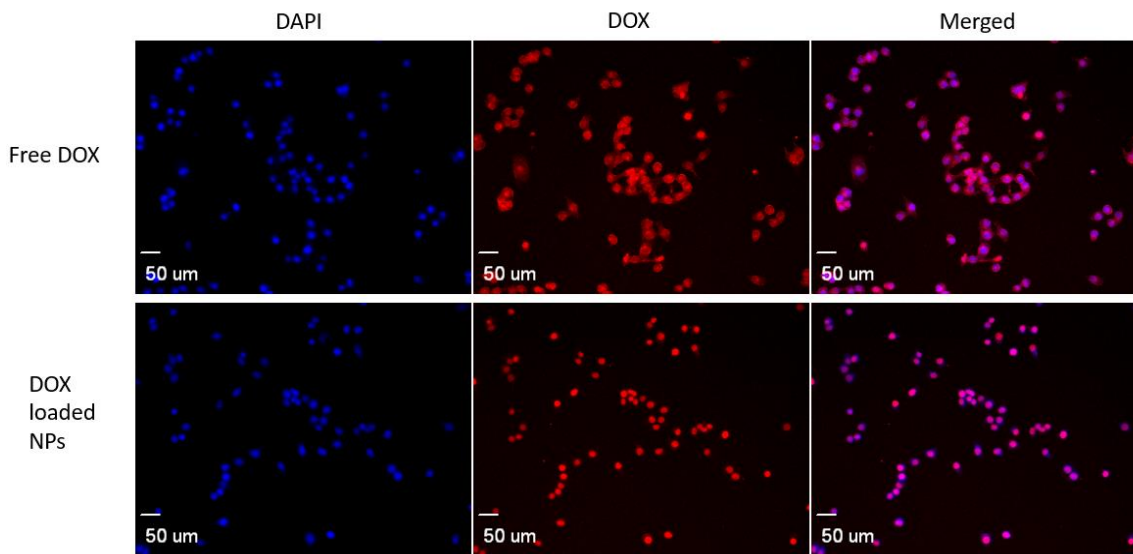
Figure 4.8. Cellular uptake analysis by confocal microscope

circulate without significant drug loss but precipitate and concentrate at places with elevated temperature. It is worth noting that the slight decrease of DOX after 30 hour for pH 7 and 40°C was because of thermal degradation of DOX at elevated temperature.[32]

Cell Uptake. Hela cells were incubated with free DOX and DOX loaded nanoparticles at 37°C. Figure 4.8 shows that after 4 hours, red fluorescence was observed around the nuclei of Hela cells in both cases, indicating that SiO_2-PMAA-b-PNIPAM nanoparticles are capable of internalizing into the nuclei of cancer cells.

4.5 Conclusions.

In this study, we demonstrated successful attachment of PMAA-b-PNIPAM block copolymers onto silica nanoparticles with high grafting density using surface-initiated RAFT polymerization. The resulting nanoparticles exhibited responses to both pH and temperature in aqueous solution as they dispersed individually at high pH and low temperature but agglomerated and precipitated out at acidic conditions or at elevated temperature. DOX was loaded onto these nanoparticles with very high loading content and entrapment efficiency and the release rate was found to be controlled by environmental pH and temperature. Cytotoxicity studies showed that DOX-loaded SiO_2-PMAA-b-PNIPAM nanoparticles are highly active against Hela cells, and more effective than free DOX of equivalent dose. The integration of these functionalities may result in SiO_2-PMAA-b-PNIPAM nanoparticles becoming ideal drug carriers for anti-cancer drug delivery and biomedical applications.

4.6 References

1. Miller, K. P.; Wang, L.; Benicewicz, B. C.; Decho, A. W., Inorganic nanoparticles engineered to attack bacteria. *Chemical Society Reviews* **2015,** *44* (21), 7787-7807.
2. Kumar, S. K.; Jouault, N.; Benicewicz, B.; Neely, T., Nanocomposites with Polymer Grafted Nanoparticles. *Macromolecules* **2013,** *46* (9), 3199-3214.
3. Erathodiyil, N.; Ying, J. Y., Functionalization of Inorganic Nanoparticles for Bioimaging Applications. *Accounts of Chemical Research* **2011,** *44* (10), 925-935.

4.   Liong, M.; Lu, J.; Kovochich, M.; Xia, T.; Ruehm, S. G.; Nel, A. E.; Tamanoi, F.; Zink, J. I., Multifunctional Inorganic Nanoparticles for Imaging, Targeting, and Drug Delivery. *ACS Nano* **2008,** *2* (5), 889-896.

5.   Li, J.; Wang, L.; Benicewicz, B. C., Synthesis of Janus Nanoparticles via a Combination of the Reversible Click Reaction and "Grafting to" Strategies. *Langmuir* **2013,** *29* (37), 11547-11553.

6.   Li, C.; Han, J.; Ryu, C. Y.; Benicewicz, B. C., A Versatile Method To Prepare RAFT Agent Anchored Substrates and the Preparation of PMMA Grafted Nanoparticles. *Macromolecules* **2006,** *39* (9), 3175-3183.

7.   Li, Y.; Krentz, T. M.; Wang, L.; Benicewicz, B. C.; Schadler, L. S., Ligand Engineering of Polymer Nanocomposites: From the Simple to the Complex. *ACS Applied Materials & Interfaces* **2014,** *6* (9), 6005-6021.

8.   Qiao, Y.; Islam, M. S.; Wang, L.; Yan, Y.; Zhang, J.; Benicewicz, B. C.; Ploehn, H. J.; Tang, C., Thiophene Polymer-Grafted Barium Titanate Nanoparticles toward Nanodielectric Composites. *Chemistry of Materials* **2014,** *26* (18), 5319-5326.

9.   Natarajan, B.; Neely, T.; Rungta, A.; Benicewicz, B. C.; Schadler, L. S., Thermomechanical Properties of Bimodal Brush Modified Nanoparticle Composites. *Macromolecules* **2013,** *46* (12), 4909-4918.

10.   Li, Y.; Wang, L.; Natarajan, B.; Tao, P.; Benicewicz, B. C.; Ullal, C.; Schadler, L. S., Bimodal "matrix-free" polymer nanocomposites. *RSC Advances* **2015,** *5* (19), 14788-14795.

11.   Zheng, Y.; Huang, Y.; Abbas, Z. M.; Benicewicz, B. C., Surface-initiated polymerization-induced self-assembly of bimodal polymer-grafted silica nanoparticles towards hybrid assemblies in one step. *Polymer Chemistry* **2016,** *7* (34), 5347-5350.

12.   Zheng, Y.; Huang, Y.; Abbas, Z. M.; Benicewicz, B. C., One-pot synthesis of inorganic nanoparticle vesicles via surface-initiated polymerization-induced self-assembly. *Polymer Chemistry* **2017,** *8* (2), 340-347.

13.   Wei, M.; Gao, Y.; Li, X.; Serpe, M. J., Stimuli-responsive polymers and their applications. *Polymer Chemistry* **2017,** *8* (1), 127-143.

14.   Liu, F.; Urban, M. W., Recent advances and challenges in designing stimuli-responsive polymers. *Progress in Polymer Science* **2010,** *35* (1–2), 3-23.

15.   Yang, Y.; Ding, X.; Urban, M. W., Chemical and physical aspects of self-healing materials. *Progress in Polymer Science* **2015,** *49–50*, 34-59.

16.   Li, Q.-L.; Xu, S.-H.; Zhou, H.; Wang, X.; Dong, B.; Gao, H.; Tang, J.; Yang, Y.-W., pH and Glutathione Dual-Responsive Dynamic Cross-Linked Supramolecular Network on Mesoporous Silica Nanoparticles for Controlled Anticancer Drug Release. *ACS Applied Materials & Interfaces* **2015,** *7* (51), 28656-28664.

17.   Zhou, H.; Wang, X.; Tang, J.; Yang, Y.-W., Tuning the growth, crosslinking, and gating effect of disulfide-containing PGMAs on the surfaces of mesoporous silica nanoparticles for redox/pH dual-controlled cargo release. *Polymer Chemistry* **2016,** *7* (12), 2171-2179.

18.   Cash, B. M.; Wang, L.; Benicewicz, B. C., The preparation and characterization of carboxylic acid-coated silica nanoparticles. *Journal of Polymer Science Part A: Polymer Chemistry* **2012,** *50* (13), 2533-2540.

19.   Li, Q.-L.; Gu, W.-X.; Gao, H.; Yang, Y.-W., Self-assembly and applications of poly(glycidyl methacrylate)s and their derivatives. *Chemical Communications* **2014,** *50* (87), 13201-13215.

20.   Schmaljohann, D., Thermo- and pH-responsive polymers in drug delivery. *Advanced Drug Delivery Reviews* **2006,** *58* (15), 1655-1670.

21.   Ma, W.-F.; Wu, K.-Y.; Tang, J.; Li, D.; Wei, C.; Guo, J.; Wang, S.-L.; Wang, C.-C., Magnetic drug carrier with a smart pH-responsive polymer network shell for controlled delivery of doxorubicin. *Journal of Materials Chemistry* **2012,** *22* (30), 15206-15214.

22.   Xu, Z.; Wang, D.; Guan, M.; Liu, X.; Yang, Y.; Wei, D.; Zhao, C.; Zhang, H., Photoluminescent Silicon Nanocrystal-Based Multifunctional Carrier for pH-Regulated Drug Delivery. *ACS Applied Materials & Interfaces* **2012,** *4* (7), 3424-3431.

23.   Wang, L.; Benicewicz, B. C., Synthesis and Characterization of Dye-Labeled Poly(methacrylic acid) Grafted Silica Nanoparticles. *ACS Macro Letters* **2013,** *2* (2), 173-176.

24.   Yang, Y.; Yan, X.; Cui, Y.; He, Q.; Li, D.; Wang, A.; Fei, J.; Li, J., Preparation of polymer-coated mesoporous silica nanoparticles used for cellular imaging by a "graft-from" method. *Journal of Materials Chemistry* **2008,** *18* (47), 5731-5737.

25.   Teresa Garay, M.; Cristina Llamas, M.; Iglesias, E., Study of polymer-polymer complexes and blends of poly(N-isopropylacrylamide) with poly(carboxylic acid): 1. Poly(acrylic acid) and poly(methacrylic acid). *Polymer* **1997,** *38* (20), 5091-5096.

26.   Ruiz-Rubio, L.; Laza, J.; Pérez, L.; Rioja, N.; Bilbao, E., Polymer–polymer complexes of poly(N-isopropylacrylamide) and poly(N,N-diethylacrylamide) with poly(carboxylic acids): a comparative study. *Colloid Polym Sci* **2014,** *292* (2), 423-430.

27.   Sahoo, B.; Devi, K. S. P.; Banerjee, R.; Maiti, T. K.; Pramanik, P.; Dhara, D., Thermal and pH Responsive Polymer-Tethered Multifunctional Magnetic Nanoparticles for Targeted Delivery of Anticancer Drug. *ACS Applied Materials & Interfaces* **2013,** *5* (9), 3884-3893.

28.   Chang, B.; Sha, X.; Guo, J.; Jiao, Y.; Wang, C.; Yang, W., Thermo and pH dual responsive, polymer shell coated, magnetic mesoporous silica nanoparticles for controlled drug release. *Journal of Materials Chemistry* **2011,** *21* (25), 9239-9247.

29.   Hu, X.; Hao, X.; Wu, Y.; Zhang, J.; Zhang, X.; Wang, P. C.; Zou, G.; Liang, X.-J., Multifunctional hybrid silica nanoparticles for controlled doxorubicin loading and release with thermal and pH dual response. *Journal of Materials Chemistry B* **2013,** *1* (8), 1109-1118.

30.   Chen, L.; Peng, Z.; Zeng, Z.; She, Y.; Wei, J.; Chen, Y., Hairy polymeric nanocapsules with ph-responsive shell and thermoresponsive brushes: Tunable permeability for controlled release of water-soluble drugs. *Journal of Polymer Science Part A: Polymer Chemistry* **2014,** *52* (15), 2202-2216.

31.   Tan, L.; Liu, J.; Zhou, W.; Wei, J.; Peng, Z., A novel thermal and pH responsive drug delivery system based on ZnO@PNIPAM hybrid nanoparticles. *Materials Science and Engineering: C* **2014,** *45* (0), 524-529.

32.   Beijnen, J.; Van der Houwen, O.; Underberg, W., Aspects of the degradation kinetics of doxorubicin in aqueous solution. *International journal of pharmaceutics* **1986,** *32* (2-3), 123-131.

33.   Wang, L.; Chen, Y. P.; Miller, K. P.; Cash, B. M.; Jones, S.; Glenn, S.; Benicewicz, B. C.; Decho, A. W., Functionalised nanoparticles complexed with antibiotic efficiently kill MRSA and other bacteria. *Chemical Communications* **2014,** *50* (81), 12030-12033.

CHAPTER 5

PREPARATION OF POLYISOPRENE-GRAFTED SILICA NANOPARTICLES AND THEIR COMPOSITES

5.1 Abstract.

The grafting of polyisoprene (PIP) to different types of silica has been studied and developed by the RAFT polymerization processes. This has been shown to be applicable for preparing grafted nanoparticles that are useful for exploring new surface interactions between silica fillers and rubber materials. Scale up approaches have been successful and detailed mechanical property studies have been conducted to assess the potential of these new graft architectures on improving rubbery composite properties.

5.2 Introduction

Polymer-grafted nanoparticles are of great interest due to their applications in sensors, coatings, optoelectronics, and nanocomposites.[1-4] RAFT polymerization has proven to be a powerful controlled radical polymerization technique for the preparation of polymer-grafted particles due to the easy attachment and precise control over the grafting densities of RAFT agents. Since the first report on the application of surface-initiated RAFT polymerization in the modification of silica particles using a surface-anchored RAFT agent by Tsujii et al.[5] to date, surface-initiated RAFT technique has been utilized in the surface modification of various nanoparticles with a wide range of polymers.[6-14]

Polyisoprene has been recognized as an important class of rubber materials and has been used in the automotive industry and medical applications.[15-17] Polyisoprene contains many double bonds in the polymer backbone which allows for further functionalization or chemical modifications. Isoprene polymers have been prepared by anionic,[15,18,19] cationic,[20,21] and radical polymerizations,[22,23] among which anionic polymerization has been the major method for the synthesis of such polymers. Anionic polymerization gives well-controlled polymerization with narrow polydispersity, however, it is expensive and is

93

not compatible with electrophilic and acidic functional groups and is challenging in the presence of contaminants.

Surface polymerization of isoprene has been reported by free radical photopolymerization and living anionic polymerization from the surface of silica particles. Binder et al.[24] applied anionic polymerization on the surface of silica nano- and glass particles. They modified the surface of particles with a diphenylethylene silane agent from which anionic addition of isoprene monomer was initiated. Derouet et al.[25] used free radical photopolymerization to graft polyisoprene onto the surface of micro-size silica particles. Particles were functionalized with N, N-diethyldithiocarbamate iniferter groups following with polymerization of isoprene under UV light.

There has been some work on controlled radical polymerization (CRP) of isoprene by RAFT and nitroxide-mediated polymerization (NMP). Perrier et al.[26] and also Wooly et al.[27] have independently reported RAFT polymerization of isoprene in bulk using a high temperature stable trithiocarbonate RAFT agent. However, to the best of our knowledge, surface polymerization of isoprene has not been performed by any of these CRP techniques. In this work, we propose an in-depth investigation of the surface-initiated RAFT polymerization of isoprene on silica nanoparticle surfaces and their dispersion and properties in polyisoprene matrices.

5.3 Experimental Section

Materials. Isoprene was obtained from TCI America and was purified by passage over a neutral alumina prior to use. The RAFT agent 4-cyano-4-(dodecylsulfanylthiocarbonyl) sulfanylpentanoic acid (DOPAT) (97%) and 2-methyl-2-

[(dodecylsulfanylthiocarbonyl) sulfanyl]propanoic acid (MDSS) (97%) were purchased from Strem Chemicals and used as received. Spherical SiO_2 nanoparticles with a diameter of 14 ± 4 nm were purchased from Nissan Chemical Co. Tetrahydrofuran (THF) (HPLC grade, Fisher), dicumyl peroxide (Acros, 99%), and aminopropyldimethylethoxysilane (Gelest, 95%) were used as received. ZEOSIL 1165mp silica powders were acquired from Solvay.

Bulk polymerization of isoprene. Isoprene (5 g, 73 mmol), DOPAT (30 mg, 74 µmol) and dicumyl peroxide initiator (4 mg, 14.3 µmol) with a ratio between species of [monomer]:[CTA]:[initiator] = 1000:1:0.2 were added to a Schlenk tube. The mixture was degassed by three freeze-pump-thaw cycles, filled with nitrogen, and then the Schlenk tube was placed in an oil bath set at 120 °C. The polymerization was stopped by quenching in ice water. Molecular weights were measured using gel permeation chromatography (GPC) in THF which was calibrated with poly(methyl methacrylate) standards.

Synthesis of DOPAT-g-SiO₂. A solution (20 mL) of colloidal silica particles (30 wt % in methyl isobutyl ketone) was added to a two-necked round bottom flask and diluted with 110 mL of THF. Dimethylmethoxy-n-octylsilane (0.1 mL) was added to improve dispersibility along with 3-aminopropyldimethylethoxysilane (0.32 mL, 2 mmol) and the mixture was refluxed in a 75 °C oil bath for 5 hours under nitrogen protection. The reaction was then cooled to room temperature and precipitated in a large amount of hexanes (500 mL). The particles were then recovered by centrifugation and dispersed in THF using sonication and precipitated in hexanes again. The amine-functionalized particles were then dispersed in 40 mL of THF for further reaction. Then 0.2 g, (0.4 mmol) of activated DOPAT was prepared and added dropwise to a THF solution of the amine functionalized

silica nanoparticles (40 mL, 6 g) at room temperature. After complete addition, the solution was stirred overnight. The reaction mixture was then precipitated into a large amount of hexanes (400 mL). The particles were recovered by centrifugation at 3000 rpm for 8 min. The particles were then redispersed in 30 mL THF and precipitated in hexanes. This dissolution−precipitation procedure was repeated 2 more times until the supernatant layer after centrifugation was colorless. The yellow DOPAT-anchored silica nanoparticles were dried at room temperature and analyzed using UV analysis to determine the chain density using a calibration curve constructed from standard solutions of free DOPAT.

Surface-initiated RAFT polymerization of isoprene. Isoprene (1.22 g, 17.8 mmol), DOPAT-g-silica NPs with surface density of 41.9 µmol/g (0.17 chs/nm^2) (80 mg, 3.27 µmol), THF (2 ml) and dicumyl peroxide initiator (0.67 mmol) with a ratio between species of [monomer]:[CTA]:[initiator] = 5000:1:0.2 were added to a Schlenk tube. The particles were dispersed into the solution via sonication for 1 min and subsequently the mixture was degassed by three freeze-pump-thaw cycles, filled with nitrogen, and then the Schlenk tube was placed in an oil bath set at 120 °C for various intervals. The polymerization was stopped by quenching in ice water. The resultant polymer grafted particles were then precipitated into a large amount of isopropanol and centrifuged at 8,000 rpm for 12 min and the particles were dispersed back into THF.

5.4 Results and Discussion

5.4.1 General RAFT polymerization of isoprene from DoPAT-functionalized silica nanoparticles

The general procedure of attaching RAFT agent onto NP surfaces and the subsequent surface initiated RAFT polymerization is illustrated in Scheme 5.1. The

attachment of DoPAT onto silica nanoparticles was confirmed by UV-vis spectrometry. The amount of RAFT agent anchored onto the modified silica nanoparticles was determined quantitatively by comparing the absorption at *ca.* 300 nm for the DoPAT anchored silica nanoparticles to a standard absorption curve made from known amounts of the free DoPAT. NPs with a wide range of graft densities were used throughout the study (0.005 chs/nm^2 to 0.42 chs/nm^2). It should be noted that graft density higher than 0.42 chs/nm^2 could also be achieved, but was not explored because higher graft density will lead to lower silica weight percent in composites, which does not meet the interest of this study.

Kinetic studies of the SI-RAFT polymerization of PIP were conducted at two different graft densities as well as using free RAFT agent. The results (Figure 5.1) showed that there is a good linear relationship between $\ln(M_0/M_t)$ vs time and Mn versus conversion, which indicates a constant radical concentration throughout the reaction and the living character of the polymerizations.
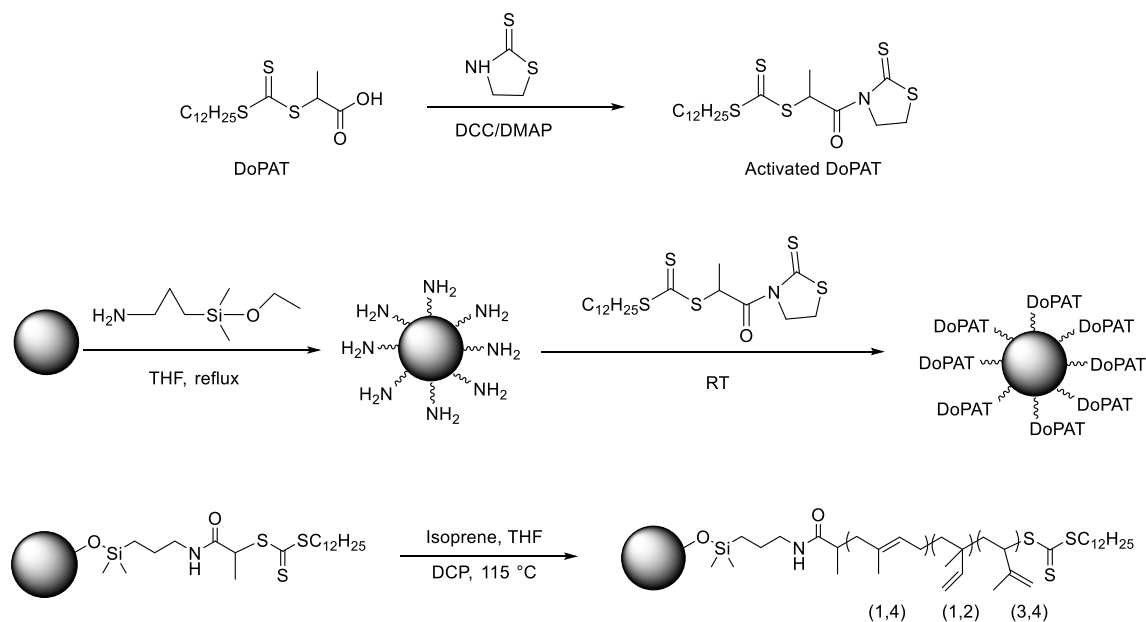
Scheme 5.1. Synthetic scheme of PIP grafted silica NPs.

97
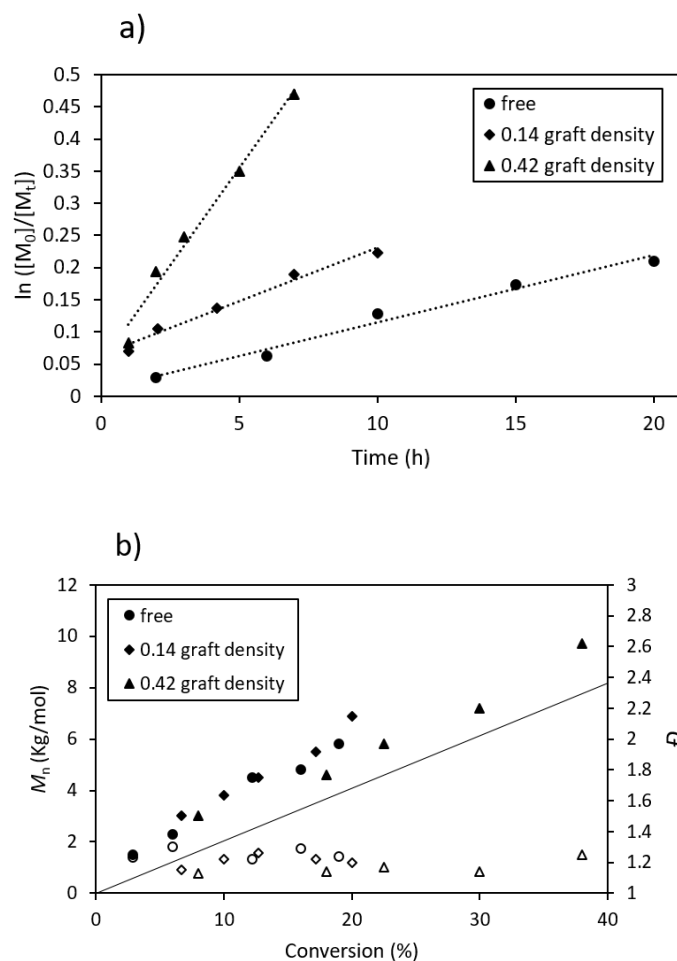
Figure 5.1. (a) First-order kinetic plots and (b) dependence of molecular weight (solid line, $M_{n, theory}$) on the conversion for the SI-RAFT polymerization of isoprene on silica nanoparticles; high surface density (triangle, 100 µmol/g, 0.42 ch/nm^2); low surface density (diamond, 32 µmol/g, 0.14 ch/nm^2); free DoPAT, (circle). All polymerizations were conducted under identical conditions with the ratio of [monomer]:[CTA]:[initiator] = 300:1:0.1.

5.4.2 Targeting high molecular weight (100K) of grafted PIP.

Although the polymerization kinetics at low monomer feed ratio was elucidated,

the preparation of high molecular weight PIP grafted NPs (>50K) remained problematic

mainly caused by gelation of the reaction system. However, high molecular weight of PIP

is desired in some cases to achieve good dispersion of NPs in polymer matrices especially

when low graft densities might be desired. We speculate there were two potential reasons

98

behind gelation. One, the poor solubility of high molecular weight PIP in the current THF

solvent system. Two, the inter-particle radical recombination that occurred when monomer

conversion was high and chain extension became ineffective. To explore this gelation

behavior, we performed studies to optimize the various reaction conditions.

Table 5.1 Polymerization details for attempts to achieve high molecular weight grafted PIP.

Sample No.	RAFT: Isoprene: Initiator	Temperature (°C)	Solvent	Solvent/ monomer ratio	Gelation Time (h)	Mn of PIP	PDI
1	1:2000:0.15	120	THF	1.5:1	3.5	18K	1.32
2	1:5000:0.2	120	THF	1:10	3.5	N/A	N/A
3	1:5000:0.2	120	4:1 Toluene/THF	1.5:1	5	54K	1.76
4	1:10000:0.2	120	15:1 Toluene/THF	2:1	9.5	41.4K	1.92
5	1:10000:0.1	115	15:1 Toluene/THF	2:1	No gelation until 32.5h	97K	1.83

As listed in the table, at high monomer feed ratio, gelation occurred soon after

polymerization started. (sample 1) This gelation time was found to be delayed to 9.5 h by

switching the solvent system from pure THF to a toluene/THF co-solvent system

presumably due to better solubility of high Mw PIP in toluene. Gelation was totally avoided

by lowering the reaction time as well as lowering the initiator feed ratio with the aim of

lowering the total radical concentration in the system. As shown in sample 5, 97K PIP

grafted NPs were prepared without gelation. Thus, we expanded our synthesis capability to a very broad range for future studies.

5.4.3 Breakdown, functionalization, and SI-Polymerization of Commercial (ZEOSIL 1165MP) silica nanoparticles.

We obtained commercially available silica powders (ZEOSIL 1165MP) and performed a series of tests to breakdown these micrometer sized particles into the nanometer range and successfully functionalized them with RAFT agent followed by coverage with PIP. As shown in Figure 5.2, we dispersed the ZEOSIL silica nanoparticles in DMF and applied sonication using a high power sonicator probe for 2 hours.
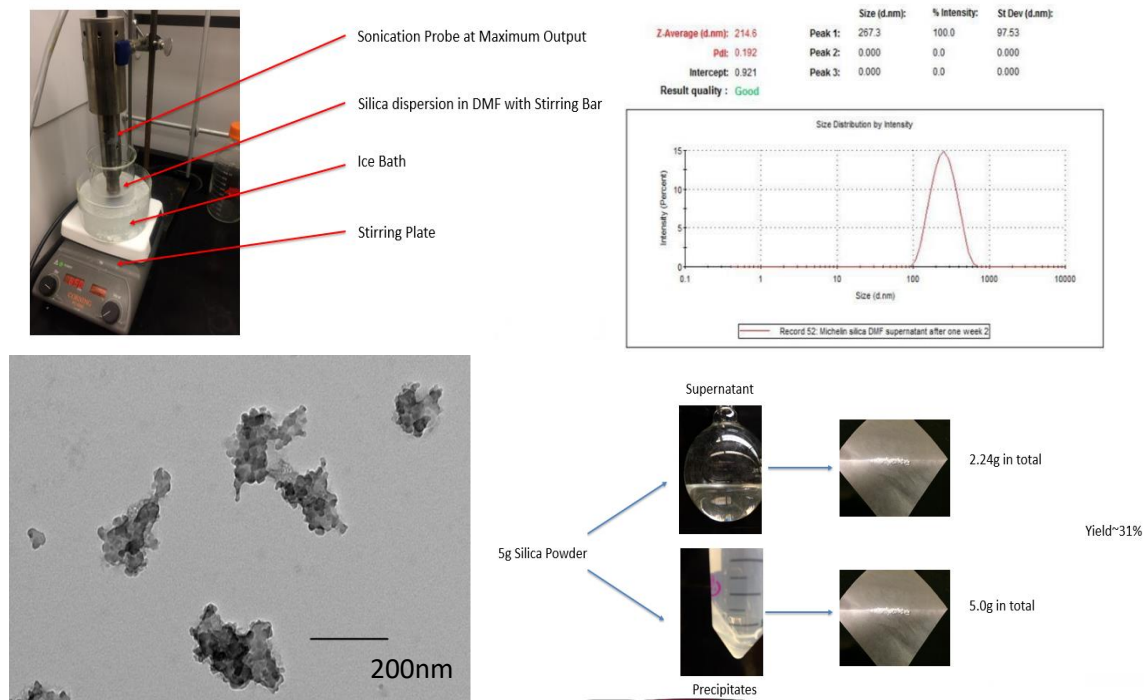
Figure 5.2. Breakdown of ZEOSIL silica particles with sonicator.

It could be seen from the DLS and TEM results that the micron-sized silica particles were broken down into nanometer range clusters. The diameters of the clusters from DLS were between 200 to 300 nm, which agreed with that observed with TEM. However, it was found that not all of the ZEOSIL 1165MP particles could be broken down even with prolonged sonication. Thus, the solution after sonication was centrifuged. The supernatant and precipitates were separated and quantified via silica content. As shown in the Figure 5.2, a typical case starting from 8g silica powder resulted in 2.24g in the form of nano-clusters in solution, and 5g undissolved precipitates, corresponding to ~31% yield. The particles were then treated with aminosilane, and activated RAFT agent. The particles acquired the yellow color after reaction, suggesting successful attachment, which was then confirmed by UV-vis analysis. SI-polymerizations from the RAFT attached particles were performed at Monomer: RAFT: Initiator=5000:1:0.2 at 120°C for 12hrs. Polymers with MW of 43.K and PDI 2.25 were obtained. With prolonged reaction times, 103K polymers with 2.27 PDI could be prepared in 24 hours. It is worth noting that the SI-polymerization from these ZEOSIL silica nanoparaticles tended to result in higher PDI than the polymerizations performed with spherical nanoparticles. We assume that the irregular shape of the cluster contributed to this PDI broadening effect. The clusters, which consist of fused primary silica nanoparticles possess silica surfaces with different accessibility. Thus, the better exposed surfaces would experience higher polymerization rates, while the less exposed surfaces would experience lower polymerization rates. As a result, PIP with higher PDI's were obtained. Thus, the complete procedure from commercially available silica micron-particles to well-defined PIP grafted silica nanocomposites was well established. Although the current research is focused on the mechanical properties of

spherical silica nanocomposites, the study of nanocomposites from these nano-clusters would be of great interest for future study.
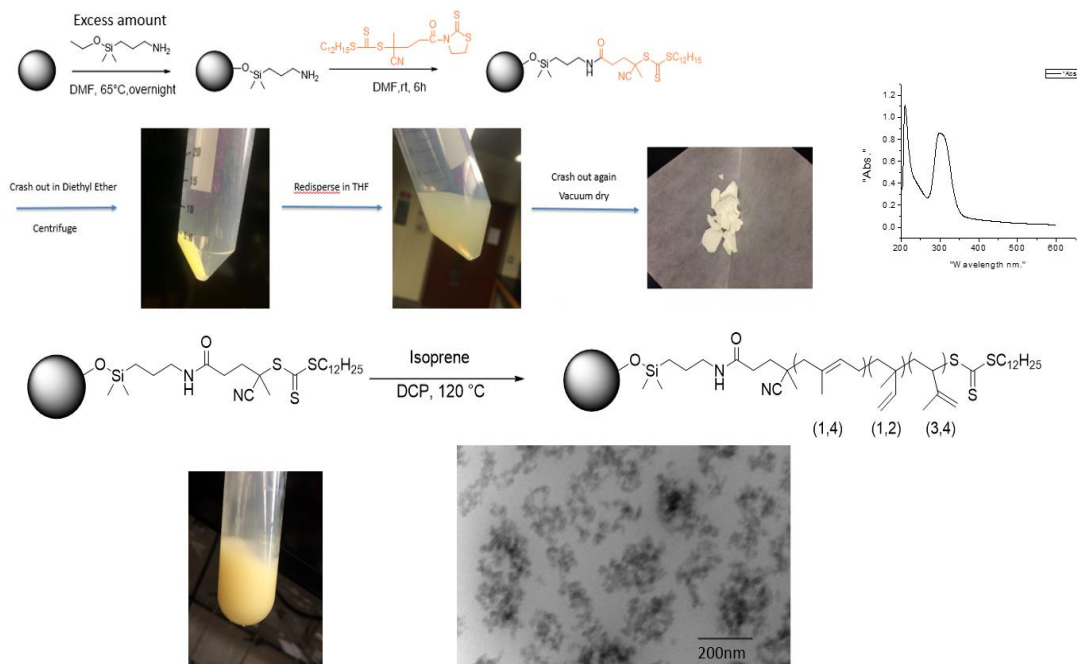
Figure 5.3. Grafting PIP from ZEOSIL silica clusters.

5.4.4 Scale-up synthesis of PIP grafted NPs.

In order to perform various mechanical testing for the PIP composites, it was necessary to scale up the current synthesis procedure to the kilogram scale. However, the simple extension of the small scale procedure to larger glassware was not appropriate with the conditions needed for the SI-Polymerization of PIP. The reaction system needs to be air-free, and capable of holding the pressure built up at reaction temperatures. Based on these needs, we converted an oven into a polymerization reactor by equipping it with a rotating arm through the center of the oven. Stainless steel tubes could be attached to this

rotating arm, thus supplying a method to continuously agitate the reaction mixture. The polymerizations could be conducted in stainless steels tubes with various sizes as shown in Figure 5.4. An air-free environment was realized by N_2 sparging, and the tubes were then sealed with stainless steel screws covered with double layer Teflon tape. This scale-up process was used routinely to prepare PIP grafted NPs at the 20g silica scale.

Figure 5.4. Experimental set-up for kilogram scale synthesis of PIP grafted NPs.

For our intended studies, we prepared the scale up samples shown in Table 5.2 using Nissan silica nanoparticles. We selected three grafting densities and targeted three different molecular weights for each sample to gain insights into the influence of each factor on mechanical behavior of the composites.

Table 5.2 Scale-up samples for PIP grafted NPs.

No.	Scale	Graft density	Molecular weight
1	~20g silica	0.08 chs/nm^2	51k
2	~20g silica	0.08 chs/nm^2	39k
3	~20g silica	0.08 chs/nm^2	15k
4	~15g silica	0.12 chs/nm^2	13k
5	~15g silica	0.12 chs/nm^2	22k
6	~15g silica	0.12 chs/nm^2	35k

5.4.5 Tensile testing of PIP silica composites.

SKI-3 polyisoprene (Mw=300 kDa, 100% cis) was used in this study as the polymer matrix. For all silica/PIP composites, 36 wt% silica loading was targeted (20 wt% silica) which is a typical loading in commercial tire applications. The PIP silica nanocomposites were prepared as follows:

20 g SKI-3 PIP matrix were dissolved in 300ml toluene. 1.6 phr VulCup® R crosslinking peroxide (Arkema) was added as a curing agent. Predetermined amounts of about solution were taken, which was then mixed with PIP grafted NP solution to achieve the target silica loading. The mixture was allowed to stir overnight and then poured into a

Teflon mold to form a thin film (0.1 to 1.0 mm thickness) under vacuum. The dried film was then hot pressed at 165 °C for 45 min (4 metric tons).

We first used 50K PIP grafted NPs with 0.015ch/nm^2 to investigate the stress-strain behavior of the PIP silica nanocomposites. The stress-strain cures are shown in Figure 5.5. It was clear that the added silica improved the stress at break compared with pure PIP matrix. The sample with bare ZEOSIL silica resulted in low tensile strain, which was due to severe agglomeration of the silica particles without surface coating. The sample with bare Nissan silica showed higher tensile stress with a decrease in tensile strain compared to the unfilled matrix. The composite with 50K PIP grafted Nissan silica showed 18% increase in elongation and 187% increase in tensile stress at break compared with pure matrix, indicating a strong reinforcement effect.
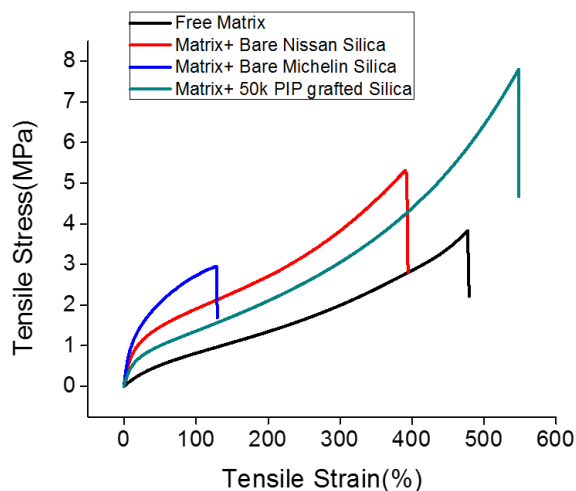
Figure 5.5. Tensile-stress curve of SKI-3 nanocomposites and unfilled matrix.

5.4.6 Effect of molecular weight on tensile-stress behavior of PIP/silica composites.

We prepared additional samples at two different graft densities and varied the molecular weight of grafted PIP for each density to investigate the effect of molecular weight and graft density on the tensile stress-strain behavior of PIP/silica composites using Nissan silica NPs. The tensile-stress curves shown in Figure 5.6 showed improved tensile stress at break for silica filled samples. One interesting finding is the appearance of a new feature in the 0.1 to 10 strain region, particularly for 39k and 51k PIP grafted NPs samples. This increase in modulus at low strain region is of particular interest in tire rubber. The 15 kDa PIP grafted NPs sample showed increased modulus in 0.1 to 1 strain region but showed no real difference with free matrix in the 1 to 10 strain regions. Comparitively 39K and 51k PIP grafted NPs samples showed significant improvement in modulus from 1 to 10 strain region, with no big difference between the two samples. Considering that the reported critical entanglement molecular weight of polyisoprene is 13300 ± 1400 g/mol determined from rheology tests by Fetters *et al.* and 14000-15000 from concentrated solutions,[28] both of which are close to 15 kDa, we can presume that the difference in properties between the 15k composite sample and the 39k & 50k composite samples is the because of different states of polymer chain entanglement. In 15k composite samples, the entanglement between surface grafted chains and the matrix is relatively weak, while in 39k and 50k composite samples such entanglement interaction is much stronger that resulted in improved mechanical properties.
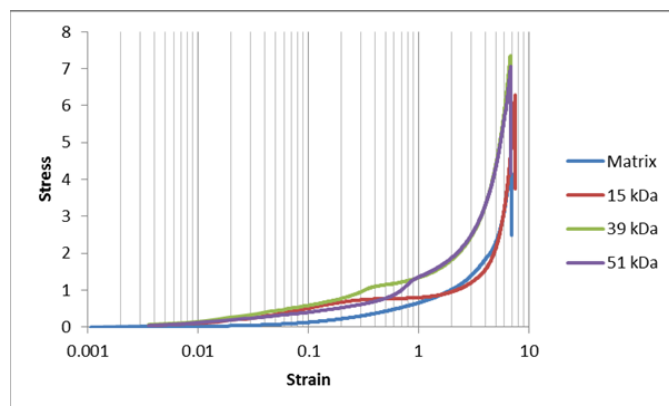
Figure 5.6. Tensile-stress curves of SKI-3 nanocomposites.

The DMA results of the 0.08 graft density NPs with different molecular weights are presented in Figure 5.7. It was clear that compared with free matrix, all three silica filled PIP samples showed significant improvements in the storage modulus in the rubbery state (top graph). There was also a slight improvement of E' with increasing molecular weight from the 15K to 39K and 51K PIP grafted NP samples which were nearly identical. In a strain-sweep test (Figure 5.7, bottom graph), all three silica filled PIP samples showed decreased E' with increasing strain. These result shows that while the added fillers did improve the storage modulus significantly, the dispersion state is not optimized. In the case of rubber composites with perfectly dispersed fillers, filler-filler interactions were minimized so that storage modulus should remain almost unchanged with an increase in strain.[29]
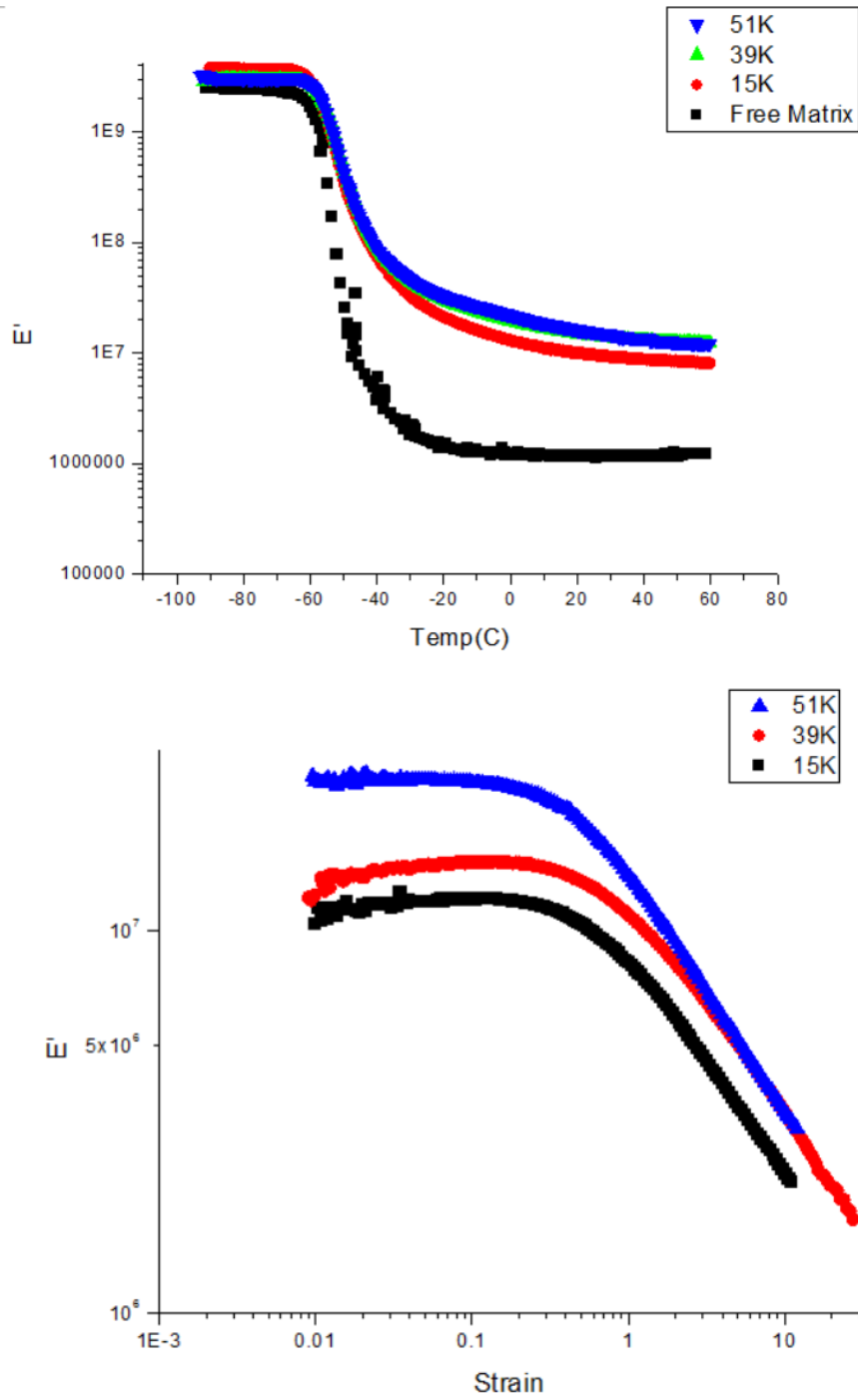
Figure 5.7. DMA analysis of SKI-3 nanocomposites. Top graph, temperature dependence of E' at 10Hz; bottom graph, strain sweep at 25°C.

5.4.7 Dispersion studies in polyisoprene matrices.

The dispersion state of PIP grafted NPs in polyisoprene matrix was studied by TEM and SAXS.

An example of 39K PIP grafted NPs in SKI-3 matrix is presented in Figure 5.8. We found that TEM may not be as good in determining particle dispersion state at these high nanoparticle loadings as at low particle loading. At 20 volume percent loading, particles may appear to be agglomerated even when they are well-distributed because of high particle density in the matrix. However, by looking at certain regions, (see arrow in the
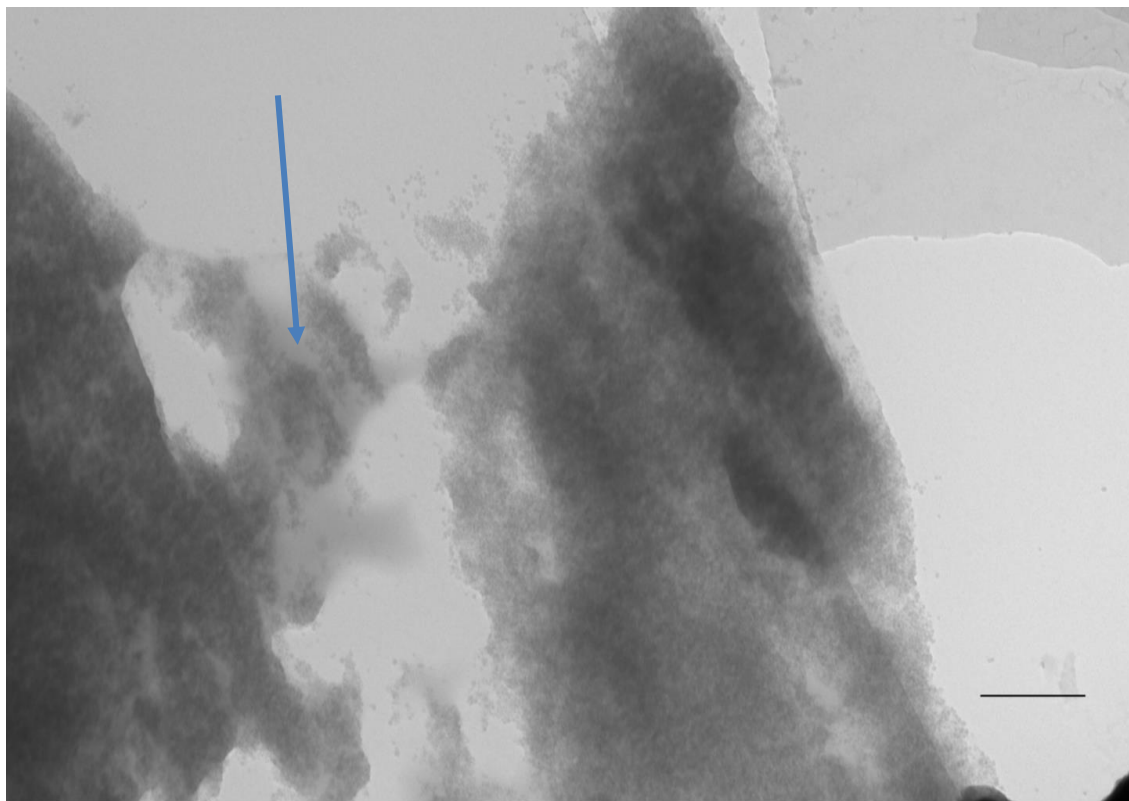
Figure 5.8. TEM of SKI-3 nanocomposites. Scale bar 500 nm.

figure), we could see regions without particle fillers and regions with particle fillers. When interpreted with previous DMA data, we can presume that good dispersion was not achieved at this graft density.
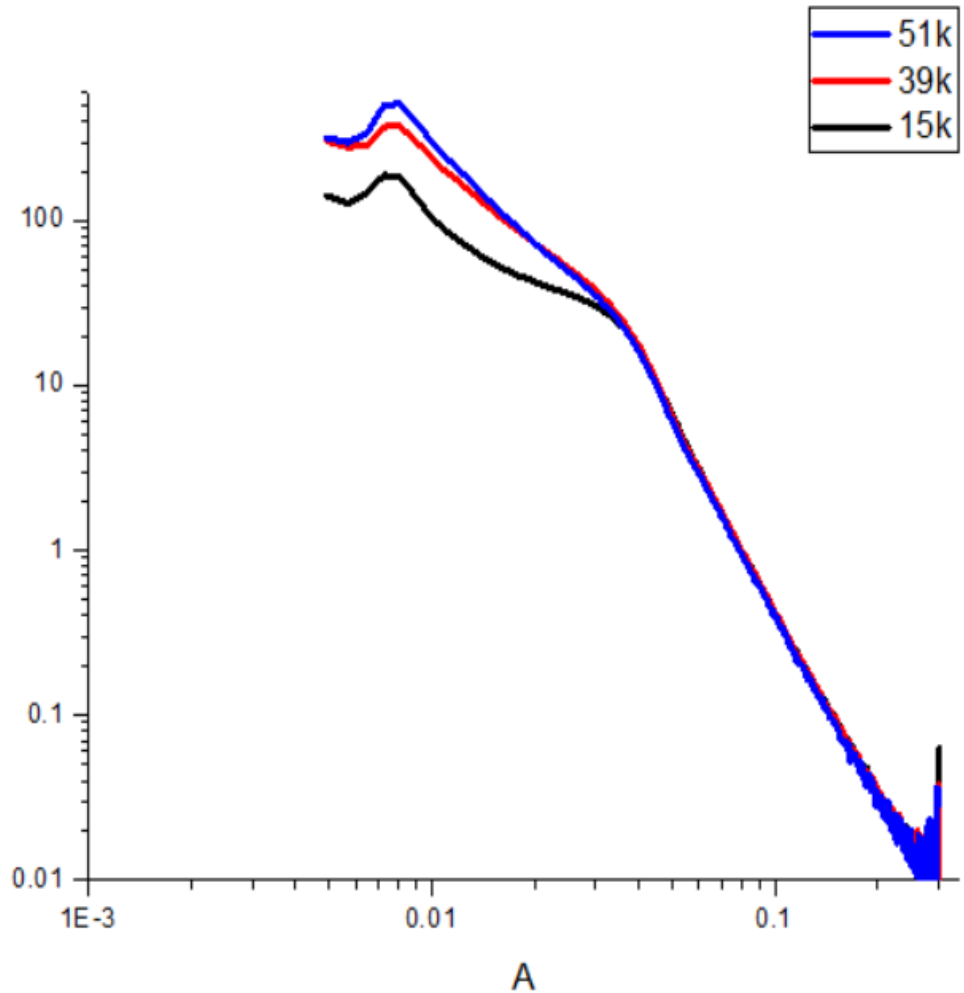
Figure 5.9. SAXS analysis of SKI-3 nanocomposites.

SAXS data (Figure 5.9) also indicate particle agglomeration at 0.08 chs/nm^2 graft density, for all three molecular weights. The q value (0.035) of the scattering peak corresponds to 18 nm particle spacing, which is very close to the diameter of the silica nanoparticles and clearly suggests that particles are together instead of separately dispersed in the matrix. However, the intensity of the peak had a decreasing trend from low m.w to high m.w, indicating some improvement in the dispersion state.

We think that there are two possible reasons for poor particle dispersion at this stage. One is the incompatibility between the SKI-matrix (pure cis PIP) and the grafted polymer (1:2 cis to trans ratio PIP). The second likely effect is the strong particle-particle interaction caused by insufficient particle surface coverage. However, if we pursue high graft density and high molecular weight of grafted polymer at the same time, it would be hard to achieve the desired silica loading (33 wt%). If fact, the silica weight percent of the PIP grafted particles has to be at least 50 wt% considering the diluting effect in the following mixing steps. As shown in Table 5.4, if we increase graft density to 0.2 chains/nm^2, then molecular weight of grafted polymer has to be limited to 20k. At 0.4 chains/nm^2 graft density, molecular weight cannot exceed 10k. On the other hand, current data suggests that both high graft density and high molecular weight is desired for better dispersion. To solve this problem, we believe that a bimodal approach should be adopted in the next step. In the bimodal approach, a high molecular weight population PIP at low graft density will be grafted in the first step. Then the uncovered surfaces remained will be grafted with a dense, low molecular weight population PIP or even small organic ligands. We would expect a much better dispersion state and even better improved mechanical properties from these rubber composites.

Table 5.4 Design of experiments of graft densities and chain MW.

	Chain MW			
Graft Dens	10000	20000	40000	100000
0.8	0.33	0.20	0.11	0.05
0.4	0.50	0.33	0.20	0.09
0.2	0.67	0.50	0.33	0.17
0.1	0.80	0.67	0.50	0.29
0.05	0.89	0.80	0.67	0.45
0.025	0.94	0.89	0.80	0.62
0.01	0.98	0.95	0.91	0.80

5.5 Conclusion

In this chapter, we studied the surface-initiated RAFT polymerization of polyisoprene from two types of silica particles. The polymerization kinetics on spherical particles were studied at different graft density and polymerization formulation was further optimized to target over 100k molecular weight grafted polymers. ZEOSIL 1165mp silica powders were used as an alternative silica source, which were broken down into ~200 nm silica clusters by sonication, which were then successfully grafted with polyisoprene as well. The synthetic procedure of PIP grafted Nissan silica nanoparticles were successfully scaled up from gram scale to kilogram scale by employing stainless steel tubes as reaction vessels in a heated oven. The PIP grafted Nissan silica nanoparticles were used as reinforcing fillers to improve the mechanical properties of SKI-3 polyisoprene matrix. Tensile testing showed that composites with 50K PIP grafted Nissan silica showed significant (187%) increase in tensile stress at break compared with pure matrix, indicating a strong reinforcement effect. Dynamic mechanical analysis showed significant improvements in the storage modulus in the rubbery state for the silica filled samples compared with unfilled matrix. Although the mechanical testing results were encouraging, TEM, SAXS and strain-sweep DMA results suggested that optimized nanoparticle dispersion has not yet been achieved. Partial nanoparticle aggregation existed probably due to insufficient particle surface coverage, which could be potentially improved by using a bimodal polymer grafting architecture.

5.6 References

(1)   Zou, H.; Wu, S.; Shen, J. Polymer/Silica Nanocomposites: Preparation, Characterization, Properties, and Applications. Chem. Rev. **2008**, *108*, 3893−3957.

(2)   Moad, G.; Rizzardo, E.; Thang, S. H. Living Radical Polymerization by the RAFT Process. Aust. J. Chem. **2005**, *58*, 379−410.

(3)   Gangopadhyay, R.; De, A. Conducting Polymer Nanocomposites: A Brief Overview. Chem. Mater. **2000**, *12*, 608–622.

(4)   Sanchez, C.; Lebeau, B.; Chaput, F.; Boilot, J. P. Optical Properties of Functional Hybrid Organic–Inorganic Nanocomposites. Adv. Mater. **2003**, *15*, 1969–1994.

(5)   Tsujii, Y.; Ejaz, M.; Sato, K.; Goto, A.; Fukuda, T. Mechanism and Kinetics of RAFT-Mediated Graft Polymerization of Styrene on a Solid Surface. 1. Experimental Evidence of Surface Radical Migration. Macromolecules **2001**, *34*, 8872–8878

(6)   Li, C. Z.; Benicewicz, B. C. Synthesis of Well-Defined Polymer Brushes Grafted onto Silica Nanoparticles via Surface Reversible Addition−Fragmentation Chain Transfer PolymerizationMacromolecules **2005**, *38*, 5929–5936.

(7)   Perrier, S.; Takolpuckdee, P.; Mars, C. A. Reversible Addition−Fragmentation Chain Transfer Polymerization: End Group Modification for Functionalized Polymers and Chain Transfer Agent Recovery. Macromolecules **2005**, *38*, 6770–6774.

(8)   Li, C.; Han, J.; Ryu, C. Y.; Benicewicz, B. C. A Versatile Method To Prepare RAFT Agent Anchored Substrates and the Preparation of PMMA Grafted Nanoparticles. Macromolecules **2006**, *39*, 3175–3183.

(9)   Zhao, Y. L.; Perrier, S. Synthesis of Well-Defined Homopolymer and Diblock Copolymer Grafted onto Silica Particles by Z-Supported RAFT Polymerization. Macromolecules **2006**, *39*, 8603–8608.

(10)   Nguyen, D. H.; Vana, P. Polym. Silica-immobilized cumyl dithiobenzoate as mediating agent in reversible addition fragmentation chain transfer (RAFT) polymerization, Adv. Technol. **2006**, *17*, 625–633.

(11)   Liu, C. H.; Pan, C. Y. Grafting polystyrene onto silica nanoparticles via RAFT polymerization. Polymer **2007**, *48*, 3679–3685.

(12)   Zhao, Y.; Perrier, S. Reversible Addition−Fragmentation Chain Transfer Graft Polymerization Mediated by Fumed Silica Supported Chain Transfer Agents. Macromolecules **2007**, *40*, 9116–9124.

(13)   Hong, C. Y.; Li, X.; Pan, C. Y. Grafting polymer nanoshell onto the exterior surface of mesoporous silica nanoparticles via surface reversible addition-fragmentation chain transfer polymerization. Eur. Polym. J. **2007**, *43*, 4114–4122.

(14)   Kaminsky, W.; Hinrichs, B. Polymeric dienes. Plast. Eng. (N.Y., U.S.) **2005**, *70*, 333-380.

(15)   Nazhat, S. N.; Parker, S.; Patel, M. P.; Braden, M. Isoprene-styrene copolymer elastomer and tetrahydrofurfuryl methacrylate mixtures for soft prosthetic applications. Biomaterials **2001**, *22*, 2411-2416.

(16)   Nazhat, S. N.; Parker, S.; Riggs, P. D.; Braden, M. Isoprene-styrene copolymer elastomer and tetrahydrofurfuryl methacrylate mixtures for soft prosthetic applications. Biomaterials **2001**, *22,* 2087-2093.

(17)   Hou, S.; Chan, W. K. Preparation of Functionalized Polystyrene-block-polyisoprene Copolymers and Their Luminescence Properties. Macromolecules **2002**, *35*, 850-856.

(18)   Lu, Z. J.; Huang, X. Y.; Huang, J. L.; Pan, G. Q. Macromol. Rapid Commun. **1998**, *19*, 527-531.

(19)   Donderer, M.; Langstein, G.; Schafer, M.; Nuyken, O. Polym. Bull. (Berlin) **2002**, *47*, 509-516.

(20)   Peng, Y.; Wang, J.; Liu, J.; Dai, H.; Cun, L. Polym. Int. **1996**, *39*, 63-68.

(21)   Kongkaew, A.; Wootthikanokkhan, J. Polym. Bull. (Berlin) **1999**, *43*, 327-332.

(22)   Wootthikanokkhan, J.; Tongrubbai, B. Compatibilization efficacy of poly(isoprene–butyl acrylate) block copolymers in natural/acrylic rubber blends. J. Appl. Polym. Sci. **2003**, *88*, 921-927.

(23)   Kir, O.; Binder, W. H.; Living anionic surface initiated polymerization (LASIP) of isoprene from silica nano- and glass particles. European Polym. J. **2013**, *49*, 3078-3088.

(24)   Derouet, D.; Thuc, C.N.H.; J. Rubb. Res. **2008**, *11*, 78-96.

(25)   Jitchum, V.; Perrier, S.; Living Radical Polymerization of Isoprene via the RAFT Process. Macromolecules **2007**, *40*, 1408- 1412.

(26)   Germack, D. S.; Wooley, K. L.; Isoprene polymerization via reversible addition fragmentation chain transfer polymerization. J. Polym. Sci., Part A: Polym. Chem. **2007**, *45*, 4100-4108.

(27)   Li, C.; Han, J.; Ryu, C. Y.; Benicewicz, B. C. A Versatile Method To Prepare RAFT Agent Anchored Substrates and the Preparation of PMMA Grafted Nanoparticles. Macromolecules **2006**, *39*, 3175–3183.

(28)   Abel-Goad, M.; Pyckhout-Hintzen, W.; Kahle, S.; Allgaier, J; Richter, D.; Feters, L. J. Rheological Properties of 1,4-Polyisoprene over a Large Molecular Weight Range. Macromolecules **2004**, *37 (21)*, 8135-8144.

(29)   Meng-Jiao Wang. Rubber Chemistry and Technology. **1998**, *71*, 3, 520-589.

CHAPTER 6

SURFACE-INITIATED REVERSIBLE ADDITION-FRAGMENTATION CHAIN

TRANSFER POLYMERIZATION OF CHLOROPRENE AND MECHANICAL

PROPERTIES OF MATRIX-FREE POLYCHLOROPRENE NANOCOMPOSITES.

6.1 Abstract

RAFT polymerization and surface-initiated RAFT polymerization (SI-RAFT) of polychloroprene was studied. The SI-RAFT polymerization rate of chloroprene was found to be slower than free solution RAFT polymerization, and further regulated by the graft density of grafted polymers. The resulting polychloroprene-grafted silica nanoparticles were directly crosslinked to get matrix-free polychloroprene nanocomposites that showed good nanoparticle dispersion and superior mechanical properties compared with unfilled polychloroprene rubber.

6.2 Introduction

Polychloroprene has been widely used in the rubber industry since its discovery by Dupont in 1931.[1] Compared with other elastomers, polychloroprene exhibits excellent resistance to oil, grease and wax, wide operating temperature range, and is resistant to ozone and harsh weather conditions. The application of polychloroprene ranges from adhesives and sealants, to hoses and automotive parts. To synthesize PCPs, uncontrolled free radical emulsion polymerization is commonly used with thio-based chain transfer agent to limit molecular weight.[2] The polymers synthesized in this way generally have very high molecular weight and broad molecular weight distribution. To obtain better control over the polymerization of chloroprene, in recent years, controlled radical polymerization has been used to synthesize polychloroprene with predetermined molecular weight and low PDI. Topham et al. demonstrated the first controlled polymerization of chloroprene using reversible addition-fragmentation chain transfer polymerization (RAFT).[3] Four different RAFT agents were examined in two different reaction medium (xylene and THF). The results showed that the dithioester 2-cyano-2-prepylbenzodithioate exhibited the highest

116

degree of control in xylene while 2-cyano-2-prepylbenzodithioate and trithiocarbonate with carboxylic acid end were most promising in THF. Yang et al. reported RAFT polymerization of chloroprene with more RAFT agents tested, and successfully synthesized polychloroprene-block-polystyrene and poly(methyl methacrylate)-block-polychloroprene copolymer.[4] Later, Fu et al. performed reverse iodine transfer polymerization of chloroprene and studied the influence of solvent, initiator and temperature.

However, to the best of our knowledge, there is no report on the surface initiated controlled polymerization of chloroprene up to date. In fact, a broader literature search indicates that while methacrylic/acrylic and styrene type of monomers have been grafted onto various of substrates using surface initiated anionic polymerization[5], surface initiated atom transfer radical polymerization[6], surface initiated nitroxide mediated polymerization,[7] and reversible fragmentation chain transfer polymerization, [8] butadiene-derivative monomers such as chloroprene, have rarely been polymerized from surfaces using any of the existing controlled polymerization techniques.

It is now well accepted that the addition of nanoparticles into a polymer matrix could result in materials with improved thermomechanical properties. To achieve optimal improvement, it requires that nanoparticles are well dispersed in the matrix instead of forming clusters to maximize the nanoparticle-matrix surface area. Grafting filler nanoparticles with the same polymer chains as the matrix has been demonstrated to be an effective way to improve nanoparticle dispersion. In this chapter, we report the surface-initiated RAFT polymerization of chloroprene from silica nanoparticles and carefully studied polymerization kinetics at different graft densities. The resulting PCP grafted silica

nanoparticles were directly crosslinked to create matrix-free nanocomposites that showed improved mechanical properties as compared to free PCP.

6.3 Experimental Section

Materials. Chloroprene monomer was synthesized according to the literature.[3] The RAFT agent 2-methyl-2-[(dodecylsulfanylthiocarbonyl) sulfanyl]propanoic acid (MDSS) (97%) was purchased from Strem Chemicals and used as received. Spherical SiO_2 nanoparticles with a diameter of 14 ± 4 nm were purchased from Nissan Chemical Co. Tetrahydrofuran (THF) (HPLC grade, Fisher), dicumyl peroxide (Acros, 99%), and aminopropyldimethylethoxysilane (Gelest, 95%) were used as received. 2.2'-Azobisisobutyronitrile (AIBN) was purified by recrystallization from methanol and dissolved in THF to make 10mM solution. All other reagents were used as received.

Characterization.

^{1}H NMR (Bruker ARX 300/ARX 400) was conducted using CD_3OD as the solvent. Molecular weights and dispersity were determined using a gel permeation chromatography (GPC) with a 515 HPLC pump, a 2410 refractive index detector, and three Styragel columns. The columns consist of HR1, HR3 and HR4 in the effective molecular weight ranges of 100-5000, 500-30000, and 5000-500000, respectively. THF was used as eluent at 30°C and flow rate was adjusted to 1.0mL/min. Molecular weights were calibrated with poly(methyl methacrylate) standards obtained from Polymer Laboratories. Dynamic Light Scattering (DLS) characterizations were conducted using Zetasizer Nano ZS90 from Malvern. Infrared spectra were obtained using a BioRad Excalibur FTS3000 spectrometer.

The transmission electron microscopy (TEM) was performed on a Hitachi H8000 TEM at an accelerating voltage of 200 KV. The samples were prepared by depositing a drop of the diluted nanoparticle solution in methanol on copper grids. Scanning electron microscopy (SEM) was performed by drop-casting 10 µl of diluted nanoparticle solution on copper grids with carbon film. Small angel X-ray scattering experiments were conducted using a SAXSLab Ganesha at the South Carolina SAXS Collaborative. A Xenocs GeniX3D microfocus source was used with a Cu target to generate a monochromic beam with a 0.154 nm wavelength. The instrument was calibrated using a silver behenate reference with the first order scattering vector $q^* = 1.076$ nm^{-1}, where $q = 4\pi\lambda^{-1} \sin\theta$ with a total scattering angle of 2θ. Thermogravimetric analysis (TGA) measurements were carried out on a TA Q5000 thermogravimetric analyzer (TA Instruments). All the samples were preheated to 150°C and kept at this temperature for 10 min to remove residual solvents. After cooling to 40°C, the samples were heated to 800 °C with a heating rate of 10 °C/min in nitrogen atmosphere. An Instron 5500 tensile tester was used to measure the stress-strain curve with a 100 N load cell and test speed of 20 mm/min at room temperature. The dog-bone shaped samples for tensile testing were cut from hot press samples with 22 mm length and 5 mm width. Each sample was tested at least three times for tensile test. Dynamic mechanical analysis (DMA) was measured by a RAS3 DMA (TA Instruments) in a tensile mode. The DMA data was collected by testing with a frequency of 1.0 Hz, 0.1% strain and a heating rate of 3 °C /min from -100 °C to 150 °C.

Free RAFT polymerization of chloroprene. In a typical polymerization, chloroprene (0.5g), MDSS (5.16mg), AIBN (141ul from 10mM stock solution) and THF (1ml) were added and mixed well in a Schlenk flask. The mixture was degassed by three freeze-pump-thaw cycles, filled with nitrogen, and the Schlenk flask was placed in an oil bath at 60°C. Aliquots of the reaction solution were withdrawn from the flask periodically since the beginning of polymerization.

Synthesis of MDSS-g-SiO$_2$. A solution (20 mL) of colloidal silica particles (30 wt % in methyl isobutyl ketone) was added to a two-necked round bottom flask and diluted with 110 mL of THF. 3-Aminopropyldimethylethoxysilane (0.32 mL, 2 mmol) and the mixture were refluxed in a 65 °C oil bath for 5 hours under nitrogen protection. The reaction was then cooled to room temperature and precipitated in a large amount of hexanes (500 mL). The particles were then recovered by centrifugation and dispersed in THF using sonication and precipitated in hexanes again. The amine-functionalized particles were redispersed in 40 mL of THF for further reaction. Then 0.2 g, (0.4 mmol) of activated MDSS was prepared as described previously and added dropwise to a THF solution of the amine functionalized silica nanoparticles (40 mL, 6 g) at room temperature. After complete addition, the solution was stirred overnight. The reaction mixture was then precipitated into a large amount of hexanes (400 mL). The particles were recovered by centrifugation at 3000 rpm for 8 min. The particles were then redispersed in 30 mL THF and precipitated in hexanes. This dissolution−precipitation procedure was repeated 2 more times until the supernatant layer after centrifugation was colorless. The yellow MDSS-anchored silica nanoparticles were dried at room temperature and analyzed using UV analysis to determine

120

the chain density using a calibration curve constructed from standard solutions of free MDSS.

Surface-initiated RAFT polymerization of chloroprene. In a typical polymerization, chloroprene (2g), MDSS-g-SiO$_2$ (0.74g 0.32ch/nm^2), AIBN (567ul from 10mM stock solution) and THF (4ml) were added and mixed well in a Schlenk flask. The mixture was degassed by three freeze-pump-thaw cycles, filled with nitrogen, and the Schlenk flask was placed in an oil bath at 60°C. Aliquots of the reaction solution were withdrawn from the flask periodically following the start of the polymerization. The resulting polychloroprene grafted particles were precipitated into a large amount of methanol and centrifuged at 8,000 rpm for 10 min and redispersed in THF.

General Procedures for cleaving Grafted Polymer from Particles. In a typical experiment, 20 mg of polychloroprene grafted silica particles was dissolved in 2mL of THF. Aqueous HF (49%, 0.2 mL) was added, and the solution was allowed to stir at room temperature overnight. The solution was poured into a PTFE Petri dish and allowed to stand in a fume hood overnight to evaporate the volatiles. The recovered polychloroprene was then subjected to SEC analyses.

Curing process of polychloroprene grafted particles.

Solvent mixing technique was used for curing. Chloroprene polymer (100eq), zinc oxide (5eq), magnesium oxide (2eq), phenyl-a-naphthylamine (2eq), stearic acid(0.5eq), 2-mercaptothiozoline(0.5eq) were mixed well in THF (15 ml for each gram of polymer). The mixtures wer then poured into Teflon petri dishes for solvent evaporation. The dried samples were hot pressed at 160° for 25 minutes to obtain vulcanized rubber sheet of 0.2 to 0.4 mm thickness.

6.4 Results and Discussion

2-Methyl-2-[(dodecylsulfanylthiocarbonyl) sulfanyl]propanoic acid (MDSS) was selected as the RAFT agent because it has been reported to have excellent control over a selection of common monomers,[3] and the end carboxylic acid group provided a convenient site for grafting onto the particle surface.

We initially examined the free RAFT polymerization of CP. The ratio between species was kept at [CP]/[RAFT]/[AIBN] = 400: 1: 0.1. The reaction was carried out in THF at 60°C, and monitored over time. As shown in Figure 6.1, $Ln(M_0/M_t)$ had a linear relationship versus time and the molecular weight increased with monomer conversion although it did show a type of hybrid behavior. This hybrid behavior, resulting in an initial high molecular weight which approaches the calculated molecular weight as conversion increases, is usually ascribed to a low chain transfer constant at initial stages of the polymerization.[9] PDI was below 1.5 during the process and the molecular distribution by GPC shows well-shaped unimodal peaks. We further studied the microstructure of PCP by NMR, which has not been reported previously. It was found that the ratio between microstructures was 71% 1,4 trans, 23% cis, 1.3% 1,2 additions and 4.7% 3,4 additions. The ratio did not change across samples at different molecular weights.
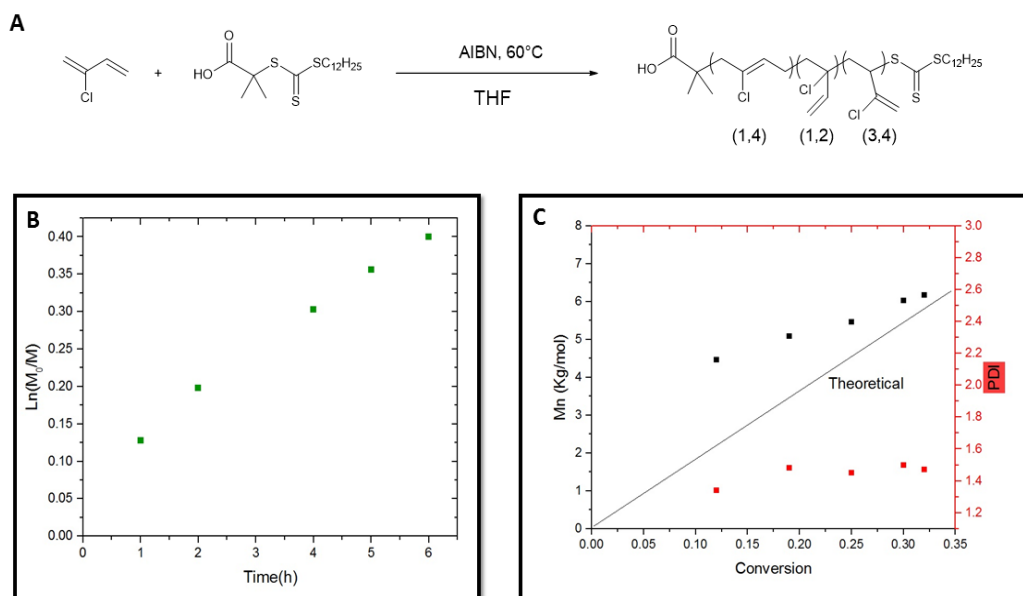
Figure 6.1. (A) Reaction scheme, (B) First-order kinetic plot and (C) Molecular weight versus conversion and polydispersity for RAFT polymerization of chloroprene in solution.

To perform surface-initiated polymerization of CP from nanoparticles, we modified particle surfaces with RAFT agents, which was realized in three steps. First, the nanoparticles were treated aminosilane agent to obtain amine functionalized NPs. Then MDSS was activated by reacting with 2-mercaptothiazoline followed by silica gel column for purification. Last, amine functionalized NPs were reacted with activated MDSS to obtain MDSS attached nanoparticles. Successfully functionalized NPs showed the light yellow color of MDSS, and graft density was calculated based on characteristic UV-vis absorbance of MDSS at 300nm.
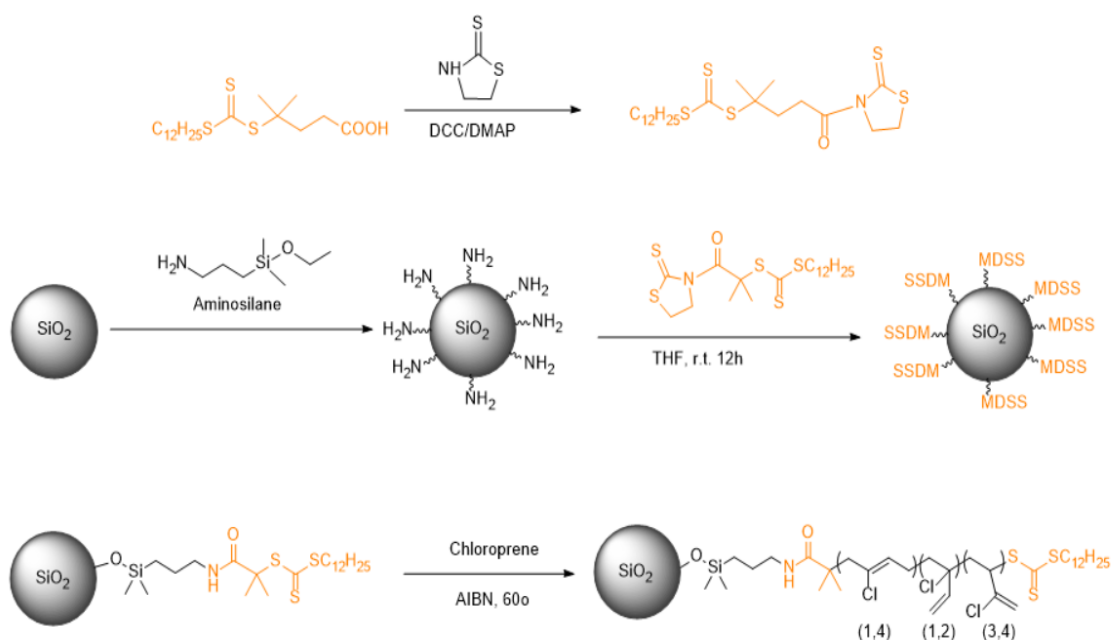
Scheme 6.1. Preparation of PCP grafted SiO_2 NPs

Surface-initiated RAFT polymerization of chloroprene was performed from MDSS grafted silica nanoparticles with 0.33chs/nm^2 graft density with ratio between [Monomer]/[CTA]/[initiator] = 400: 1: 0.1. Reaction conditions were kept exactly the same as free solution polymerization including the ratio between monomers and solvent.

The polymerization kinetics are shown in Figure 6.2. Molecular weight increased with monomer conversion with slight hybrid behavior and PDIs were typically less than 1.6. The linearity of the pseudo first order kinetic plot implies a constant radical concentration during the 26h polymerization period. These results indicated that surface anchored MDSS as well as free MDSS could be employed to control the polymerization of CP.
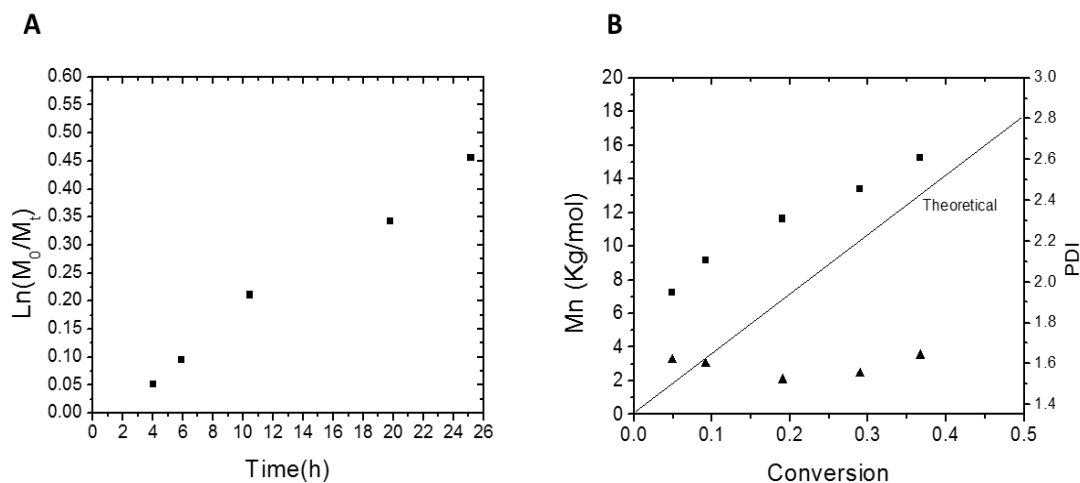
124

Figure 6.2. (A) First-order kinetic plot and (b) molecular weight and polydispersity versus conversion of the surfaced initiated RAFT polymerization of CP with 0.32chs/nm^2 graft density, [monomer]/[CTA]/[initiator] = 400: 1: 0.1.

It is interesting to compare the reaction kinetics between free RAFT polymerization in solution, and the surface-initiated RAFT polymerization on particles. By comparing the kinetics of SI-RAFT in Figure 6.2 and the one for free RAFT mediated polymerization in Figure 6.1, it is obvious that the free RAFT agent mediated polymerization was much faster than SI-RAFT polymerization. Approximately 25% conversion was achieved in 4 hours for free RAFT mediated polymerization and the same conversion was not achieved until 20 hours for SI-RAFT with 0.32chs/nm^2 graft density. This observation implied a retardation effect with SI-RAFT polymerization of CP. Similar observations have been reported for SI-RAFT polymerization of methyl methacrylate (MMA) using 4-cyanopentanoic acid dithiobenzoate (CPDB) as RAFT agent. We reason that such

observation could be ascribed to the "localized high RAFT agent concentration" effect.[8] In the case of SI-RAFT polymerization, the local concentration of RAFT agent was much higher than free RAFT agent mediated polymerization due to the immobilization onto particle surfaces. Therefore, surface radicals could transfer between adjacent RAFT agents instead of propagation via monomer addition, which resulted in retardation of polymerization observed here and reported in the literature.

To provide further evidence for the hypothesis, we studied the SI-RAFT polymerization of CP with a different graft density (0.15ch/nm^2), and plotted the reaction kinetics along with the two prior cases. (Figure 6.3)
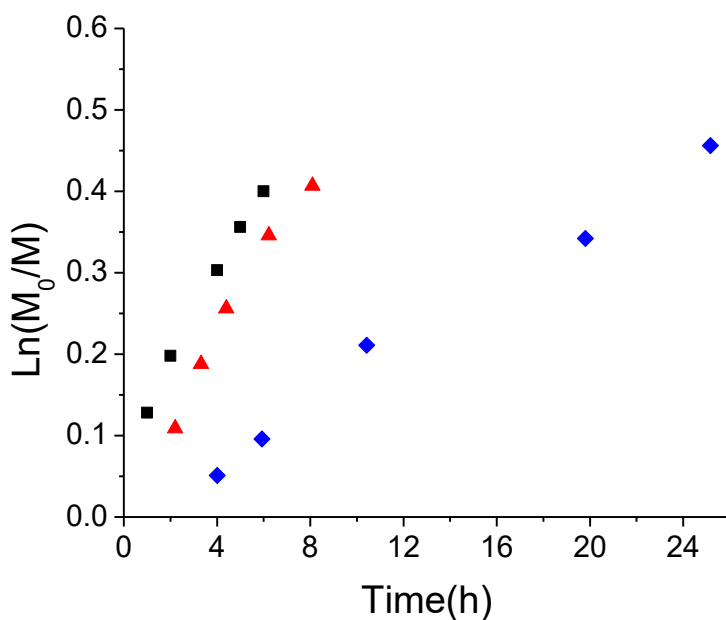

Figure 6.3. Pseudo first-order kinetic plots for the polymerization of chloroprene with ratio between species [monomer]/[CTA]/[initiator] = 400: 1: 0.1 with free MDSS (black square); MDSS grafted particles with 0.15 ch/nm^2 density (red triangle); MDSS grafted particles with 0.32 chs/nm^2 density (blue diamond).

We find that the kinetic curve of SI-RAFT polymerization at 0.15ch/nm^2 graft density is intermediate between the curves of free RAFT polymerization and SI-RAFT polymerization at 0.32ch/nm^2 density, which agrees with our hypothesis. For SI-RAFT polymerization of CP, at low-to -medium graft density, the "localized high RAFT agent concentration" effect is not as pronounced as the case for high graft density, and the polymerization kinetics was similar to the free RAFT polymerization of CP.

Mechanical properties of matrix-free PCP grafted silica nanoparticle composites.

To investigate the mechanical properties of matrix-free PCP grafted silica nanoparticle composites, we prepared a series of composites from NPs with the same graft density (0.1 chs/nm^2), but different molecular weights of grafted polymer. The details of the samples are listed in Table 6.1.

Table 6.1. Sample details of matrix-free PCP grafted silica nanoparticle composites.

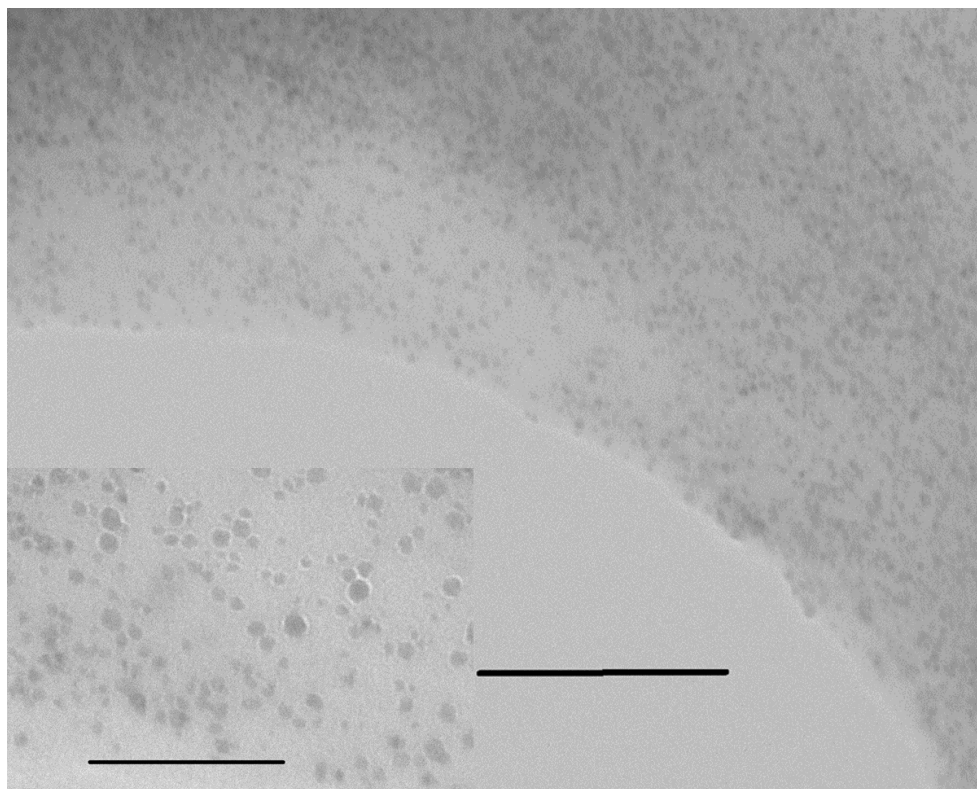| Sample name	Graft density (chs/nm^2)	Mn	Silica content%	Tensile strength(MPa)	Elongation at break
PCP unfilled	N/A	50 kDa	0	1.8	10.3
MF-47K	0.1	47 kDa	50	12.9	3.9
MF-55K	0.1	55 kDa	45	11.0	5.3
MF-70K	0.1	70 kDa	40	11.0	7.7
MF-100K	0.1	100 kDa	30	6.1	10.9

Figure 6.4. TEM image of 100 kDa PCP grafted silica nanocomposites at 30 silica wt%. Scale bar 500nm (bottom middle) and 200nm (bottom left).

The PCP grafted silica nanoparticles were directly crosslinked as matrix-free composites. MgO and ZnO were used as crosslinking agents. PCP grafted silica nanoparticles were mixed with curing agents in solution and then solvents were allowed to evaporate under vacuum. Then dried samples were hot pressed at 160 °C for 25 minutes to obtain vulcanized rubber sheet of 0.2 to 0.4 mm thickness. The advantage of matrix-free nanocomposites over conventional composite materials is to achieve better nanoparticle dispersion. Conventional composite synthesis procedures require the mixing of particles with polymer matrix, which introduces additional complexity into the system, and often results in agglomeration of particles especially at high nanoparticle loading due to unsatisfactory interface compatibility. In matrix-free systems, the particles are inherently

128

separated from each other by the grafted polymers. Thus, good dispersion could be easily achieved.[10-12]

As shown in Figure 6.4, good particle dispersion was achieved with 100 kDa PCP grafted silica nanocomposites at 30 wt% silica. There was no significant clustering of particles even at high silica loading. However, a closer view revealed there is no well-defined pattern of particle distribution and interparticle spacing was not uniform, which is most likely due to the large size disparity of the core silica particles.
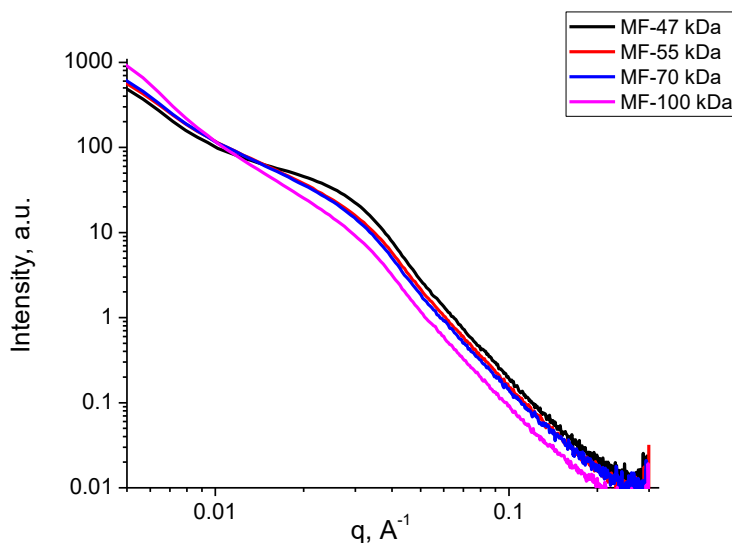
Figure 6.5. Representative small-angle X-ray scattering (SAXS) intensity for matrix-free PCP grafted silica nanocomposites.

Small-angle X-ray scattering (SAXS) was used to obtain more information on the particle dispersion state of the crosslinked samples. No agglomeration was detected from the X-ray scattering pattern at low q. The intensity of all the peaks was relatively weak, indicating a broad distribution of interparticle spacing. The location of the peak did not

change much between the samples, which corresponded to a d spacing ~23nm, and seems

reasonable considering the size of silica core (15nm) plus the grafted polymers.

The matrix-free nanocomposites were crosslinked as films and cut into dog-bones

for tensile testing. It was found that the properties of the composites were directly related

to the molecular weight of the grafted polymers.

Figure 6.6. Stress-strain curves of crosslinked unfilled and filled composites.

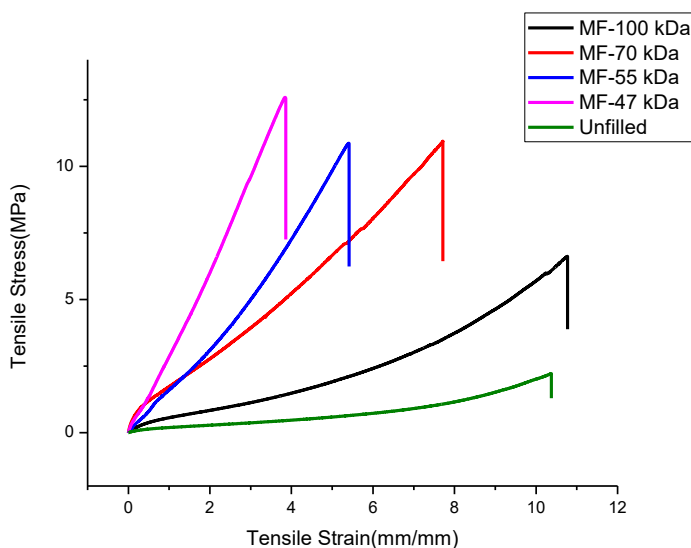Tensile stress-stain curves of matrix-free PCP silica nanocomposites are shown in

Figure 6.6. All the matrix-free composites have significantly improved tensile strength

compared with unfilled PCP. Furthermore, the tensile stress at break increased with silica

loading with a corresponding decrease in elongation at break. This general trend is

consistent with literature that the crosslink density increase continuously with increasing silica loading.[13-14] [15] For matrix-free nanocomposite systems, the increase in molecular weight of the grafted polymers causes a decrease in silica loading at a fixed graft density. Thus, as molecular weight increased, the elongation at break increased due to better entanglement between polymer chains while the tensile strength decreased due to lower silica loading.
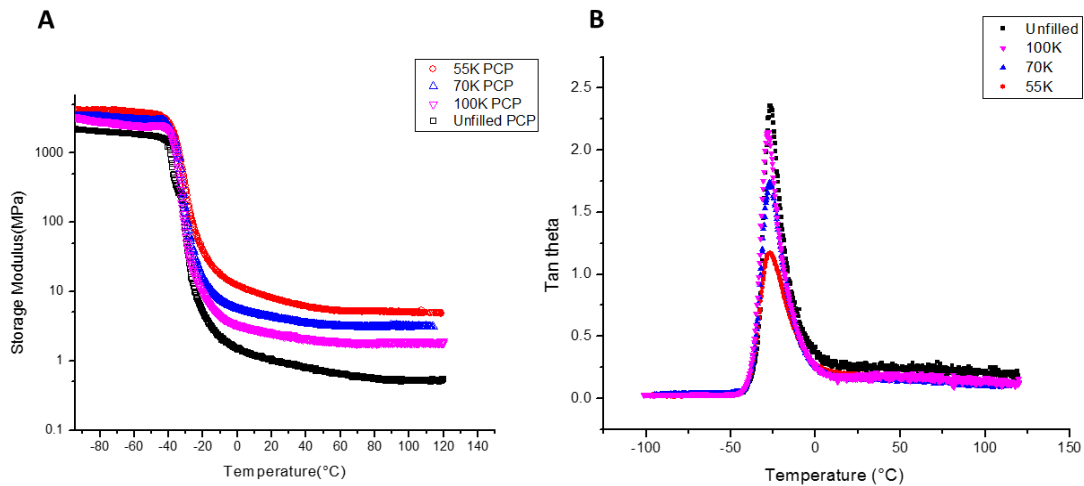
Figure 6.7. Temperature dependence of storage modulus of crosslinked unfilled PCP and matrix-free PCP silica nanocomposites.

The dynamic mechanical behavior was measured at constant strain and frequency for the PCP crosslinked silica nanocomposites and the crosslinked unfilled PCP. Figure 6.7 shows that matrix-free PCP silica composites showed higher storage modulus in the rubbery plateau region relative to the unfilled PCP corresponding to the increase in silica content. The glass transition temperature of the matrix-free composites was not altered compared with unfilled PCP as observed in Figure 7B, however, the reduction of tan delta

131

peak height increased with silica loading, which also suggests better reinforcing effect and stronger rubber-filler interaction at high silica loading. [16]

6.5 Conclusion

A facile method was demonstrated for the synthesis of polychloroprene grafted silica NPs using surface-initiated RAFT polymerization. A trithioester RAFT agent was anchored onto the surface of silica NPs with controlled graft density, and controlled radical polymerizations were conducted to produce surface grafted PCP of predetermined molecular weight and relatively narrow PDI. The polymerization kinetics was studied and it was found that the grafting-from polymerization rate was dependent on the graft density and generally slower than chloroprene polymerization mediated by free RAFT agent. The PCP grafted silica NPs were directly crosslinked to form matrix-free nanocomposites that showed uniform particle dispersion and improved mechanical properties than unfilled PCP. These strong, tough composite materials could be useful in many applications that also require the improved solvent and environmental resistance inherent in polychloroprene rubbers.

6.6 References.

1.   Carothers, W. H.; Williams, I.; Collins, A. M.; Kirby, J. E., ACETYLENE POLYMERS AND THEIR DERIVATIVES. II. A NEW SYNTHETIC RUBBER: CHLOROPRENE AND ITS POLYMERS. *Journal of the American Chemical Society* **1931,** *53* (11), 4203-4225.
2.   Itoyama, K.; Hirashima, N.; Hirano, J.; Kadowaki, T., Emulsion Polymerization of Chloroprene. Polymerization Mechanism and Evaluation of Crosslinking Density. *Polym J* **1991,** *23* (7), 859-864.
3.   Pullan, N.; Liu, M.; Topham, P. D., Reversible addition-fragmentation chain transfer polymerization of 2-chloro-1,3-butadiene. *Polymer Chemistry* **2013,** *4* (7), 2272-2277.

4. Hui, J.; Dong, Z.; Shi, Y.; Fu, Z.; Yang, W., Reversible-deactivation radical polymerization of chloroprene and the synthesis of novel polychloroprene-based block copolymers by the RAFT approach. *RSC Advances* **2014,** *4* (98), 55529-55538.

5. Zhou, Q.; Fan, X.; Xia, C.; Mays, J.; Advincula, R., Living Anionic Surface Initiated Polymerization (SIP) of Styrene from Clay Surfaces. *Chemistry of Materials* **2001,** *13* (8), 2465-2467.

6. Ohno, K.; Morinaga, T.; Koh, K.; Tsujii, Y.; Fukuda, T., Synthesis of Monodisperse Silica Particles Coated with Well-Defined, High-Density Polymer Brushes by Surface-Initiated Atom Transfer Radical Polymerization. *Macromolecules* **2005,** *38* (6), 2137-2142.

7. Matsuno, R.; Otsuka, H.; Takahara, A., Polystyrene-grafted titanium oxide nanoparticles prepared through surface-initiated nitroxide-mediated radical polymerization and their application to polymer hybrid thin films. *Soft Matter* **2006,** *2* (5), 415-421.

8. Li, C.; Han, J.; Ryu, C. Y.; Benicewicz, B. C., A Versatile Method To Prepare RAFT Agent Anchored Substrates and the Preparation of PMMA Grafted Nanoparticles. *Macromolecules* **2006,** *39* (9), 3175-3183.

9. Moad, G.; Barner-Kowollik, C., The Mechanism and Kinetics of the RAFT Process: Overview, Rates, Stabilities, Side Reactions, Product Spectrum and Outstanding Challenges. In *Handbook of RAFT Polymerization*, Wiley-VCH Verlag GmbH & Co. KGaA: 2008; pp 51-104.

10. Grabowski, C. A.; Koerner, H.; Meth, J. S.; Dang, A.; Hui, C. M.; Matyjaszewski, K.; Bockstaller, M. R.; Durstock, M. F.; Vaia, R. A., Performance of Dielectric Nanocomposites: Matrix-Free, Hairy Nanoparticle Assemblies and Amorphous Polymer–Nanoparticle Blends. *ACS Applied Materials & Interfaces* **2014,** *6* (23), 21500-21509.

11. Yan, J.; Kristufek, T.; Schmitt, M.; Wang, Z.; Xie, G.; Dang, A.; Hui, C. M.; Pietrasik, J.; Bockstaller, M. R.; Matyjaszewski, K., Matrix-free Particle Brush System with Bimodal Molecular Weight Distribution Prepared by SI-ATRP. *Macromolecules* **2015,** *48* (22), 8208-8218.

12. Li, Y.; Wang, L.; Natarajan, B.; Tao, P.; Benicewicz, B. C.; Ullal, C.; Schadler, L. S., Bimodal "matrix-free" polymer nanocomposites. *RSC Advances* **2015,** *5* (19), 14788-14795.

13. Sae-oui, P.; Sirisinha, C.; Thepsuwan, U.; Hatthapanit, K., Dependence of mechanical and aging properties of chloroprene rubber on silica and ethylene thiourea loadings. *European Polymer Journal* **2007,** *43* (1), 185-193.

14. Sae-oui, P.; Sirisinha, C.; Thepsuwan, U.; Hatthapanit, K., Roles of silane coupling agents on properties of silica-filled polychloroprene. *European Polymer Journal* **2006,** *42* (3), 479-486.

15. Kapgate, B. P.; Das, C.; Das, A.; Basu, D.; Wiessner, S.; Reuter, U.; Heinrich, G., Reinforced chloroprene rubber by in situ generated silica particles: Evidence of bound rubber on the silica surface. *Journal of Applied Polymer Science* **2016,** *133* (30), n/a-n/a.

16. Kumnuantip, C.; Sombatsompop, N., Dynamic mechanical properties and swelling behaviour of NR/reclaimed rubber blends. *Materials Letters* **2003,** *57* (21), 3167-3174.

CHAPTER 7

CONCLUSIONS AND OUTLOOK

7.1 Conclusions

Multifunctional polymer grafted nanoparticles were synthesized, characterized and investigated for various applications. The composition, structure, molecular weight, graft density and architecture of the grafted polymers were carefully selected to meet the specific requirements for each application. For drug delivery applications, water-soluble, stimuli responsive block copolymers were selected to provide biocompatibility and enhanced drug release at a tumor environment. For self-assembly applications, amphiphilic polymers with mixed brush architecture were selected to provide the delicate balance of overall hydrophilicity to induce the self-assembly. For tire reinforcement applications, low Tg polymers with exact composition as target matrices were selected to provide the optimum compatibility between nanofillers and polymer matrices.

The self-assembly behavior of amphiphilic polymer grafted nanoparticles were systematically studied. A new self-assembly technique, namely surface-initiated polymerization-induced self-assembly (SI-PISA) was developed that enabled the one-pot synthesis of hybrid nano-objects with different shapes including 1D strings, 2D disks, 3D vesicles and solid spheres. The SI-PISA was established based on a bimodal polymer-grafted NP structure. A solvent-miscible brush was first grafted onto 15 nm silica NPs, and self-assembly was subsequently induced by the polymerization of a second brush that was solvent-immiscible. Self-assembly occurred *in situ* with the SI-polymerization of the second brush. The shape of the nano-objects was found to be controlled by the chemical structure of grafted polymers, chain length of grafted polymers, and reaction media.

A reversed monomer addition sequence was successfully utilized to prepare bimodal polymer grafted nanoparticles and resulted in a significantly condensed synthetic procedure. The procedure started from surface-initiated RAFT polymerization of styrene from silica nanoparticles and then the polystyrene macro RAFT agents were chain extended with poly(methacrylic acid), which was in the reversed monomer addition sequence for building well-defined block copolymers. The composition of the grafted polymers was analyzed by GPC deconvolution. Approximately 10% of the grafted PS macro-initiators were chain extended while the majority remained "unreacted" or were terminated by radical coupling. It was shown that this procedure of grafting block polymers with reversed monomer addition sequence could be employed as a "quick and dirty" method of preparing mixed brush polymer grafted nanoparticles. The SiO_2-g-(PS_{396}, PS_{396}-b-$PMAA_x$) nanoparticles showed unique self-assembly behavior and formed solid spherical aggregates. The degree of aggregation could be controlled in the range between 1 to several hundred by adjusting the PS/PMAA ratio and initial nanoparticle concentration. It is expected that these assemblies will find wide application in the nanotechnology field.

A pH and thermal dual-responsive nanocarrier with silica as the core and block copolymer composed of poly(methacrylic acid) (PMAA) and poly(N-isopropylacrylamide) (PNIPAM) as the shell was prepared by surface initiated RAFT polymerization. The resulting SiO_2-PMAA-b-PNIPAM particles dispersed individually in aqueous solution at high pH and low temperature but reversibly agglomerated at acidic conditions or at elevated temperature. These dual-responsive nanoparticles were used as carriers to deliver the model drug doxorubicin (DOX) with unusually high entrapment efficiency and loading content. The release rate was controlled by both pH and temperature

of the surrounding medium. Moreover, these particles selectively precipitated at acidic conditions with increased temperature, which may enhance their ability to accumulate at tumor sites. Cytotoxicity studies demonstrated that DOX-loaded nanoparticles are highly active against Hela cells, and more effective than free DOX of equivalent dose. A cellular uptake study revealed that SiO_2-PMAA-b-PNIPAM nanoparticles could successfully deliver DOX molecules into the nuclei of Hela cells. All these features indicated that SiO_2-PMAA-b-PNIPAM nanoparticles are a promising candidate for therapeutic applications.

We studied the surface-initiated RAFT polymerization of polyisoprene from two types of silica particles. The polymerization kinetics on spherical particles were studied at different graft densities and the polymerization formulation was further optimized to target over 100 kDa molecular weight grafted polymers. ZEOSIL 1165mp silica powders were used as an alternative silica source, which were broken down into ~200 nm silica clusters by sonication, which were then successfully grafted with polyisoprene as well. The synthetic procedure of PIP grafted Nissan silica nanoparticles were successfully scaled up from gram scale to kilogram scale by employing stainless steel tubes as a reaction vessel in a heated oven. The PIP grafted Nissan silica nanoparticles were used as reinforcing fillers to improve the mechanical properties of SKI-3 polyisoprene matrix. Tensile testing showed that composites with 50 kDa PIP grafted Nissan silica showed significant (187%) increase in tensile stress at break compared with pure matrix, indicating a strong reinforcement effect. Dynamic mechanical analysis showed significant improvements in the storage modulus in the rubbery state for the silica filled samples compared with unfilled matrix. Although the mechanical testing results were encouraging, TEM, SAXS and strain-sweep DMA results suggested that perfect nanoparticle dispersion has not yet been

achieved. Partial nanoparticle aggregation existed probably due to insufficient particle surface coverage, which could be potentially improved by using a bimodal polymer grafting architecture.

A facile method was demonstrated for the synthesis of polychloroprene grafted silica NPs using surface-initiated RAFT polymerization. A trithioester RAFT agent was anchored onto the surface of silica NPs with controlled graft density, and controlled radical polymerizations were conducted to produce surface grafted PCP of predetermined molecular weight and relatively narrow PDI. The polymerization kinetic was studied and it was found that the grafting-from polymerization rate was dependent on the graft density and generally slower than chloroprene polymerization mediated by free RAFT agent. The PCP grafted silica NPs were directly crosslinked to form matrix-free nanocomposites that showed uniform particle dispersion and improved mechanical properties than unfilled PCP. These strong, tough composite materials could be useful in many applications that also require the reported solvent and environmental resistance inherent in polychloroprene rubbers.

7.2 Future work

The SI-PISA method developed in this work is a new self-assembly technique with huge potential in terms of versatility, efficiency and cost-effectiveness to produce hybrid nano-assemblies. One important extension of the current state-of-the-art would be to try this formula on other types of nanoparticles, for example magnetic nanoparticles and gold nanoparticles. In this context, robust synthesis methods for surface-initiated RAFT polymerization from magnetic or gold nanoparticles need to be developed. It would be very useful to expand the current SI-PISA to other solvent systems like water and non-polar

solvents. The key to success would be to find the right combination of polymer brushes where the first brush provides sufficient solubility and the second brush becomes insoluble when polymerized to induce the self-assembly. In this context, we could utilize the large body of literature of pure polymer PISA recipes. Block copolymer based PISA systems have been successfully expanded into various solvent systems including water, ionic liquids, and non-polar solvents. Testing the polymer combinations from PISA would be a good starting point to explore future SI-PISA. However, there are also some factors that should be considered because the SI-PISA system is based on mixed brush grafted nanoparticles which is far more complicated than block copolymers. For example, the compatibility between the first polymer brush and the agents used to introduce second surface grafted RAFT agents should be considered. Our preliminary results show that acid containing polymer may not be suitable for stabilization brushes because they could potentially absorb the aminosilane agents which then subsequently decompose the surface RAFT agents.

In this thesis, we successfully synthesized and scaled up polyisoprene grafted silica nanoparticles that significantly improved mechanical properties of polyisoprene tire rubber. However, characterizations including TEM, SAXS and DMA indicated that perfect nanoparticle dispersions were not achieved. More work should be done to tackle this problem. Current data suggests that at low to medium graft densities, the dispersion state of the nanoparticles is not ideal. The uncovered silica surface could be contributing to particle agglomeration due to the particle-particle interaction. As a future direction, high graft density regime with short brushes should be explored, eliminating particle-particle interaction to achieve a better dispersion state. A second factor that may affect particle

dispersion is the lack of compatibility between the largely *trans* configuration polyisoprene and the pure *cis* configuration matrix. Experiments with different matrices should be carried out to help elucidate and address the incompatibility. For example, free polyisoprene matrix synthesized by RAFT could be used to guarantee the exact same polymer configuration between matrix polymer and grafted polymers. In addition to exploring high graft density regimen, we also propose the bimodal polymer architecture to address the issue. One potential problem with monomodal, high graft density polymer grafted nanoparticles is that polymer content tends to be relatively high especially when targeting high molecular weight at the same time. This trend is unfavorable in terms of tire rubber reinforcement application because high silica loading (~33 wt%) is desired for practical applications. Bimodal polymer architecture could solve this problem by using two populations of grafted polyisoprene chains. The first population should be high in molecular weight (>80 kDa), but very low in graft destiny(<0.05 chs/nm^2). They provide the entanglement between fillers and the matrix while not accounting for too much weight percent. The second population should be very low in molecular weight ($<$ 5 kDa), but with high graft density. They would saturate the silica surface, eliminating particle-particle interaction. These bimodal polymer-grafted nanoparticles would be ideal candidates to achieve perfect particle dispersion and optimal mechanical properties.